

# ON OPTIMAL CELL AVERAGE DECOMPOSITION FOR HIGH-ORDER BOUND-PRESERVING SCHEMES OF HYPERBOLIC CONSERVATION LAWS

SHUMO CUI, SHENGRONG DING, AND KAILIANG WU

**ABSTRACT.** This paper presents the first systematic study on the fundamental problem of seeking optimal cell average decomposition (OCAD), which arises from constructing efficient high-order bound-preserving (BP) numerical methods within Zhang–Shu framework. Since proposed in 2010, Zhang–Shu framework has attracted extensive attention and been applied to developing many high-order BP discontinuous Galerkin and finite volume schemes for various hyperbolic equations. An essential ingredient in the framework is the decomposition of the cell averages of the numerical solution into a convex combination of the solution values at certain quadrature points. The classic CAD originally proposed by Zhang and Shu has been widely used in the past decade. However, the feasible CADs are not unique, and different CAD would affect the theoretical BP CFL condition and thus the computational costs. Zhang and Shu only checked, for the 1D  $\mathbb{P}^2$  and  $\mathbb{P}^3$  spaces, that their classic CAD based on the Gauss–Lobatto quadrature is *optimal* in the sense of achieving the mildest BP CFL conditions. However, it was recently discovered that the classic CAD is generally not optimal for the multidimensional  $\mathbb{P}^2$  and  $\mathbb{P}^3$  spaces. It remained unclear what CAD is optimal for general polynomial spaces, especially in the multiple dimensions. In this paper, we establish the general theory for studying the OCAD problem on Cartesian meshes in 1D and 2D. We rigorously prove that the classic CAD is optimal for general 1D  $\mathbb{P}^k$  spaces and general 2D  $\mathbb{Q}^k$  spaces of an arbitrary  $k$ . For the widely used 2D  $\mathbb{P}^k$  spaces, the classic CAD is not optimal, and we establish the general approach to find out the genuine OCAD and propose a more practical quasi-optimal CAD, both of which provide much milder BP CFL conditions than the classic CAD. As a result, our OCAD and quasi-optimal CAD notably improve the efficiency of high-order BP schemes for a large class of hyperbolic or convection-dominated equations, at the little cost of only a slight and local modification to the implementation code. The remarkable advantages in efficiency are further confirmed by several numerical examples covering four hyperbolic partial differential equations.

The proposed analysis and theory of OCADs are highly nontrivial and involve novel techniques from several branches of mathematics. We prove several key properties of the OCAD problem, including the existence of OCAD by using Carathéodory’s theorem from convex geometry. Through transformation onto a reference cell, we simplify the 2D OCAD problem to a symmetric OCAD problem based on the invariant theory of symmetric group in abstract algebra. Most notably, we discover that the symmetric OCAD problem is closely related to polynomial optimization of a positive linear functional on the positive polynomial cone, thereby establishing four useful criteria for examining the optimality of a feasible CAD. Some geometric insights are also provided to interpret our critical findings.

## 1. INTRODUCTION

This paper is concerned with robust and efficient high-order numerical methods for hyperbolic conservation laws

$$(1.1) \quad \begin{cases} u_t + \nabla \cdot \mathbf{f}(u) = 0, & (\mathbf{x}, t) \in \mathbb{R}^d \times \mathbb{R}^+, \\ u(\mathbf{x}, 0) = u_0(\mathbf{x}), & \mathbf{x} \in \mathbb{R}^d, \end{cases}$$

where  $\mathbf{x}$  denotes the spatial coordinate variable(s) in  $d$ -dimensional space,  $t$  denotes the time, the conservative variable(s)  $u$  takes values in  $\mathbb{R}^m$ , and the flux  $\mathbf{f}$  takes values in  $(\mathbb{R}^m)^d$ . Our discussions in this paper can also be applicable to other related hyperbolic or convection dominated equations.

Solutions to the hyperbolic equations (1.1) typically satisfy certain bounds, which define a convex invariant region  $G \subset \mathbb{R}^m$ . For example, the entropy solution to scalar conservation laws

---

2020 *Mathematics Subject Classification.* Primary 35L65, 65M12, 65M60, 65M08.

*Key words and phrases.* Discontinuous Galerkin methods, hyperbolic conservation laws, bound-preserving schemes, cell average decomposition.

The third author is the corresponding author. This work is supported in part by NSFC grant 12171227.

( $m = 1$ ) satisfies the maximum principle [36]:

$$(1.2) \quad u(\mathbf{x}, t) \in G := [U_{\min}, U_{\max}] \quad \forall t \geq 0$$

with  $U_{\min} := \min_{\mathbf{x}} u_0(\mathbf{x})$  and  $U_{\max} := \max_{\mathbf{x}} u_0(\mathbf{x})$ . Other important examples include but are not limited to:

- the positivity of water height in shallow water equations [30];
- the positivity of density and pressure in compressible Euler equations [37];
- the subluminal constraint on fluid velocity, the positivity of pressure, and the positivity of rest-mass density in relativistic hydrodynamics [29, 16, 22].

When numerically solving such hyperbolic equations, it is highly desirable or even essential to preserve the intrinsic bounds, namely, to preserve the numerical solutions in the region  $G$ . In fact, if the numerical solutions go outside the bounds, for example, negative density or negative pressure is produced when solving the Euler equations, the discrete problem would become ill-posed due to the loss of hyperbolicity of the system, leading to the instability or breakdown of the numerical computation.

As well known for scalar conservation laws, the first-order monotone schemes

$$(1.3) \quad \bar{u}_j^{n+1} = \bar{u}_j^n - \lambda \left( \hat{f}(\bar{u}_j^n, \bar{u}_{j+1}^n) - \hat{f}(\bar{u}_{j-1}^n, \bar{u}_j^n) \right) =: H_\lambda(\bar{u}_{j-1}^n, \bar{u}_j^n, \bar{u}_{j+1}^n)$$

with  $H_\lambda$  monotonically increasing in all of its arguments, have been proved to preserve the bounds (1.2) under a suitable CFL condition

$$(1.4) \quad a\lambda \leq c_0,$$

where  $\lambda = \Delta t / \Delta x$  is the ratio of the temporal and spatial step-sizes,  $a$  denotes the maximum characteristic speed, and  $c_0$  is the maximum allowable CFL number. Examples of such first-order monotone schemes include the Godunov scheme, the Lax–Friedrichs scheme, and the Engquist–Osher scheme, etc. These first-order bound-preserving (BP) schemes were also extended to many hyperbolic systems.

However, constructing high-order accurate BP schemes is rather nontrivial. In [36, 37], Zhang and Shu proposed a general framework of designing high-order BP discontinuous Galerkin (DG) and finite volume (FV) schemes for hyperbolic conservation laws on rectangular meshes. Later, Zhang, Xia, and Shu further extended the framework to unstructured triangular meshes in [39]. Over the past decade, their framework has attracted extensive attention and been generalized to various hyperbolic or convection dominated equations; see, for example, [30, 20, 40, 29, 16, 35, 22, 5, 6, 24] and the survey papers [38, 33]. Recently, inspired by a series of BP study on magnetohydrodynamics [23, 25, 27], the geometric quasilinearization (GQL) framework was established in [28] for BP problems involving nonlinear constraints. The readers are also referred to [32, 31, 29, 10, 12, 7, 1] for some other BP techniques.

The Zhang–Shu approach [36, 37] classifies the loss of BP property in high-order FV and DG schemes into two cases: The first case is that the updated cell averages of the numerical solutions may be outside the set  $G$ , while the second is that the point values of the piecewise polynomial solutions, either reconstructed in a FV scheme or evolved by a DG scheme, may be out of the region  $G$ . As long as the BP property of the updated cell averages is guaranteed, then a simple scaling BP limiter can be employed to enforce the pointwise bounds of the piecewise polynomial solutions without affecting the high-order accuracy [36, 37]. Therefore, the key task is to ensure that the cell averages are always preserved within the region  $G$  during the updating process. Let us consider the evolution equation of cell averages for a high-order FV or DG scheme for the one-dimensional (1D) scalar conservation laws, which can be written in a unified form as

$$(1.5) \quad \bar{u}_j^{n+1} = \bar{u}_j^n - \lambda \left( \hat{f}(u_{j+\frac{1}{2}}^-, u_{j+\frac{1}{2}}^+) - \hat{f}(u_{j-\frac{1}{2}}^-, u_{j-\frac{1}{2}}^+) \right).$$

Here  $\bar{u}_j^n$  denotes the average on cell  $\Omega_j := [x_{j-\frac{1}{2}}, x_{j+\frac{1}{2}}]$  at time level  $n$ , and the limiting values at the cell interfaces are computed by

$$u_{j-\frac{1}{2}}^+ = p_j(x_{j-\frac{1}{2}}), \quad u_{j+\frac{1}{2}}^- = p_j(x_{j+\frac{1}{2}}) \quad \forall j,$$

where the polynomial  $p_j(x)$  of degree  $k$  is either evolved in a DG scheme or reconstructed in a FV scheme on  $\Omega_j$  with its cell average on  $\Omega_j$  equaling  $\bar{u}_j^n$ . Assume the numerical flux  $\hat{f}(\cdot, \cdot)$  is monotone, so that the corresponding first-order scheme (1.3) is BP under the CFL condition (1.4). It can be verified that the high-order scheme (1.5) is increasing only with  $\bar{u}_j^n$  and the exterior limiting values  $\{u_{j+\frac{1}{2}}^+, u_{j-\frac{1}{2}}^-\}$ , but decreasing with the interior limiting values  $\{u_{j+\frac{1}{2}}^-, u_{j-\frac{1}{2}}^+\}$ . Therefore, the monotonically increasing property is invalid to achieve the BP property for the high-order scheme (1.5). To address this issue, Zhang and Shu [36] proposed a novel strategy by using the cell average  $\bar{u}_j^n$  to control the effect of the interior limiting values  $\{u_{j+\frac{1}{2}}^-, u_{j-\frac{1}{2}}^+\}$ . They decomposed the cell average  $\bar{u}_j^n$  into a convex combination of some point values via the  $L$ -point Gauss–Lobatto quadrature with  $L = \lceil \frac{k+3}{2} \rceil$ , which is exact for polynomials of degree up to  $k$ . This implies

$$(1.6) \quad \bar{u}_j^n = \frac{1}{\Delta x} \int_{\Omega_j} p_j(x) dx = \sum_{\ell=1}^L \omega_\ell^{\text{GL}} p_j(x_{j,\ell}^{\text{GL}}) = \sum_{\ell=2}^{L-1} \omega_\ell^{\text{GL}} p_j(x_{j,\ell}^{\text{GL}}) + \omega_1^{\text{GL}} u_{j-\frac{1}{2}}^+ + \omega_L^{\text{GL}} u_{j+\frac{1}{2}}^-,$$

where  $\{\omega_\ell^{\text{GL}}\}$  are the Gauss–Lobatto quadrature weights (which are all positive), and  $\{x_{j,\ell}^{\text{GL}}\}$  are the quadrature nodes with  $x_{j,1}^{\text{GL}} = x_{j-\frac{1}{2}}$  and  $x_{j,L}^{\text{GL}} = x_{j+\frac{1}{2}}$ . Based on the cell average decomposition (1.6), Zhang and Shu rewrote the scheme (1.5) equivalently as

$$\bar{u}_j^{n+1} = \omega_1^{\text{GL}} H_{\frac{\lambda}{\omega_1^{\text{GL}}}} \left( u_{j-\frac{1}{2}}^-, u_{j-\frac{1}{2}}^+, u_{j+\frac{1}{2}}^- \right) + \omega_L^{\text{GL}} H_{\frac{\lambda}{\omega_L^{\text{GL}}}} \left( u_{j-\frac{1}{2}}^+, u_{j+\frac{1}{2}}^-, u_{j+\frac{1}{2}}^+ \right) + \sum_{\ell=2}^{L-1} \omega_\ell^{\text{GL}} p_j(x_{j,\ell}^{\text{GL}}),$$

which is a convex combination form of the formally first-order scheme. If we use a simple accuracy-maintaining BP limiter [36] to enforce

$$(1.7) \quad p_j(x_{j,\ell}^{\text{GL}}) \in G \quad \forall j, \ell,$$

then by the convexity of  $G$ , the high-order scheme (1.5) preserves  $\bar{u}_j^{n+1} \in G$  under the CFL condition

$$(1.8) \quad a\lambda \leq c_0 \min\{\omega_1^{\text{GL}}, \omega_L^{\text{GL}}\}.$$

For the  $L$ -point Gauss–Lobatto quadrature,  $\omega_1^{\text{GL}} = \omega_L^{\text{GL}} = \frac{1}{L(L-1)}$ .

As we have seen, the cell average decomposition (CAD) in (1.6) plays a critical role in constructing high-order BP schemes in Zhang–Shu framework. The classic decomposition (1.6) originally proposed by Zhang and Shu has been widely used over the past decade. Clearly, the *feasible* decomposition strategies, as defined below, are not unique. The classic CAD (1.6) is obviously feasible.

**Definition 1.1** (1D Feasible CAD). Let  $\mathbb{P}^k$  denote the space of 1D polynomials of degree up to  $k$ . Let  $\langle p \rangle_{\Omega_j}$  denote the average of a polynomial  $p$  over a closed interval  $\Omega_j = [x_{j-\frac{1}{2}}, x_{j+\frac{1}{2}}]$ . A 1D cell average decomposition

$$(1.9) \quad \langle p \rangle_{\Omega_j} := \frac{1}{\Delta x} \int_{\Omega_j} p(x) dx = \omega^- p(x_{j-\frac{1}{2}}) + \omega^+ p(x_{j+\frac{1}{2}}) + \sum_{s=1}^S \omega_s p(x_j^{(s)})$$

is said to be *feasible* for the space  $\mathbb{P}^k$ , if it simultaneously satisfies the following three conditions:

- (i) the identity (1.9) exactly holds for all  $p \in \mathbb{P}^k$ ;
- (ii) the weights  $\{\omega^\pm, \omega_s\}$  are all positive (their summation equals one);
- (iii) the internal node set  $\mathbb{S}_j := \{x_j^{(s)}\}_{s=1}^S \subset \Omega_j$ .

Note that different decomposition strategies would give different values of  $\min\{\omega^-, \omega^+\}$  and lead to different BP CFL condition

$$(1.10) \quad a\lambda \leq c_0 \min\{\omega^-, \omega^+\},$$

which affects the computational costs of the overall scheme. In view of the efficiency, it is natural to ask a fundamental and important question:

What is the optimal CAD (OCAD) such that the maximum BP CFL number  $c_0 \min\{\omega^-, \omega^+\}$  is largest?

**Problem 1.2** (1D OCAD Problem). *Given  $k \in \mathbb{N}_+$ , find the optimal decomposition in the form of (1.9) that is feasible and maximizes*

$$\mathcal{G}_1(\omega^-, \omega^+) := \min\{\omega^-, \omega^+\}$$

among all feasible CADs, or equivalently, find the 1D positive quadrature rule<sup>1</sup> on  $\Omega_j$ , with the degree of algebraic accuracy being at least  $k$  and the quadrature nodes including the two endpoints of  $\Omega_j$ , that provides the maximum  $\mathcal{G}_1(\omega^-, \omega^+)$ .

In the trivial case of  $k = 1$ , the classic decomposition (1.6) based on the Gauss–Lobatto quadrature is evidently optimal, because  $\omega_1^{\text{GL}} = \omega_L^{\text{GL}} = \frac{1}{2}$ . Zhang and Shu mentioned in [36, Remark 2.7] that they had checked that the decomposition (1.6) is optimal in the special cases of  $2 \leq k \leq 3$ .

*It remains unclear whether the CAD (1.6) is also optimal for general  $k \geq 4$ .*

Compared to the 1D OCAD problem, the multi-dimensional OCAD problems [4] are much more complicated and challenging. In this paper, we focus on two classes of two-dimensional (2D) polynomial spaces: the polynomial space of total degree up to  $k$  (denoted by  $\mathbb{P}^k$ ) and the tensor-product polynomial space of degree up to  $k$  (denoted by  $\mathbb{Q}^k$ ). On 2D rectangular meshes, the feasible CAD for high-order BP schemes can be defined as follows.

**Definition 1.3** (2D Feasible CAD). Let the 2D polynomial space  $\mathbb{V}^k$  be either  $\mathbb{P}^k$  or  $\mathbb{Q}^k$ . Let

$$\langle p \rangle_{\Omega_{ij}} := \frac{1}{\Delta x \Delta y} \int_{x_{i-\frac{1}{2}}}^{x_{i+\frac{1}{2}}} \int_{y_{j-\frac{1}{2}}}^{y_{j+\frac{1}{2}}} p(x, y) dy dx$$

denote the average of a 2D polynomial  $p$  over a rectangular cell  $\Omega_{ij} = [x_{i-\frac{1}{2}}, x_{i+\frac{1}{2}}] \times [y_{j-\frac{1}{2}}, y_{j+\frac{1}{2}}]$ . A 2D CAD

$$(1.11) \quad \begin{aligned} \langle p \rangle_{\Omega_{ij}} &= \frac{1}{\Delta y} \int_{y_{j-\frac{1}{2}}}^{y_{j+\frac{1}{2}}} \left( \omega_1^- p(x_{i-\frac{1}{2}}, y) + \omega_1^+ p(x_{i+\frac{1}{2}}, y) \right) dy \\ &+ \frac{1}{\Delta x} \int_{x_{i-\frac{1}{2}}}^{x_{i+\frac{1}{2}}} \left( \omega_2^- p(x, y_{j-\frac{1}{2}}) + \omega_2^+ p(x, y_{j+\frac{1}{2}}) \right) dx + \sum_{s=1}^S \omega_s p(x_{ij}^{(s)}, y_{ij}^{(s)}) \end{aligned}$$

is said to be *feasible* for the space  $\mathbb{V}^k$ , if it simultaneously satisfies the following three conditions:

- (i) the identity (1.11) exactly holds for all  $p \in \mathbb{V}^k$ ;
- (ii) the weights  $\{\omega_1^\pm, \omega_2^\pm, \omega_s\}$  are all positive (their summation equals one);
- (iii) the point set  $\mathbb{S}_{ij} := \{(x_{ij}^{(s)}, y_{ij}^{(s)})\}_{s=1}^S \subset \Omega_{ij}$ .

For convenience, we refer to  $\{\omega_1^\pm, \omega_2^\pm\}$  as the **boundary weights** and  $\omega_s$  as the **internal weights**, and refer to the node set  $\mathbb{S}_{ij}$  as the set of **internal nodes**.

In 2D high-order FV or DG methods, the integration of numerical fluxes on the cell interface should be discretized by a suitable 1D Gauss quadrature rule, which is exact for polynomials up to degree  $k$ . Applying this Gauss quadrature to the line integrals in (1.11), we can equivalently rewrite the feasible CAD (1.11) as

$$(1.12) \quad \begin{aligned} \langle p \rangle_{\Omega_{ij}} &= \sum_{q=1}^Q \omega_q^{\text{G}} \left( \omega_1^- p(x_{i-\frac{1}{2}}, y_{j,q}^{\text{G}}) + \omega_1^+ p(x_{i+\frac{1}{2}}, y_{j,q}^{\text{G}}) \right) \\ &+ \sum_{q=1}^Q \omega_q^{\text{G}} \left( \omega_2^- p(x_{i,q}^{\text{G}}, y_{j-\frac{1}{2}}) + \omega_2^+ p(x_{i,q}^{\text{G}}, y_{j+\frac{1}{2}}) \right) + \sum_{s=1}^S \omega_s p(x_{ij}^{(s)}, y_{ij}^{(s)}), \end{aligned}$$

where  $\{x_{i,q}^{\text{G}}\}$  and  $\{y_{j,q}^{\text{G}}\}$  are the Gauss quadrature nodes in the intervals  $[x_{i-\frac{1}{2}}, x_{i+\frac{1}{2}}]$  and  $[y_{j-\frac{1}{2}}, y_{j+\frac{1}{2}}]$ , respectively, and  $\{\omega_q^{\text{G}}\}$  are the Gauss weights. As long as the feasible decomposition (1.11) or

<sup>1</sup>A quadrature rule is said to be positive, if its weights are all positive.

(1.12) is available, one can construct high-order BP schemes on 2D rectangular meshes under the following CFL condition (see [4])

$$(1.13) \quad \Delta t \leq c_0 \min \left\{ \frac{\omega_1^- \Delta x}{a_1}, \frac{\omega_1^+ \Delta x}{a_1}, \frac{\omega_2^- \Delta y}{a_2}, \frac{\omega_2^+ \Delta y}{a_2} \right\} =: c_0 \mathcal{G}_2(\omega_1^-, \omega_1^+, \omega_2^-, \omega_2^+),$$

where  $a_1$  and  $a_2$  are the maximum characteristic speeds in the  $x$ - and  $y$ -directions, respectively. It is natural to seek the optimal decomposition such that the CFL condition (1.13) is mildest.

**Problem 1.4** (2D OCAD Problem). *Given  $k \in \mathbb{N}_+$ , the space  $\mathbb{V}^k$  and  $\{a_1 > 0, a_2 > 0, \Delta x > 0, \Delta y > 0\}$ , find the optimal feasible decomposition (1.11) that maximizes  $\mathcal{G}_2(\omega_1^-, \omega_1^+, \omega_2^-, \omega_2^+)$ . This is equivalent to find the 2D positive quadrature rule on  $\Omega_{ij}$ , which is exact for all  $p \in \mathbb{V}^k$  with the quadrature nodes including all the Gauss nodes on  $\partial\Omega_{ij}$  and maximizes  $\mathcal{G}_2(\omega_1^-, \omega_1^+, \omega_2^-, \omega_2^+)$ .*

The 2D OCAD problem is much more challenging than the 1D case. Based on the tensor product of the  $Q$ -point Gauss quadrature and the  $L$ -point Gauss–Lobatto quadrature, Zhang and Shu proposed the following feasible CAD in [36, 37]:

$$(1.14) \quad \begin{aligned} \langle p \rangle_{\Omega_{ij}} &= \frac{a_1/\Delta x}{a_1/\Delta x + a_2/\Delta y} \omega_1^{\text{GL}} \sum_{q=1}^Q \omega_q^{\text{G}} \left( p(x_{i-\frac{1}{2}}, y_{j,q}^{\text{G}}) + p(x_{i+\frac{1}{2}}, y_{j,q}^{\text{G}}) \right) \\ &+ \frac{a_2/\Delta y}{a_1/\Delta x + a_2/\Delta y} \omega_1^{\text{GL}} \sum_{q=1}^Q \omega_q^{\text{G}} \left( p(x_{i,q}^{\text{G}}, y_{j-\frac{1}{2}}) + p(x_{i,q}^{\text{G}}, y_{j+\frac{1}{2}}) \right) \\ &+ \sum_{\ell=2}^{L-1} \sum_{q=1}^Q \omega_\ell^{\text{GL}} \omega_q^{\text{G}} \left( \frac{a_1/\Delta x}{a_1/\Delta x + a_2/\Delta y} p(x_{i,\ell}^{\text{GL}}, y_{j,q}^{\text{G}}) + \frac{a_2/\Delta y}{a_1/\Delta x + a_2/\Delta y} p(x_{i,q}^{\text{G}}, y_{j,\ell}^{\text{GL}}) \right), \end{aligned}$$

which corresponds to  $\omega_1^\pm = \frac{a_1 \Delta y \omega_1^{\text{GL}}}{a_1 \Delta y + a_2 \Delta x}$  and  $\omega_2^\pm = \frac{a_2 \Delta x \omega_1^{\text{GL}}}{a_1 \Delta y + a_2 \Delta x}$ . As a special case of (1.13), the CAD (1.14) leads to the following BP CFL condition [36, 37]:

$$(1.15) \quad \Delta t \leq \frac{c_0 \omega_1^{\text{GL}}}{a_1/\Delta x + a_2/\Delta y},$$

namely, the corresponding maximum CFL number is  $c_0 \omega_1^{\text{GL}}$ . It is natural to ask: Is the classic CAD (1.14) optimal in the 2D case? This question had been open until our recent work in [4]. We found that the classic Zhang–Shu CAD (1.14) is generally not optimal for  $\mathbb{P}^k$  spaces in multiple dimensions, and we successfully constructed the OCAD for the multidimensional  $\mathbb{P}^2$  and  $\mathbb{P}^3$  spaces; see [4] for details.

*It is still unclear what CAD is optimal for general polynomial spaces, including 2D  $\mathbb{P}^k$  spaces with  $k \geq 4$  and 2D  $\mathbb{Q}^k$  spaces.*

This paper makes the first attempt to systematically study the OCAD problems for general 1D and 2D polynomial spaces. Our efforts and findings are summarized as follows.

- We rigorously prove that, in the 1D case, the classic CAD (1.6) is optimal for general  $\mathbb{P}^k$  spaces of an arbitrary  $k \in \mathbb{N}_+$ . The key point of the proof is to first relate the OCAD problem to a new optimization problem (Problem 2.2) with infinitely many linear constraints described by non-negative polynomials, and then to construct a non-negative polynomial in  $\mathbb{P}^k$  vanishing at all the internal nodes of (1.6).
- We establish the general theory for studying the 2D OCAD problem on Cartesian meshes. This is highly nontrivial and involves novel techniques from several branches of mathematics. We prove several key properties of the OCAD problem, including the existence of OCAD by using Carathéodory’s theorem from convex geometry. Through transformation onto a reference cell, we simplify the 2D OCAD problem to a symmetric OCAD problem (Problem 3.13) based on the invariant theory of symmetric group. Most notably, we discover that the symmetric OCAD problem is closely related to polynomial optimization of a positive linear functional on the positive polynomial cone, thereby establishing four

useful criteria for examining the optimality of a feasible CAD. Some geometric insights are also provided to interpret our critical findings.

- Based on the proposed theory, we rigorously prove that, in the 2D case, the classic CAD (1.14) is optimal for general  $\mathbb{Q}^k$  spaces of an arbitrary  $k \in \mathbb{N}_+$ .
- It is observed that the classic CAD (1.14) is *not* optimal for 2D  $\mathbb{P}^k$  spaces. As the polynomial degree  $k$  increases, seeking the genuine OCAD becomes more and more difficult. We develop a systematical approach to find the genuinely optimal CADs for the 2D  $\mathbb{P}^k$  spaces, which is a highly nontrivial task. We derive the analytical formulas of OCADs for  $\mathbb{P}^k$  spaces with  $k \leq 7$ . A general algorithm is also proposed to construct the OCADs for  $\mathbb{P}^k$  spaces with  $k \geq 8$ . The discovery of OCAD is highly nontrivial yet meaningful, as it leads to an improvement of high-order BP schemes for a large class of hyperbolic or convection-dominated equations, at the little cost of only a slight and local modification to the implementation code; see Table 1 for a comparison.
- Based on geometric insights, we also propose a more practical quasi-optimal CAD, which can be easily constructed via a convex combination of the OCADs in three special cases. It is demonstrated that the quasi-optimal CAD can achieve a near-optimal BP CFL condition, which is very close to the optimal one.
- We apply the proposed OCAD and quasi-optimal CAD to designing more efficient BP high-order schemes with milder CFL condition for hyperbolic conservation laws. The notable advantages in efficiency are also demonstrated by several examples covering four hyperbolic partial differential equations, including the convection equation, the inviscid Burgers' equation, the compressible Euler equations, and the relativistic hydrodynamic equations.

The paper is organized as illustrated in Figure 1. We analyze the 1D OCAD problem in Section 2 and prove that classic CAD (1.6) is optimal in the 1D case. Section 3 proposes the general theory for the 2D OCAD problem. The OCADs for 2D  $\mathbb{Q}^k$  spaces and 2D  $\mathbb{P}^k$  spaces are studied in Section 4 and Section 5, respectively. Section 6 discusses the 2D quasi-optimal CAD for  $\mathbb{P}^k$  spaces. We apply the OCAD and quasi-optimal CAD to design efficient BP high-order schemes in Section 7. Several numerical tests are presented in Section 8, before concluding the paper in Section 9.

TABLE 1. Comparison of optimal BP CFL number  $\bar{\omega}_* c_0$ , classic BP CFL number  $\omega_1^{\text{GL}} c_0$ , and standard linearly stable CFL number  $\frac{1}{2k+1}$ , in the case of  $c_0 = 1$  and  $a_1 \Delta y = a_2 \Delta x$  for  $\mathbb{P}^k$ -based DG methods with  $1 \leq k \leq 9$ .

$k$	standard ( $\frac{1}{2k+1}$ )	classic ( $\omega_1^{\text{GL}}$ )	optimal ( $\bar{\omega}_*$ )
1	$\frac{1}{3} = 0.3333$	$\frac{1}{2} = 0.5$	$\frac{1}{2} = 0.5$
2	$\frac{1}{5} = 0.2$	$\frac{1}{6} = 0.1667$	$\frac{1}{4} = 0.25$
3	$\frac{1}{7} = 0.1429$	$\frac{1}{6} = 0.1667$	$\frac{1}{4} = 0.25$
4	$\frac{1}{9} = 0.1111$	$\frac{1}{12} = 0.08333$	$2 - \frac{\sqrt{14}}{2} = 0.1292$
5	$\frac{1}{11} = 0.09091$	$\frac{1}{12} = 0.08333$	$2 - \frac{\sqrt{14}}{2} = 0.1292$
6	$\frac{1}{13} = 0.07692$	$\frac{1}{20} = 0.05$	$1 - \frac{\sqrt{30}}{6} = 0.08713$
7	$\frac{1}{15} = 0.06667$	$\frac{1}{20} = 0.05$	$1 - \frac{\sqrt{30}}{6} = 0.08713$
8	$\frac{1}{17} = 0.05882$	$\frac{1}{30} = 0.03333$	0.05767
9	$\frac{1}{19} = 0.05263$	$\frac{1}{30} = 0.03333$	0.05767

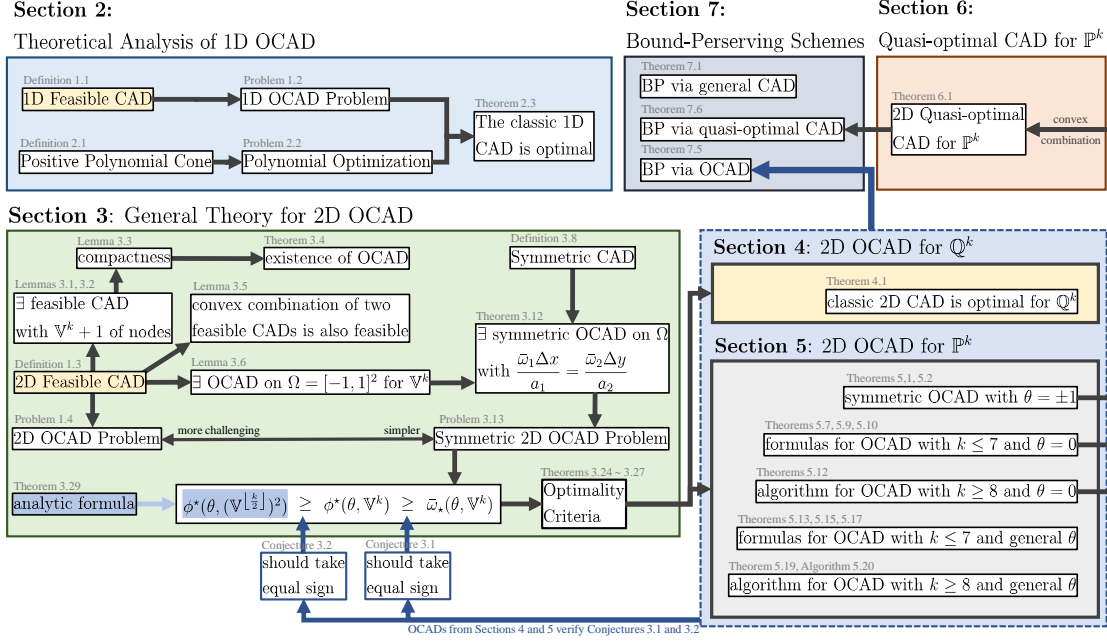


FIGURE 1. Structure of the present paper

## 2. THEORETICAL ANALYSIS OF 1D OCAD

In this section, we rigorously prove that the classic 1D CAD (1.6) is optimal for general polynomial spaces  $\mathbb{P}^k$  of an arbitrary degree  $k \in \mathbb{N}_+$ .

**Definition 2.1** (Positive Polynomial Cone). Let  $\mathbb{P}_+^k(\Omega_j)$  denote the set of 1D polynomials of degree at most  $k$  and nonnegative on  $\Omega_j$ , namely,

$$(2.1) \quad \mathbb{P}_+^k(\Omega_j) := \{p \in \mathbb{P}^k : p(x) \geq 0 \forall x \in \Omega_j\}.$$

Since the set  $\mathbb{P}_+^k(\Omega_j)$  is a closed convex cone satisfying

$$t_1 p_1 + t_2 p_2 \in \mathbb{P}_+^k(\Omega_j), \quad \forall p_1, p_2 \in \mathbb{P}_+^k(\Omega_j), \quad \forall t_1, t_2 \geq 0,$$

we call  $\mathbb{P}_+^k(\Omega_j)$  a *positive polynomial cone* on  $\Omega_j$ .

We observe that the 1D OCAD problem is closely related to the following optimization problem, as shown in Theorem 2.3.

**Problem 2.2.** For a given  $k \in \mathbb{N}_+$ , maximize  $\mathcal{G}_1(\omega^-, \omega^+)$  subject to the constraint

$$\langle p \rangle_{\Omega_j} - \omega^- p(x_{j-\frac{1}{2}}) - \omega^+ p(x_{j+\frac{1}{2}}) \geq 0, \quad \forall p \in \mathbb{P}_+^k(\Omega_j).$$

**Theorem 2.3.** Problem 2.2 has a unique optimal solution. The boundary weights in the 1D OCAD, denoted by  $(\omega_\star^-, \omega_\star^+)$ , are unique and given by

$$\omega_\star^- = \omega_\star^+ = \omega_1^{\text{GL}} = \frac{1}{L(L-1)}, \quad L = \left\lceil \frac{k+3}{2} \right\rceil,$$

which is also the optimal solution to Problem 2.2. This means the classic CAD (1.6) based on the  $L$ -point Gauss-Lobatto quadrature is the OCAD in the 1D case.

*Proof.* Recall the Gauss-Lobatto quadrature weights satisfy  $\omega_1^{\text{GL}} = \omega_L^{\text{GL}} = \frac{1}{L(L-1)}$ . Since the CAD (1.6) is feasible, we have

$$(2.2) \quad \omega_1^{\text{GL}} = \omega_L^{\text{GL}} = \mathcal{G}_1(\omega_1^{\text{GL}}, \omega_L^{\text{GL}}) \leq \mathcal{G}_1(\omega_\star^-, \omega_\star^+).$$

Let  $(\omega_\square^-, \omega_\square^+)$  be an optimal solution to Problem 2.2 and satisfy

$$(2.3) \quad \langle p \rangle_{\Omega_j} - \omega_\square^- p(x_{j-\frac{1}{2}}) - \omega_\square^+ p(x_{j+\frac{1}{2}}) \geq 0 \quad \forall p \in \mathbb{P}_+^k(\Omega_j).$$

Using (1.9) gives  $\langle p \rangle_{\Omega_j} - \omega_{\star}^{-} p(x_{j-\frac{1}{2}}) - \omega_{\star}^{+} p(x_{j+\frac{1}{2}}) = \sum_{s=1}^S \omega_s p(x_j^{(s)}) \geq 0$  for all  $p \in \mathbb{P}_{+}^k(\Omega_j)$ , which implies that  $(\omega_{\star}^{-}, \omega_{\star}^{+})$  is a feasible solution to Problem 2.2. This yields

$$(2.4) \quad \mathcal{G}_1(\omega_{\star}^{-}, \omega_{\star}^{+}) \leq \mathcal{G}_1(\omega_{\square}^{-}, \omega_{\square}^{+}).$$

Define

$$(2.5) \quad p^*(x) := \prod_{\ell=2}^{L-1} (x - x_{j,\ell}^{\text{GL}})^2,$$

where  $\{x_{j,\ell}^{\text{GL}}\}$  are the Gauss–Lobatto nodes. Clearly,  $p^*(x) \geq 0$  for all  $x$ , and the degree of  $p^*$  is  $2(L-2) = 2(\lceil \frac{k+3}{2} \rceil - 2) \leq k$ . Hence  $p^* \in \mathbb{P}_{+}^k$ . Noting that

$$p^*(x_{j,\ell}^{\text{GL}}) = 0, \quad 2 \leq \ell \leq L-1; \quad p^*(x_{j,1}^{\text{GL}}) > 0, \quad p^*(x_{j,L}^{\text{GL}}) > 0,$$

and using (2.3) for  $p = p^*$ , we obtain

$$(2.6) \quad \begin{aligned} 0 &\leq \langle p^* \rangle_{\Omega_j} - \omega_{\square}^{-} p^*(x_{j-\frac{1}{2}}) - \omega_{\square}^{+} p^*(x_{j+\frac{1}{2}}) \\ &= \sum_{\ell=1}^L \omega_{\ell}^{\text{GL}} p^*(x_{j,\ell}^{\text{GL}}) - \omega_{\square}^{-} p^*(x_{j-\frac{1}{2}}) - \omega_{\square}^{+} p^*(x_{j+\frac{1}{2}}) \\ &= (\omega_1^{\text{GL}} - \omega_{\square}^{-}) p^*(x_{j-\frac{1}{2}}) + (\omega_1^{\text{GL}} - \omega_{\square}^{+}) p^*(x_{j+\frac{1}{2}}) \\ &\leq (\omega_1^{\text{GL}} - \min\{\omega_{\square}^{-}, \omega_{\square}^{+}\}) (p^*(x_{j-\frac{1}{2}}) + p^*(x_{j+\frac{1}{2}})). \end{aligned}$$

Since  $p^*(x_{j-\frac{1}{2}}) + p^*(x_{j+\frac{1}{2}}) > 0$ , we therefore have

$$(2.7) \quad \omega_1^{\text{GL}} \geq \min\{\omega_{\square}^{-}, \omega_{\square}^{+}\} = \mathcal{G}_1(\omega_{\square}^{-}, \omega_{\square}^{+}).$$

Combining (2.2)–(2.4) with (2.7) gives  $\mathcal{G}_1(\omega_{\star}^{-}, \omega_{\star}^{+}) = \mathcal{G}_1(\omega_{\square}^{-}, \omega_{\square}^{+}) = \omega_1^{\text{GL}}$ . Without loss of generality, assume that  $\omega_{\square}^{-} \geq \omega_{\square}^{+}$ , then  $\mathcal{G}_1(\omega_{\square}^{-}, \omega_{\square}^{+}) = \omega_{\square}^{+} = \omega_1^{\text{GL}}$  and using (2.6) gives  $(\omega_1^{\text{GL}} - \omega_{\square}^{-}) p^*(x_{j-\frac{1}{2}}) \geq 0$ . This leads to  $\omega_1^{\text{GL}} \geq \omega_{\square}^{-} \geq \omega_{\square}^{+} = \omega_1^{\text{GL}}$ . Therefore,  $\omega_{\square}^{-} = \omega_{\square}^{+} = \omega_1^{\text{GL}}$ , which demonstrates the uniqueness of the optimal solution to Problem 2.2. Because  $\mathcal{G}_1(\omega_{\star}^{-}, \omega_{\star}^{+}) = \mathcal{G}_1(\omega_{\square}^{-}, \omega_{\square}^{+})$ , we have that  $(\omega_{\star}^{-}, \omega_{\star}^{+})$  is an optimal solution to Problem 2.2. By the uniqueness, we have  $\omega_{\star}^{-} = \omega_{\star}^{+} = \omega_{\square}^{-} = \omega_{\square}^{+} = \omega_1^{\text{GL}}$ . This completes the proof.  $\square$

As proved in Theorem 2.3, the classic 1D CAD (1.6) proposed in [36] is optimal for all  $k \in \mathbb{N}_{+}$ . This confirms the conjecture of Zhang and Shu in [36, Remark 2.7].

### 3. GENERAL THEORY FOR 2D OCAD

In this section, we establish the general theory for studying the 2D OCAD problem (Problem 1.4) on an arbitrary rectangular cell  $\Omega_{ij} := [x_{i-\frac{1}{2}}, x_{i+\frac{1}{2}}] \times [y_{j-\frac{1}{2}}, y_{j+\frac{1}{2}}]$  for 2D polynomial space  $\mathbb{V}^k$ , which can be  $\mathbb{P}^k$  or  $\mathbb{Q}^k$  or other suitable subspaces of  $\mathbb{Q}^k$ .

**3.1. Existence.** We first prove the existence of the 2D OCAD, i.e., Problem 1.4 always has at least one OCAD solution.

For convenience, we introduce the following notations

$$\langle p \rangle_{\Omega_{ij}}^{\pm x} := \frac{1}{\Delta y} \int_{y_{j-\frac{1}{2}}}^{y_{j+\frac{1}{2}}} p(x_{i \pm \frac{1}{2}}, y) dy \quad \text{and} \quad \langle p \rangle_{\Omega_{ij}}^{\pm y} := \frac{1}{\Delta x} \int_{x_{i-\frac{1}{2}}}^{x_{i+\frac{1}{2}}} p(x, y_{j \pm \frac{1}{2}}) dx.$$

Then a 2D feasible CAD (1.11) can be written as

$$(3.1) \quad \langle p \rangle_{\Omega_{ij}} = \omega_1^{-} \langle p \rangle_{\Omega_{ij}}^{-x} + \omega_1^{+} \langle p \rangle_{\Omega_{ij}}^{+x} + \omega_2^{-} \langle p \rangle_{\Omega_{ij}}^{-y} + \omega_2^{+} \langle p \rangle_{\Omega_{ij}}^{+y} + \sum_{s=1}^S \omega_s p(x_{ij}^{(s)}, y_{ij}^{(s)}).$$

For ease of the following discussions in this subsection, we may relax the condition (ii) in Definition 1.3 to a milder one—“the weights  $\{\omega_1^{\pm}, \omega_2^{\pm}, \omega_s\}$  are all *nonnegative*”. Note that such a relaxation does not affect the OCAD problem, because the zero boundary weights lead to  $\mathcal{G}_2 = 0$  and obviously do not correspond to an OCAD, while the zero weights in  $\{\omega_s\}$  can be safely removed in the CAD.



Notice that only the boundary weights  $(\omega_1^-, \omega_1^+, \omega_2^-, \omega_2^+)$  are involved in the objective function  $\mathcal{G}_2(\omega_1^-, \omega_1^+, \omega_2^-, \omega_2^+)$ . Let  $\mathbb{A}_\omega \subset \mathbb{R}^4$  denote the set of the boundary weights of all feasible CADs. Evidently, the set  $\mathbb{A}_\omega \subset [0, 1]^4$  is bounded. We would like to show that the set  $\mathbb{A}_\omega$  is both *compact* and *convex* in  $\mathbb{R}^4$ .

**Lemma 3.1.** *Given a feasible CAD (3.1) for  $\mathbb{V}^k$ , there always exists a “conciser” feasible CAD with the same boundary weights as (3.1) and with only  $(\dim \mathbb{V}^k + 1)$  or less internal nodes, namely, there exists a feasible CAD*

$$(3.2) \quad \langle p \rangle_{\Omega_{ij}} = \omega_1^- \langle p \rangle_{\Omega_{ij}}^{-x} + \omega_1^+ \langle p \rangle_{\Omega_{ij}}^{+x} + \omega_2^- \langle p \rangle_{\Omega_{ij}}^{-y} + \omega_2^+ \langle p \rangle_{\Omega_{ij}}^{+y} + \sum_{s \in \mathbb{S}} \tilde{\omega}_s p(x_{ij}^{(s)}, y_{ij}^{(s)})$$

with

$$(3.3) \quad \mathbb{S} \subseteq \{1, 2, \dots, S\} \quad \text{and} \quad \#\mathbb{S} \leq \dim \mathbb{V}^k + 1.$$

*Proof.* If  $S \leq \dim \mathbb{V}^k + 1$ , the claim (3.3) is obviously true with  $\mathbb{S} = \{1, 2, \dots, S\}$ . Let

$$\omega_0 := 1 - \omega_1^- - \omega_1^+ - \omega_2^- - \omega_2^+ = \sum_{s=1}^S \omega_s \in [0, 1].$$

If  $\omega_0 = 0$ , then we know  $\omega_s = 0$  for all  $s = 1, \dots, S$ . In this case, we can safely remove all the internal nodes in the CAD (3.1) without affecting its feasibility, resulting in a feasible CAD with  $\mathbb{S} = \emptyset$  and  $\#\mathbb{S} = 0$ , implying the claim (3.3) is true.

Now, we consider the case  $S > \dim \mathbb{V}^k + 1$  and  $\omega_0 > 0$ . Let  $D = \dim \mathbb{V}^k$  and  $\{b_1 \equiv 1, b_2, \dots, b_D\}$  be a basis for  $\mathbb{V}^k$ . Define the vector

$$\mathbf{m} := (m_1, m_2, \dots, m_d)^\top \in \mathbb{R}_+^D$$

with

$$m_i := \langle b_i \rangle_{\Omega_{ij}} - \omega_1^- \langle b_i \rangle_{\Omega_{ij}}^{-x} - \omega_1^+ \langle b_i \rangle_{\Omega_{ij}}^{+x} - \omega_2^- \langle b_i \rangle_{\Omega_{ij}}^{-y} - \omega_2^+ \langle b_i \rangle_{\Omega_{ij}}^{+y},$$

and define the following point set

$$\mathcal{B} := \left\{ \omega_0 \mathbf{b}(x_{ij}^{(1)}, y_{ij}^{(1)}), \dots, \omega_0 \mathbf{b}(x_{ij}^{(S)}, y_{ij}^{(S)}) \right\} \subseteq \mathbb{R}^D$$

with  $\mathbf{b} := (b_1, b_2, \dots, b_D)^\top$ . The feasibility condition (i) of CAD (3.1) implies

$$\mathbf{m} = \sum_{s=1}^S \omega_s \mathbf{b}(x_{ij}^{(s)}, y_{ij}^{(s)}) = \sum_{s=1}^S \frac{\omega_s}{\omega_0} \cdot \omega_0 \mathbf{b}(x_{ij}^{(s)}, y_{ij}^{(s)}).$$

Notice that  $\mathbf{m}$  lies in the *convex hull* of the set  $\mathcal{B}$ , because  $\sum_{s=1}^S \frac{\omega_s}{\omega_0} = 1$  and  $\frac{\omega_s}{\omega_0} > 0$ . According to *Carathéodory's theorem* [2], the vector  $\mathbf{m}$  can be written as the convex combination of at most  $(D + 1)$  points in  $\mathcal{B}$ , namely,

$$(3.4) \quad \mathbf{m} = \sum_{s \in \mathbb{S}} \hat{\omega}_s \omega_0 \mathbf{b}(x_{ij}^{(s)}, y_{ij}^{(s)}) = \sum_{s \in \mathbb{S}} \tilde{\omega}_s \mathbf{b}(x_{ij}^{(s)}, y_{ij}^{(s)})$$

with

$$\begin{aligned} \hat{\omega}_s > 0, \quad \tilde{\omega}_s = \hat{\omega}_s \omega_0 > 0 \quad \forall s \in \mathbb{S} \subseteq \{1, 2, \dots, S\}, \\ \sum_{s \in \mathbb{S}} \hat{\omega}_s = 1, \quad \sum_{s \in \mathbb{S}} \tilde{\omega}_s = \omega_0, \quad \#\mathbb{S} \leq D + 1. \end{aligned}$$

The equality (3.4) implies that the CAD (3.2) holds for all the basis functions  $\{b_i\}_{i=1}^D$  of  $\mathbb{V}^k$ , thus for any  $p \in \mathbb{V}^k$ . The feasibility condition (i) is verified. Notice that  $\tilde{\omega}_s > 0$  for all  $s \in \mathbb{S}$  and  $\omega_1^- + \omega_1^+ + \omega_2^- + \omega_2^+ + \sum_{s \in \mathbb{S}} \tilde{\omega}_s = 1$ , the feasibility condition (ii) is verified. Finally, the feasibility condition (iii) is true, because  $(x_{ij}^{(s)}, y_{ij}^{(s)}) \in \Omega_{ij} \forall s \in \mathbb{S}$ . To conclude, (3.2) is a 2D feasible CAD for the space  $\mathbb{V}^k$ . The proof is completed.  $\square$

As a direct consequence of Lemma 3.1, we have the following result.

**Lemma 3.2.** *For any  $(\omega_1^-, \omega_1^+, \omega_2^-, \omega_2^+) \in \mathbb{A}_\omega$ , there always exists a feasible CAD in the form (3.1) with  $(\omega_1^-, \omega_1^+, \omega_2^-, \omega_2^+)$  as its boundary weights and with  $S = \dim \mathbb{V}^k + 1$ .*

*Proof.* Due to Lemma 3.1, there exists a feasible CAD like (3.1) with boundary weights  $(\omega_1^-, \omega_1^+, \omega_2^-, \omega_2^+)$  and  $S \leq \dim \mathbb{V}^k + 1$ . Since we have relaxed the condition (ii) in Definition 1.3 to allow  $\{\omega_s\}$  being zero, we can add some nodes with zero weight such that  $S = \dim \mathbb{V}^k + 1$ .  $\square$

**Lemma 3.3.** *The set  $\mathbb{A}_\omega$  is compact.*

*Proof.* Since  $\mathbb{A}_\omega \subset [0, 1]^4$  is bounded, it remains to prove that  $\mathbb{A}_\omega$  is closed, namely, the limit of every convergent sequence contained in  $\mathbb{A}_\omega$  is also an element of  $\mathbb{A}_\omega$ . Assume that  $\{\omega_n := (\omega_{1,n}^-, \omega_{1,n}^+, \omega_{2,n}^-, \omega_{2,n}^+)\}_{n \geq 1}$  is an arbitrary convergent sequence in  $\mathbb{A}_\omega$ , and denote

$$\lim_{n \rightarrow \infty} \omega_n = \omega =: (\omega_1^-, \omega_1^+, \omega_2^-, \omega_2^+).$$

It suffices to show the limit  $\omega \in \mathbb{A}_\omega$ . For every  $\omega_n \in \mathbb{A}_\omega$ , Lemma 3.2 tells us that there exists a feasible CAD with  $\omega_n$  as its boundary weights in the following form

$$(3.5) \quad \langle p \rangle_{\Omega_{ij}} = \omega_{1,n}^- \langle p \rangle_{\Omega_{ij}}^{-x} + \omega_{1,n}^+ \langle p \rangle_{\Omega_{ij}}^{+x} + \omega_{2,n}^- \langle p \rangle_{\Omega_{ij}}^{-y} + \omega_{2,n}^+ \langle p \rangle_{\Omega_{ij}}^{+y} + \sum_{s=1}^S \omega_{s,n} p \left( x_{ij}^{(s,n)}, y_{ij}^{(s,n)} \right)$$

with  $S = \dim \mathbb{V}^k + 1$ . Note that for all  $n \geq 1$ ,  $\omega_{s,n} \in [0, 1]$  and  $(x_{ij}^{(s,n)}, y_{ij}^{(s,n)}) \in \Omega_{ij}$ . According to the *Bolzano–Weierstrass theorem*, the bounded sequence

$$\left\{ (\omega_{1,n}, \dots, \omega_{S,n}, x_{ij}^{(1,n)}, \dots, x_{ij}^{(S,n)}, y_{ij}^{(1,n)}, \dots, y_{ij}^{(S,n)}) \right\}_{n \geq 1} \subseteq [0, 1]^S \times [x_{i-\frac{1}{2}}, x_{i+\frac{1}{2}}]^S \times [y_{j-\frac{1}{2}}, y_{j+\frac{1}{2}}]^S$$

has a convergent subsequence, denoted by

$$(3.6) \quad \lim_{\ell \rightarrow \infty} \omega_{s,n_\ell} = \omega_s \in [0, 1], \quad \lim_{\ell \rightarrow \infty} \left( x_{ij}^{(s,n_\ell)}, y_{ij}^{(s,n_\ell)} \right) = \left( x_{ij}^{(s)}, y_{ij}^{(s)} \right) \in \Omega_{ij}, \quad s = 1, 2, \dots, S.$$

Taking  $n = n_\ell$  in (3.5) and letting  $\ell \rightarrow +\infty$ , we obtain for any  $p \in \mathbb{V}^k$  that

$$(3.7) \quad \langle p \rangle_{\Omega_{ij}} = \omega_1^- \langle p \rangle_{\Omega_{ij}}^{-x} + \omega_1^+ \langle p \rangle_{\Omega_{ij}}^{+x} + \omega_2^- \langle p \rangle_{\Omega_{ij}}^{-y} + \omega_2^+ \langle p \rangle_{\Omega_{ij}}^{+y} + \sum_{s=1}^S \omega_s p \left( x_{ij}^{(s)}, y_{ij}^{(s)} \right),$$

which is a feasible CAD, because  $\omega_1^\pm \geq 0$ ,  $\omega_2^\pm \geq 0$ ,  $\omega_s \geq 0$ , and  $(x_{ij}^{(s)}, y_{ij}^{(s)}) \in \Omega_{ij}$ . Therefore,  $\omega = (\omega_1^-, \omega_1^+, \omega_2^-, \omega_2^+) \in \mathbb{A}_\omega$ . In conclusion, the set  $\mathbb{A}_\omega$  is closed and thus compact.  $\square$

**Theorem 3.4.** *The 2D OCAD always exists, i.e., Problem 1.4 has at least one OCAD solution. Moreover, there exists an OCAD whose boundary weights  $(\omega_{1,\star}^-, \omega_{1,\star}^+, \omega_{2,\star}^-, \omega_{2,\star}^+)$  maximize  $\mathcal{G}_2$  and also satisfy*

$$(3.8) \quad \frac{\omega_{1,\star}^- \Delta x}{a_1} = \frac{\omega_{1,\star}^+ \Delta x}{a_1} = \frac{\omega_{2,\star}^- \Delta y}{a_2} = \frac{\omega_{2,\star}^+ \Delta y}{a_2} = \max \mathcal{G}_2.$$

*Proof.* According to Lemma 3.3, the feasible region  $\mathbb{A}_\omega$  is compact. Since the objective function  $\mathcal{G}_2$  is continuous, by the *Weierstrass extreme value theorem*, Problem 1.4 has at least one OCAD solution.

Consider an OCAD in the form (3.1) which attains  $\max \mathcal{G}_2$ . Define

$$\omega_{1,\star}^- = \omega_{1,\star}^+ = a_1 \max \mathcal{G}_2 / \Delta x, \quad \omega_{2,\star}^- = \omega_{2,\star}^+ = a_2 \max \mathcal{G}_2 / \Delta y,$$

which satisfy (3.8). From the definition of  $\mathcal{G}_2$ , one can observe that

$$\omega_1^\pm - \omega_{1,\star}^\pm \geq 0, \quad \omega_2^\pm - \omega_{2,\star}^\pm \geq 0.$$

It follows that

$$\begin{aligned} \langle p \rangle_{\Omega_{ij}} &= \omega_{1,\star}^- \langle p \rangle_{\Omega_{ij}}^{-x} + \omega_{1,\star}^+ \langle p \rangle_{\Omega_{ij}}^{+x} + \omega_{2,\star}^- \langle p \rangle_{\Omega_{ij}}^{-y} + \omega_{2,\star}^+ \langle p \rangle_{\Omega_{ij}}^{+y} + \sum_{s=1}^S \omega_s p(x_{ij}^{(s)}, y_{ij}^{(s)}) \\ &+ \sum_{q=1}^Q \omega_q^G \left( (\omega_1^- - \omega_{1,\star}^-) p(x_{i-\frac{1}{2}}, y_{j,q}^G) + (\omega_1^+ - \omega_{1,\star}^+) p(x_{i+\frac{1}{2}}, y_{j,q}^G) \right) \\ &+ \sum_{q=1}^Q \omega_q^G \left( (\omega_2^- - \omega_{2,\star}^-) p(x_{i,q}^G, y_{j-\frac{1}{2}}) + (\omega_2^+ - \omega_{2,\star}^+) p(x_{i,q}^G, y_{j+\frac{1}{2}}) \right), \end{aligned}$$

which is also an OCAD and satisfies (3.8). The proof is completed.  $\square$

### 3.2. Convexity.

**Lemma 3.5.** *A convex combination of any two feasible CADs is also a feasible CAD. Furthermore,  $\mathbb{A}_\omega$  is a convex set.*

*Proof.* Consider two arbitrary 2D feasible CADs

$$(3.9) \quad \langle p \rangle_{\Omega_{ij}} = \omega_1^- \langle p \rangle_{\Omega_{ij}}^{-x} + \omega_1^+ \langle p \rangle_{\Omega_{ij}}^{+x} + \omega_2^- \langle p \rangle_{\Omega_{ij}}^{-y} + \omega_2^+ \langle p \rangle_{\Omega_{ij}}^{+y} + \sum_{s=1}^S \omega_s p(x_{ij}^{(s)}, y_{ij}^{(s)}),$$

$$(3.10) \quad \langle p \rangle_{\Omega_{ij}} = \widehat{\omega}_1^- \langle p \rangle_{\Omega_{ij}}^{-x} + \widehat{\omega}_1^+ \langle p \rangle_{\Omega_{ij}}^{+x} + \widehat{\omega}_2^- \langle p \rangle_{\Omega_{ij}}^{-y} + \widehat{\omega}_2^+ \langle p \rangle_{\Omega_{ij}}^{+y} + \sum_{s=1}^{\widehat{S}} \widehat{\omega}_s p(\widehat{x}_{ij}^{(s)}, \widehat{y}_{ij}^{(s)}).$$

Their convex combination

$$(3.11) \quad \begin{aligned} \langle p \rangle_{\Omega_{ij}} &= [\lambda \omega_1^- + (1-\lambda) \widehat{\omega}_1^-] \langle p \rangle_{\Omega_{ij}}^{-x} + [\lambda \omega_1^+ + (1-\lambda) \widehat{\omega}_1^+] \langle p \rangle_{\Omega_{ij}}^{+x} \\ &\quad + [\lambda \omega_2^- + (1-\lambda) \widehat{\omega}_2^-] \langle p \rangle_{\Omega_{ij}}^{-y} + [\lambda \omega_2^+ + (1-\lambda) \widehat{\omega}_2^+] \langle p \rangle_{\Omega_{ij}}^{+y} \\ &\quad + \lambda \sum_{s=1}^S \omega_s p(x_{ij}^{(s)}, y_{ij}^{(s)}) + (1-\lambda) \sum_{s=1}^{\widehat{S}} \widehat{\omega}_s p(\widehat{x}_{ij}^{(s)}, \widehat{y}_{ij}^{(s)}) \end{aligned}$$

is also a 2D feasible CAD for any  $\lambda \in [0, 1]$ . Thus, the set  $\mathbb{A}_\omega$  is convex.  $\square$

**3.3. Transformation to a reference cell  $\Omega = [-1, 1]^2$ .** For convenience, we propose to transform the 2D OCAD problem on an arbitrary rectangular cell  $\Omega_{ij}$  into the OCAD problem on a reference cell  $\Omega = [-1, 1]^2$ . It should be noted that the objective function  $\mathcal{G}_2(\omega_1^-, \omega_1^+, \omega_2^-, \omega_2^+)$  depends on the cell size  $\{\Delta x, \Delta y\}$ . Hence, such a transformation is **not** exactly equivalent to directly considering the OCAD problem on the reference cell  $\Omega = [-1, 1]^2$ , because  $\Delta x$  and  $\Delta y$  in  $\mathcal{G}_2$  are generally not equal to 2.

**Lemma 3.6.** *The existence of a feasible CAD on  $\Omega_{ij} = [x_{i-\frac{1}{2}}, x_{i+\frac{1}{2}}] \times [y_{j-\frac{1}{2}}, y_{j+\frac{1}{2}}]$  for  $\mathbb{V}^k$  of the form*

$$(3.12) \quad \langle p \rangle_{\Omega_{ij}} = \omega_1^- \langle p \rangle_{\Omega_{ij}}^{-x} + \omega_1^+ \langle p \rangle_{\Omega_{ij}}^{+x} + \omega_2^- \langle p \rangle_{\Omega_{ij}}^{-y} + \omega_2^+ \langle p \rangle_{\Omega_{ij}}^{+y} + \sum_{s=1}^S \omega_s p(x_{ij}^{(s)}, y_{ij}^{(s)}) \quad \forall p \in \mathbb{V}^k$$

is equivalent to the existence of a feasible CAD on  $\Omega = [-1, 1]^2$  for  $\mathbb{V}^k$  of the form

$$(3.13) \quad \langle q \rangle_{\Omega} = \omega_1^- \langle q \rangle_{\Omega}^{-x} + \omega_1^+ \langle q \rangle_{\Omega}^{+x} + \omega_2^- \langle q \rangle_{\Omega}^{-y} + \omega_2^+ \langle q \rangle_{\Omega}^{+y} + \sum_{s=1}^S \omega_s p(x^{(s)}, y^{(s)}), \quad \forall q \in \mathbb{V}^k,$$

where

$$(3.14) \quad x^{(s)} = \frac{x_{ij}^{(s)} - x_i}{\Delta x/2}, \quad y^{(s)} = \frac{y_{ij}^{(s)} - y_j}{\Delta y/2}, \quad x_i := \frac{x_{i-\frac{1}{2}} + x_{i+\frac{1}{2}}}{2}, \quad y_j := \frac{y_{j-\frac{1}{2}} + y_{j+\frac{1}{2}}}{2}.$$

*Proof.* For any  $p \in \mathbb{V}^k$ , we define another polynomial  $q \in \mathbb{V}^k$  as

$$(3.15) \quad q(x, y) := p\left(x_i + \frac{\Delta x}{2}x, y_j + \frac{\Delta y}{2}y\right).$$

The polynomials  $p$  and  $q$  have the following connections

$$(3.16) \quad \langle p \rangle_{\Omega_{ij}} = \langle q \rangle_{\Omega}, \quad \langle p \rangle_{\Omega_{ij}}^{\pm x} = \langle q \rangle_{\Omega}^{\pm x}, \quad \langle p \rangle_{\Omega_{ij}}^{\pm y} = \langle q \rangle_{\Omega}^{\pm y}, \quad p(x_{ij}^{(s)}, y_{ij}^{(s)}) = q(x^{(s)}, y^{(s)}) \quad \forall s.$$

Thus, (3.13) implies (3.12). Conversely, given an arbitrary  $q \in \mathbb{V}^k$ , we can construct a polynomial  $p \in \mathbb{V}^k$  similar to (3.15), which satisfies the relations in (3.16). It immediately follows that (3.12) implies (3.13).  $\square$

**3.4. Symmetric CAD.** The reference cell  $\Omega = [-1, 1]^2$  is symmetric with respect to  $x$ - and  $y$ -axes. It is natural to seek a feasible CAD with the same symmetry.

In order to precisely describe such symmetric structures, we can invoke the concept of invariance [19, Section 1.3] with respect to the following symmetric group of transformations:

$$(3.17) \quad \mathcal{G}_s := \{(x, y) \mapsto (x, y), (x, y) \mapsto (-x, y), (x, y) \mapsto (x, -y), (x, y) \mapsto (-x, -y)\}.$$

Clearly, the reference cell  $\Omega = [-1, 1]^2$  is  $\mathcal{G}_s$ -invariant, namely,  $g(\Omega) = \Omega$  for all  $g \in \mathcal{G}_s$ . In addition, the space  $\mathbb{V}^k$  (either  $\mathbb{P}^k$  or  $\mathbb{Q}^k$ ) is  $\mathcal{G}_s$ -invariant, namely,

$$(3.18) \quad g(p) := p(g(x, y)) \in \mathbb{V}^k \quad \forall g \in \mathcal{G}_s.$$

**Definition 3.7.** ( $\mathcal{G}_s$ -invariant subspace) The polynomial space

$$\mathbb{V}^k(\mathcal{G}_s) := \{p \in \mathbb{V}^k : g(p) = p \ \forall g \in \mathcal{G}_s\}$$

is called the  $\mathcal{G}_s$ -invariant subspace of  $\mathbb{V}^k$ .

**Definition 3.8** (Symmetric CAD). A feasible CAD on  $\Omega$  is called a symmetric CAD, if it can be written as the following form

$$(3.19) \quad \langle p \rangle_\Omega = 2\bar{\omega}_1 \langle p \rangle_\Omega^x + 2\bar{\omega}_2 \langle p \rangle_\Omega^y + \sum_{s=1}^S \overline{\omega_s p(x^{(s)}, y^{(s)})} \quad \forall p \in \mathbb{V}^k,$$

where  $\bar{\omega}_1 > 0$ ,  $\bar{\omega}_2 > 0$ ,  $\omega_s > 0$ , and  $(x^{(s)}, y^{(s)}) \in [0, 1]^2$  for all  $s$ , and

$$(3.20) \quad \langle p \rangle_\Omega^x := \frac{1}{2}(\langle p \rangle_\Omega^{-x} + \langle p \rangle_\Omega^{+x}), \quad \langle p \rangle_\Omega^y := \frac{1}{2}(\langle p \rangle_\Omega^{-y} + \langle p \rangle_\Omega^{+y})$$

$$(3.21) \quad \overline{p(x^{(s)}, y^{(s)})} := \frac{1}{4} \left[ p(x^{(s)}, y^{(s)}) + p(-x^{(s)}, y^{(s)}) + p(x^{(s)}, -y^{(s)}) + p(-x^{(s)}, -y^{(s)}) \right].$$

*Remark 3.9.* All the internal nodes involved in the classic CAD (1.14) are symmetrically distributed in  $\Omega_{ij}$ , and the weights associated symmetric nodes are equal. Hence the classic CAD (1.14) is symmetric.

The symmetry of a CAD is helpful for relaxing the feasibility requirement in condition (i) of Definition 1.3, as shown in the following lemma.

**Lemma 3.10.** *If a symmetric CAD (3.19) is feasible for the  $\mathcal{G}_s$ -invariant subspace  $\mathbb{V}^k(\mathcal{G}_s)$ , then it is feasible for  $\mathbb{V}^k$ .*

*Proof.* The symmetric CAD (3.19) is associated with the following linear functional of  $p$  on  $\mathbb{V}^k$ :

$$\mathcal{F}(p) = \langle p \rangle_\Omega - 2\bar{\omega}_1 \langle p \rangle_\Omega^x - 2\bar{\omega}_2 \langle p \rangle_\Omega^y - \sum_{s=1}^S \overline{\omega_s p(x^{(s)}, y^{(s)})}.$$

Since the CAD (3.19) is feasible for  $\mathbb{V}^k(\mathcal{G}_s)$ , we have

$$(3.22) \quad \mathcal{F}(p) = 0 \quad \forall p \in \mathbb{V}^k(\mathcal{G}_s).$$

We aim to show that  $\mathcal{F}(p) = 0$  for all  $p \in \mathbb{V}^k$ . Let us prove this by contradiction. Assume that there exists a  $p_0 \in \mathbb{V}^k$  such that  $\mathcal{F}(p_0) \neq 0$ . Notice that for every  $g \in \mathcal{G}_s$ ,

$$\langle g(p_0) \rangle_\Omega = \langle p_0 \rangle_\Omega, \quad \langle g(p_0) \rangle_\Omega^x = \langle p_0 \rangle_\Omega^x, \quad \langle g(p_0) \rangle_\Omega^y = \langle p_0 \rangle_\Omega^y, \quad \overline{p_0(g(x^{(s)}, y^{(s)}))} = \overline{p_0(x^{(s)}, y^{(s)})},$$

which imply

$$(3.23) \quad \mathcal{F}(g(p_0)) = \mathcal{F}(p_0) \neq 0 \quad \forall g \in \mathcal{G}_s.$$

Then for every  $h \in \mathcal{G}_s$ , we have

$$h \left( \sum_{g \in \mathcal{G}_s} g(p_0) \right) = \sum_{g \in \mathcal{G}_s} h(g(p_0)) = \sum_{hg \in \mathcal{G}_s} h(g(p_0)) = \sum_{g \in \mathcal{G}_s} g(p_0),$$

Thus,  $p_1 := \sum_{g \in \mathcal{G}_s} g(p_0) \in \mathbb{V}^k(\mathcal{G}_s)$ . However,

$$\mathcal{F}(p_1) = \mathcal{F}\left(\sum_{g \in \mathcal{G}_s} g(p_0)\right) = \sum_{g \in \mathcal{G}_s} \mathcal{F}(g(p_0)) \stackrel{(3.23)}{=} \sum_{g \in \mathcal{G}_s} \mathcal{F}(p_0) = |\mathcal{G}_s| \mathcal{F}(p_0) \neq 0,$$

which contradicts (3.22). Hence the assumption is incorrect. We have proved that  $\mathcal{F}(p) = 0$  for all  $p \in \mathbb{V}^k$ , which means the symmetric CAD (3.19) is feasible for  $\mathbb{V}^k$ .  $\square$

*Remark 3.11.* Lemma 3.10 can be considered as a corollary of the Sobolev theorem [18]. Note that the dimension of the subspace  $\mathbb{V}^k(\mathcal{G}_s)$  is typically much smaller than the dimension of  $\mathbb{V}^k$ . For example, for  $\mathbb{P}^3 = \text{span}\{1, x, y, x^2, xy, y^2, x^3, x^2y, xy^2, y^3\}$ , we have  $\mathbb{P}^3(\mathcal{G}_s) = \text{span}\{1, x^2, y^2\}$ , and  $\dim \mathbb{P}^3(\mathcal{G}_s) = 3 \ll \dim \mathbb{P}^3 = 10$ . Therefore, Lemma 3.10 helps to greatly simplify the feasibility requirement and will be very useful for seeking OCADs in Section 5.

**3.5. Symmetric OCAD problem.** After careful observation, we find that there always exists an OCAD that is symmetric. This new insight gives significant simplification of the 2D OCAD problem, motivating us to consider the simplified symmetric OCAD problem in the next subsection.

**Theorem 3.12.** *There exists a symmetric OCAD on  $\Omega$  with*

$$(3.24) \quad \frac{\bar{\omega}_1 \Delta x}{a_1} = \frac{\bar{\omega}_2 \Delta y}{a_2}.$$

*Proof.* According to Theorem 3.4, there exists an OCAD on  $\Omega$  of the form

$$(3.25) \quad \langle p \rangle_\Omega = \omega_1^- \langle p \rangle_\Omega^{-x} + \omega_1^+ \langle p \rangle_\Omega^{+x} + \omega_2^- \langle p \rangle_\Omega^{-y} + \omega_2^+ \langle p \rangle_\Omega^{+y} + \sum_{s=1}^S \omega_s p(x^{(s)}, y^{(s)}),$$

which maximizes  $\mathcal{G}_2(\omega_1^-, \omega_1^+, \omega_2^-, \omega_2^+)$  and satisfies

$$(3.26) \quad \frac{\omega_1^- \Delta x}{a_1} = \frac{\omega_1^+ \Delta x}{a_1} = \frac{\omega_2^- \Delta y}{a_2} = \frac{\omega_2^+ \Delta y}{a_2}.$$

For any  $p \in \mathbb{V}^k$ , we define  $q(x, y) := p(-x, y)$ , then  $q \in \mathbb{V}^k$  due to (3.18) and moreover,

$$\langle q \rangle_\Omega = \langle p \rangle_\Omega, \quad \langle q \rangle_\Omega^{\pm x} = \langle p \rangle_\Omega^{\mp x}, \quad \langle q \rangle_\Omega^{\pm y} = \langle p \rangle_\Omega^{\pm y}, \quad q(x^{(s)}, y^{(s)}) = p(-x^{(s)}, y^{(s)}).$$

Applying the OCAD (3.25) to  $q$ , we find that the following CAD is feasible:

$$(3.27) \quad \langle p \rangle_\Omega = \omega_1^+ \langle p \rangle_\Omega^{-x} + \omega_1^- \langle p \rangle_\Omega^{+x} + \omega_2^- \langle p \rangle_\Omega^{-y} + \omega_2^+ \langle p \rangle_\Omega^{+y} + \sum_{s=1}^S \omega_s p(-x^{(s)}, y^{(s)}).$$

Similarly, we obtain the following two feasible CADs:

$$(3.28) \quad \langle p \rangle_\Omega = \omega_1^- \langle p \rangle_\Omega^{-x} + \omega_1^+ \langle p \rangle_\Omega^{+x} + \omega_2^+ \langle p \rangle_\Omega^{-y} + \omega_2^- \langle p \rangle_\Omega^{+y} + \sum_{s=1}^S \omega_s p(x^{(s)}, -y^{(s)}),$$

$$(3.29) \quad \langle p \rangle_\Omega = \omega_1^+ \langle p \rangle_\Omega^{-x} + \omega_1^- \langle p \rangle_\Omega^{+x} + \omega_2^+ \langle p \rangle_\Omega^{-y} + \omega_2^- \langle p \rangle_\Omega^{+y} + \sum_{s=1}^S \omega_s p(-x^{(s)}, -y^{(s)}).$$

Taking an average of the four feasible CADs (3.25) and (3.27)–(3.29), we obtain the following feasible CAD

$$(3.30) \quad \langle p \rangle_\Omega = \frac{\omega_1^- + \omega_1^+}{2} \left[ \langle p \rangle_\Omega^{+x} + \langle p \rangle_\Omega^{-x} \right] + \frac{\omega_2^- + \omega_2^+}{2} \left[ \langle p \rangle_\Omega^{+y} + \langle p \rangle_\Omega^{-y} \right] + \sum_{s=1}^S \omega_s \overline{p(x^{(s)}, y^{(s)})}.$$

or equivalently,

$$(3.31) \quad \langle p \rangle_\Omega = (\omega_1^- + \omega_1^+) \langle p \rangle_\Omega^x + (\omega_2^- + \omega_2^+) \langle p \rangle_\Omega^y + \sum_{s=1}^S \omega_s \overline{p(|x^{(s)}|, |y^{(s)}|)},$$

which is a symmetric CAD with  $(|x^{(s)}|, |y^{(s)}|) \in [0, 1]^2$  for all  $s$ . Moreover, because

$$\bar{\omega}_1 := \frac{\omega_1^- + \omega_1^+}{2} \geq \min \{\omega_1^-, \omega_1^+\} \quad \text{and} \quad \bar{\omega}_2 := \frac{\omega_2^- + \omega_2^+}{2} \geq \min \{\omega_2^-, \omega_2^+\},$$

we have

$$\begin{aligned} \mathcal{G}_2(\bar{\omega}_1, \bar{\omega}_1, \bar{\omega}_2, \bar{\omega}_2) &= \min \left\{ \frac{\bar{\omega}_1 \Delta x}{a_1}, \frac{\bar{\omega}_2 \Delta y}{a_2} \right\} \\ &\geq \min \left\{ \frac{\omega_1^- \Delta x}{a_1}, \frac{\omega_1^+ \Delta x}{a_1}, \frac{\omega_2^- \Delta y}{a_2}, \frac{\omega_2^+ \Delta y}{a_2} \right\} = \mathcal{G}_2(\omega_1^-, \omega_1^+, \omega_2^-, \omega_2^+), \end{aligned}$$

which implies the symmetric CAD (3.31) is also an OCAD. Moreover, (3.26) implies (3.24).  $\square$

Let  $\mathbb{B}_\omega \subset \mathbb{R}^2$  denote the set of the boundary weights  $(\bar{\omega}_1, \bar{\omega}_2)$  for all feasible symmetric CADs, namely,

$$(3.32) \quad \mathbb{B}_\omega := \left\{ (\bar{\omega}_1, \bar{\omega}_2) \in [0, 1]^2 : \exists \text{ symmetric CAD } \langle p \rangle_\Omega = 2\bar{\omega}_1 \langle p \rangle_\Omega^x + 2\bar{\omega}_2 \langle p \rangle_\Omega^y + \sum_s \omega_s \overline{p(x^{(s)}, y^{(s)})} \right\}.$$

In fact, the set  $\mathbb{B}_\omega$  is a projection of the set  $\mathbb{A}_\omega$ . Since  $\mathbb{A}_\omega \subset [0, 1]^4$  is compact (Lemma 3.3) and convex (Lemma 3.5), we know that  $\mathbb{B}_\omega \subset [0, 1]^2$  is also compact and convex. Figure 2 illustrates the region  $\mathbb{B}_\omega$  (shaded in green) for  $\mathbb{V}^k = \mathbb{Q}^2$  or  $\mathbb{Q}^3$  and  $\mathbb{V}^k = \mathbb{P}^2$  or  $\mathbb{P}^3$ , respectively.

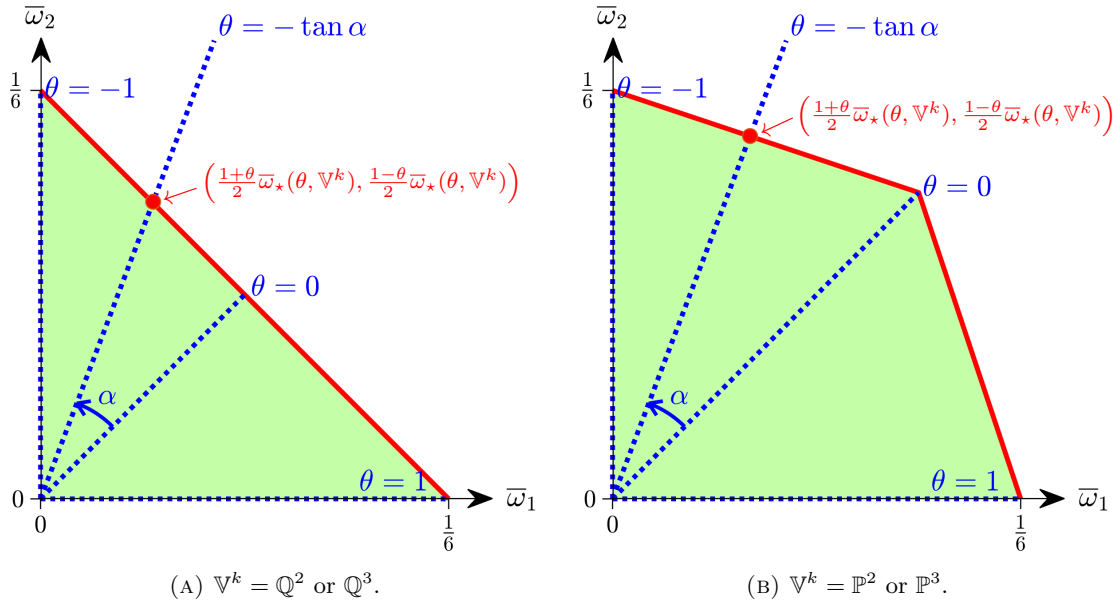


FIGURE 2. The region  $\mathbb{B}_\omega$  (shaded in green) and the geometric interpretation of the transformation (3.35) for Problem 3.13.

Thanks to Lemma 3.6 and Theorem 3.12, we only need to seek the symmetric OCAD on the reference cell  $\Omega$  that maximizes

$$(3.33) \quad \min \left\{ \frac{\bar{\omega}_1 \Delta x}{a_1}, \frac{\bar{\omega}_2 \Delta y}{a_2} \right\} \quad \text{with} \quad \frac{\bar{\omega}_1 \Delta x}{a_1} = \frac{\bar{\omega}_2 \Delta y}{a_2}.$$

Define

$$(3.34) \quad \theta := \frac{a_1/\Delta x - a_2/\Delta y}{a_1/\Delta x + a_2/\Delta y} \in [-1, 1],$$

and introduce a new quantity  $\bar{\omega}$  to automatically meet the constraint  $\frac{\bar{\omega}_1 \Delta x}{a_1} = \frac{\bar{\omega}_2 \Delta y}{a_2}$  as follows:

$$(3.35) \quad \bar{\omega}_1 = \frac{1}{2} \bar{\omega} (1 + \theta), \quad \bar{\omega}_2 = \frac{1}{2} \bar{\omega} (1 - \theta).$$

See Figure 2 for the geometric interpretation of the transformation (3.35). Then a symmetric CAD (3.19) can be rewritten as

$$(3.36) \quad \langle p \rangle_\Omega = \bar{\omega} [(1 + \theta) \langle p \rangle_\Omega^x + (1 - \theta) \langle p \rangle_\Omega^y] + \sum_{s=1}^S \overline{\omega_s p(x^{(s)}, y^{(s)})} \quad \forall p \in \mathbb{V}^k,$$

and the objective function (3.33) is simplified to  $\bar{\omega}/(a_1/\Delta x + a_2/\Delta y)$ . This procedure greatly simplifies the 2D OCAD problem to the following Problem 3.13.

**Problem 3.13** (Symmetric 2D OCAD Problem). *For  $k \in \mathbb{N}_+$  and any given  $\theta \in [-1, 1]$ , find the symmetric OCAD on the reference cell  $\Omega$  with the maximum boundary weight  $\bar{\omega}_*(\theta, \mathbb{V}^k)$ :*

$$(3.37) \quad \langle p \rangle_\Omega = \bar{\omega}_*(\theta, \mathbb{V}^k) [(1 + \theta) \langle p \rangle_\Omega^x + (1 - \theta) \langle p \rangle_\Omega^y] + \sum_{s=1}^S \overline{\omega_s p(x^{(s)}, y^{(s)})} \quad \forall p \in \mathbb{V}^k,$$

where  $\omega_s > 0$  and  $(x^{(s)}, y^{(s)}) \in [0, 1]^2$  for all  $s$ .

In the following, we will mainly focus on the simplified Problem 3.13 on the reference cell  $\Omega$ . The resulting optimal CFL condition will be

$$(3.38) \quad \Delta t \leq c_0 \max \mathcal{G}_2 = \frac{c_0 \bar{\omega}_*}{a_1/\Delta x + a_2/\Delta y}.$$

Once Problem 3.13 is solved, we immediately obtain an OCAD on the rectangular cell  $\Omega_{ij}$  with the corresponding nodes  $\{(x_{ij}^{(s)}, y_{ij}^{(s)})\}$  given by the inverse transformation of (3.14).

**Lemma 3.14** (Monotonicity). *The optimal weight  $\bar{\omega}_*(\theta, \mathbb{V}^k)$  is monotonically non-increasing with respect to  $k$ , namely,*

$$(3.39) \quad \bar{\omega}_*(\theta, \mathbb{V}^{k_1}) \geq \bar{\omega}_*(\theta, \mathbb{V}^{k_2}) \quad \text{if } k_1 < k_2.$$

*Proof.* If  $k_1 < k_2$ , then  $\mathbb{V}^{k_1} \subseteq \mathbb{V}^{k_2}$ . Any OCAD for  $\mathbb{V}^{k_2}$  is a feasible CAD for  $\mathbb{V}^{k_1}$ . Hence we have (3.39).  $\square$

**Lemma 3.15.** *For any  $k \in \mathbb{N}_+$ , the symmetric OCAD on  $\Omega$  for the space  $\mathbb{V}^{2k}$  is also a symmetric OCAD for the space  $\mathbb{V}^{2k+1}$ . Furthermore,*

$$(3.40) \quad \bar{\omega}_*(\theta, \mathbb{V}^{2k+1}) = \bar{\omega}_*(\theta, \mathbb{V}^{2k}) \quad \forall \theta \in [-1, 1].$$

*Proof.* Let

$$(3.41) \quad \langle p \rangle_\Omega = \bar{\omega}_*(\theta, \mathbb{V}^{2k}) [(1 + \theta) \langle p \rangle_\Omega^x + (1 - \theta) \langle p \rangle_\Omega^y] + \sum_{s=1}^S \overline{\omega_s p(x^{(s)}, y^{(s)})}$$

be a symmetric OCAD on the reference cell  $\Omega$  for the space  $\mathbb{V}^{2k}$ . For any polynomial  $q(x, y) = \sum_{\|\mathbf{i}\| \leq 2k+1} a_{i_1 i_2} x^{i_1} y^{i_2} \in \mathbb{V}^{2k+1}$ , define the truncated polynomial  $p(x, y) := \sum_{\|\mathbf{i}\| \leq 2k} a_{i_1 i_2} x^{i_1} y^{i_2} \in \mathbb{V}^{2k}$ , where the norm  $\|\mathbf{i}\| = i_1 + i_2$  for  $\mathbb{V}^{2k} = \mathbb{P}^{2k}$  and  $\|\mathbf{i}\| = \max\{i_1, i_2\}$  for  $\mathbb{V}^{2k} = \mathbb{Q}^{2k}$ . Note that the polynomial  $q(x, y) - p(x, y)$  is odd with respect to either  $x$  or  $y$ . Thanks to the symmetry, we have

$$\langle q - p \rangle_\Omega = \langle q - p \rangle_\Omega^x = \langle q - p \rangle_\Omega^y = \overline{(q - p)(x^{(s)}, y^{(s)})} = 0.$$

It then follows from (3.41) that

$$(3.42) \quad \langle q \rangle_\Omega = \bar{\omega}_*(\theta, \mathbb{V}^{2k}) [(1 + \theta) \langle q \rangle_\Omega^x + (1 - \theta) \langle q \rangle_\Omega^y] + \sum_{s=1}^S \overline{\omega_s q(x^{(s)}, y^{(s)})} \quad \forall q \in \mathbb{V}^{2k+1}.$$

This means (3.42) is a symmetric feasible CAD for  $\mathbb{V}^{2k+1}$ , and thus  $\bar{\omega}_*(\theta, \mathbb{V}^{2k}) \leq \bar{\omega}_*(\theta, \mathbb{V}^{2k+1})$ . On the other hand, Lemma 3.14 yields  $\bar{\omega}_*(\theta, \mathbb{V}^{2k}) \geq \bar{\omega}_*(\theta, \mathbb{V}^{2k+1})$ . Therefore,  $\bar{\omega}_*(\theta, \mathbb{V}^{2k}) = \bar{\omega}_*(\theta, \mathbb{V}^{2k+1})$ , and (3.42) is also a symmetric OCAD for  $\mathbb{V}^{2k+1}$ . The proof is completed.  $\square$

*Remark 3.16.* Thanks to Lemma 3.15, we only need to seek the symmetric OCAD for  $\mathbb{V}^{2k}$  of even degrees.

**Lemma 3.17.** *The symmetric CAD*

$$(3.43) \quad \langle p \rangle_\Omega = \bar{\omega} [(1 + \theta) \langle p \rangle_\Omega^x + (1 - \theta) \langle p \rangle_\Omega^y] + \sum_{s=1}^S \overline{\omega_s p(x^{(s)}, y^{(s)})}$$

is feasible for  $\mathbb{V}^k$  if and only if the CAD

$$(3.44) \quad \langle p \rangle_\Omega = \bar{\omega} [(1 - \theta) \langle p \rangle_\Omega^x + (1 + \theta) \langle p \rangle_\Omega^y] + \sum_{s=1}^S \overline{\omega_s p(y^{(s)}, x^{(s)})}$$

is feasible for  $\mathbb{V}^k$ . This implies the region  $\mathbb{B}_\omega$  is symmetric with respect to the line  $\bar{\omega}_1 = \bar{\omega}_2$ .

*Proof.* The feasibility of a CAD, as defined in Definition 1.3, requires three conditions. The satisfaction of condition (ii) for CADs (3.43) and (3.44) is equivalent. The satisfaction of condition (iii) is also equivalent for both CADs, due to the geometric symmetry of  $\Omega$ .

Let us verify the equivalence for condition (i). Assume the condition (i) of (3.43) is satisfied. For any  $p(x, y) \in \mathbb{V}^k$ ,  $q(x, y) := p(y, x)$  is also a polynomial in  $\mathbb{V}^k$ . Note that

$$\langle p \rangle_\Omega = \langle q \rangle_\Omega, \quad \langle p \rangle_\Omega^x = \langle q \rangle_\Omega^y, \quad \langle p \rangle_\Omega^y = \langle q \rangle_\Omega^x, \quad \overline{p(y^{(s)}, x^{(s)})} = \overline{q(x^{(s)}, y^{(s)})},$$

we have

$$\begin{aligned} & \langle p \rangle_\Omega - \bar{\omega} [(1 - \theta) \langle p \rangle_\Omega^x + (1 + \theta) \langle p \rangle_\Omega^y] - \sum_{s=1}^S \overline{\omega_s p(y^{(s)}, x^{(s)})} \\ &= \langle q \rangle_\Omega - \bar{\omega} [(1 - \theta) \langle q \rangle_\Omega^y + (1 + \theta) \langle q \rangle_\Omega^x] - \sum_{s=1}^S \overline{\omega_s q(x^{(s)}, y^{(s)})} = 0. \end{aligned}$$

Thus, the condition (i) of (3.43) is a sufficient condition of the condition (i) of (3.44). The necessity can be similarly proved, and the proof of Lemma 3.17 is completed.  $\square$

**Lemma 3.18.** *The function  $\bar{\omega}_*(\theta, \mathbb{V}^k)$  is even with  $\theta$ , namely,*

$$\bar{\omega}_*(-\theta, \mathbb{V}^k) = \bar{\omega}_*(\theta, \mathbb{V}^k) \quad \theta \in [-1, 1].$$

*Proof.* Consider a symmetric OCAD (3.37) for  $\mathbb{V}^k$ . By Lemma 3.17, the following symmetric CAD is also feasible for  $\mathbb{V}^k$ :

$$(3.45) \quad \langle p \rangle_\Omega = \bar{\omega}_*(\theta, \mathbb{V}^k) [(1 - \theta) \langle p \rangle_\Omega^x + (1 + \theta) \langle p \rangle_\Omega^y] + \sum_{s=1}^S \overline{\omega_s p(y^{(s)}, x^{(s)})},$$

which implies  $\bar{\omega}_*(-\theta, \mathbb{V}^k) \geq \bar{\omega}_*(\theta, \mathbb{V}^k)$ . Similar, one has  $\bar{\omega}_*(\theta, \mathbb{V}^k) \geq \bar{\omega}_*(-\theta, \mathbb{V}^k)$ . Hence  $\bar{\omega}_*(-\theta, \mathbb{V}^k) = \bar{\omega}_*(\theta, \mathbb{V}^k)$ , and (3.45) is a symmetric OCAD for  $(-\theta, \mathbb{V}^k)$ .  $\square$

*Remark 3.19.* Thanks to Lemma 3.18, we only need to investigate the symmetric 2D OCAD problem (Problem 3.13) for  $\theta \in [-1, 0]$ . For  $\theta \in [0, 1]$ , the corresponding symmetric OCAD can then be directly obtained by (3.45).

**3.6. Optimality criteria.** Let  $\mathbb{V}_+^k$  denote the set of all the polynomials in  $\mathbb{V}^k$  that is non-negative over  $\Omega$ . The following lemma establishes the close connection between  $\bar{\omega}_*(\theta, \mathbb{V}^k)$  and  $\mathbb{V}_+^k$ .

**Lemma 3.20.** *Given  $k \in \mathbb{N}_+$ , for any  $p \in \mathbb{V}_+^k$ , define*

$$\phi(p; \theta) := \begin{cases} \frac{\langle p \rangle_\Omega}{(1 + \theta) \langle p \rangle_\Omega^x + (1 - \theta) \langle p \rangle_\Omega^y} & \text{if } (1 + \theta) \langle p \rangle_\Omega^x + (1 - \theta) \langle p \rangle_\Omega^y \neq 0, \\ +\infty & \text{if } (1 + \theta) \langle p \rangle_\Omega^x + (1 - \theta) \langle p \rangle_\Omega^y = 0, \end{cases}$$

then

$$(3.46) \quad \phi^*(\theta, \mathbb{V}_+^k) := \inf_{p \in \mathbb{V}_+^k} \phi(p; \theta) \geq \bar{\omega}_*(\theta, \mathbb{V}^k).$$



*Proof.* For a symmetric OCAD (3.37) on  $\Omega$ , we have for all  $p \in \mathbb{V}_+^k \setminus \{0\}$  that

$$\begin{aligned} \langle p \rangle_\Omega &= \bar{\omega}_*(\theta, \mathbb{V}^k) [(1 + \theta) \langle p \rangle_\Omega^x + (1 - \theta) \langle p \rangle_\Omega^y] + \sum_{s=1}^S \overline{\omega_s p(x^{(s)}, y^{(s)})} \\ &\geq \bar{\omega}_*(\theta, \mathbb{V}^k) [(1 + \theta) \langle p \rangle_\Omega^x + (1 - \theta) \langle p \rangle_\Omega^y], \end{aligned}$$

which implies

$$\phi(p; \theta) \geq \bar{\omega}_*(\theta, \mathbb{V}^k) \quad \forall p \in \mathbb{V}_+^k.$$

Taking the infimum for  $p$  on the above inequality completes the proof.  $\square$

For any  $p \in \mathbb{V}_+^k$ ,  $\phi(p; \theta)$  is an upper bound of  $\bar{\omega}_*(\theta, \mathbb{V}^k)$ . As suggested by Lemma 3.20, one may minimize  $\phi(p; \theta)$  in  $\mathbb{V}_+^k$  and obtain  $\phi^*(\theta, \mathbb{V}_+^k)$  as a sharp upper bound for  $\bar{\omega}_*(\theta, \mathbb{V}^k)$ . Very interestingly, for all the 2D OCADs found in this paper, we discover that  $\phi^*(\theta, \mathbb{V}_+^k) = \bar{\omega}_*(\theta, \mathbb{V}^k)$ , which will be further discussed in Conjecture 3.1. This motivates us to consider the following problem.

**Problem 3.21.** *Given  $k \in \mathbb{N}^+$  and  $\theta \in [-1, 1]$ , minimize  $\phi(p; \theta)$  for  $p \in \mathbb{V}_+^k$ .*

For given  $\theta \in [-1, 1]$  and  $\mathbb{V}_+^k$ , if there exists a  $p^* \in \mathbb{V}_+^k \setminus \{0\}$  such that

$$(3.47) \quad p^* := \arg \min_{p \in \mathbb{V}_+^k} \phi(p; \theta),$$

then we call  $p^*$  a *critical positive polynomial* for  $\phi^*(\theta, \mathbb{V}_+^k)$ .

*Remark 3.22.* It is worth noting that, for given  $\theta \in [-1, 1]$  and  $k \in \mathbb{N}^+$ , the critical positive polynomial for  $\phi^*(\theta, \mathbb{V}_+^k)$  and the symmetric OCAD for  $\mathbb{V}^k$  can be possibly not unique.

**Lemma 3.23.** *If two different nonzero nonnegative polynomials,  $p_1^*, p_2^* \in \mathbb{V}_+^k \setminus \{0\}$ , are both critical positive polynomials for  $\phi^*(\theta, \mathbb{V}_+^k)$ , namely,*

$$(3.48) \quad \phi^*(\theta, \mathbb{V}_+^k) = \phi(p_1^*; \theta) = \phi(p_2^*; \theta),$$

then for any  $\alpha_1, \alpha_2 \in \mathbb{R}_+$ , the positively combined polynomial

$$\alpha_1 p_1^* + \alpha_2 p_2^* \in \mathbb{V}_+^k \setminus \{0\}$$

is also a critical positive polynomial for  $\phi^*(\theta, \mathbb{V}_+^k)$ .

*Proof.* We observe for any  $\alpha_1, \alpha_2 \in \mathbb{R}_+$  that

$$\begin{aligned} \frac{1}{\phi(\alpha_1 p_1^* + \alpha_2 p_2^*; \theta)} &= \frac{(1 + \theta) \langle \alpha_1 p_1^* + \alpha_2 p_2^* \rangle_\Omega^x + (1 - \theta) \langle \alpha_1 p_1^* + \alpha_2 p_2^* \rangle_\Omega^y}{\langle \alpha_1 p_1^* + \alpha_2 p_2^* \rangle_\Omega} \\ &= \frac{\alpha_1 \langle p_1^* \rangle_\Omega}{\alpha_1 \langle p_1^* \rangle_\Omega + \alpha_2 \langle p_2^* \rangle_\Omega} \frac{1}{\phi(p_1^*; \theta)} + \frac{\alpha_2 \langle p_1^* \rangle_\Omega}{\alpha_1 \langle p_1^* \rangle_\Omega + \alpha_2 \langle p_2^* \rangle_\Omega} \frac{1}{\phi(p_2^*; \theta)} \\ &\stackrel{(3.48)}{=} \frac{1}{\phi^*(\theta, \mathbb{V}_+^k)}, \end{aligned}$$

which yields  $\phi(\alpha_1 p_1^* + \alpha_2 p_2^*; \theta) = \phi^*(\theta, \mathbb{V}_+^k)$ . Hence  $\alpha_1 p_1^* + \alpha_2 p_2^*$  is also a critical positive polynomial.  $\square$

We discover that the symmetric OCAD problem (Problem 3.13) is strongly connected with Problem 3.21. Their connection leads to the following optimality criteria, which are very useful for examining the optimality of a feasible symmetric CAD:

$$(3.49) \quad \langle p \rangle_\Omega = \bar{\omega} [(1 + \theta) \langle p \rangle_\Omega^x + (1 - \theta) \langle p \rangle_\Omega^y] + \sum_{s=1}^S \overline{\omega_s p(x^{(s)}, y^{(s)})} \quad \forall p \in \mathbb{V}^k.$$

**Theorem 3.24** (Optimality Criterion #1). *If  $\bar{\omega} = \phi^*(\theta, \mathbb{V}_+^k)$ , then  $\bar{\omega}_*(\theta, \mathbb{V}^k) = \phi^*(\theta, \mathbb{V}_+^k)$  and the CAD (3.49) is a symmetric OCAD for  $\mathbb{V}^k$ .*

*Proof.* Lemma 3.20 tells us that

$$\phi^*(\theta, \mathbb{V}_+^k) \geq \bar{\omega}_*(\theta, \mathbb{V}^k) \geq \bar{\omega}.$$

If  $\bar{\omega} = \phi^*(\theta, \mathbb{V}^k)$ , then  $\bar{\omega} = \bar{\omega}_*(\theta, \mathbb{V}^k) = \phi^*(\theta, \mathbb{V}^k)$  and the symmetric CAD (3.49) is optimal for  $\mathbb{V}^k$ .  $\square$

**Theorem 3.25** (Optimality Criterion #2). *For a given  $\theta \in [-1, 1]$ , if there exists a polynomial  $p^* \in \mathbb{V}_+^k \setminus \{0\}$  such that  $p^*(x^{(s)}, y^{(s)}) = 0$  for all  $s$ , then we have:*

- $\bar{\omega}_*(\theta, \mathbb{V}^k) = \phi^*(\theta, \mathbb{V}_+^k)$ ;
- the CAD (3.49) is a symmetric OCAD for  $\mathbb{V}^k$ ;
- the polynomial  $p^*$  is a critical positive polynomial for  $\phi^*(\theta, \mathbb{V}_+^k)$ .

*Proof.* Taking  $p = p^*$  in (3.49) gives

$$\langle p^* \rangle_\Omega = \bar{\omega} [(1 + \theta) \langle p^* \rangle_\Omega^x + (1 - \theta) \langle p^* \rangle_\Omega^y].$$

Since  $p^* \neq 0$ , we have  $\langle p^* \rangle_\Omega \neq 0$  and  $\phi(p^*; \theta) = \bar{\omega}$ . Thanks to Lemma 3.20, we obtain

$$\bar{\omega} = \phi(p^*; \theta) \geq \inf_{p \in \mathbb{V}_+^k} \phi(p; \theta) \geq \bar{\omega}_*(\theta, \mathbb{V}^k) \geq \bar{\omega},$$

which implies  $\bar{\omega} = \bar{\omega}_*(\theta, \mathbb{V}^k) = \phi(p^*; \theta) = \min_{p \in \mathbb{V}_+^k} \phi(p; \theta) = \phi^*(\theta, \mathbb{V}_+^k)$ . Hence the CAD (3.49) is optimal, and  $p^*$  is a critical positive polynomial.  $\square$

**Theorem 3.26** (Optimality Criterion #3). *For a given  $\theta \in [-1, 1]$ , if there exists a polynomial  $q_* \in \mathbb{V}^{\lfloor \frac{k}{2} \rfloor} \setminus \{0\}$  such that  $q_*(x^{(s)}, y^{(s)}) = 0$  for all  $s$ , then we have:*

- $\bar{\omega}_*(\theta, \mathbb{V}^k) = \phi^*(\theta, \mathbb{V}_+^k) = \phi(q_*^2; \theta) = \inf_{q \in \mathbb{V}^{\lfloor \frac{k}{2} \rfloor}} \phi(q^2; \theta)$ ;
- the CAD (3.49) is a symmetric OCAD for  $\mathbb{V}^k$ ;
- the polynomial  $p^* := q_*^2$  is a critical positive polynomial for  $\phi^*(\theta, \mathbb{V}_+^k)$ .

*Proof.* Since  $q_* \in \mathbb{V}^{\lfloor \frac{k}{2} \rfloor} \setminus \{0\}$ , we have  $p^* := q_*^2 \in \mathbb{V}_+^k \setminus \{0\}$ . Moreover,  $p^*(x^{(s)}, y^{(s)}) = 0$  for all  $s$ . By Theorem 3.25, we have  $\bar{\omega}_*(\theta, \mathbb{V}^k) = \phi^*(\theta, \mathbb{V}_+^k) = \phi(q_*^2; \theta)$ , (3.49) is a symmetric OCAD for  $\mathbb{V}^k$ , and  $p^*$  is a critical positive polynomial. Noting  $q^2 \in \mathbb{V}_+^k$  for all  $q \in \mathbb{V}^{\lfloor \frac{k}{2} \rfloor}$ , we have  $(\mathbb{V}^{\lfloor \frac{k}{2} \rfloor})^2 \subset \mathbb{V}_+^k$ , which implies

$$\phi(q_*^2; \theta) \geq \inf_{q \in \mathbb{V}^{\lfloor \frac{k}{2} \rfloor}} \phi(q^2; \theta) \geq \inf_{p \in \mathbb{V}_+^k} \phi(p; \theta) = \phi^*(\theta, \mathbb{V}_+^k).$$

Therefore,  $\phi(q_*^2; \theta) = \inf_{q \in \mathbb{V}^{\lfloor \frac{k}{2} \rfloor}} \phi(q^2; \theta) = \phi^*(\theta, \mathbb{V}_+^k)$ . The proof is completed.  $\square$

**Theorem 3.27** (Optimality Criterion #4). *Define  $\phi^*(\theta, (\mathbb{V}^{\lfloor \frac{k}{2} \rfloor})^2) := \inf_{q \in \mathbb{V}^{\lfloor \frac{k}{2} \rfloor}} \phi(q^2; \theta)$ . If there is a feasible CAD (3.49) with  $\bar{\omega} = \phi^*(\theta, (\mathbb{V}^{\lfloor \frac{k}{2} \rfloor})^2)$ , then we have:*

- $\bar{\omega}_*(\theta, \mathbb{V}^k) = \phi^*(\theta, \mathbb{V}_+^k) = \phi^*(\theta, (\mathbb{V}^{\lfloor \frac{k}{2} \rfloor})^2)$ ;
- the CAD (3.49) is a symmetric OCAD for  $\mathbb{V}^k$ .

*Proof.* Recalling  $(\mathbb{V}^{\lfloor \frac{k}{2} \rfloor})^2 \subset \mathbb{V}_+^k$  and (3.46), we have

$$\bar{\omega} \leq \bar{\omega}_*(\theta, \mathbb{V}^k) \leq \phi^*(\theta, \mathbb{V}_+^k) \leq \phi^*(\theta, (\mathbb{V}^{\lfloor \frac{k}{2} \rfloor})^2).$$

If  $\bar{\omega} = \phi^*(\theta, (\mathbb{V}^{\lfloor \frac{k}{2} \rfloor})^2)$ , we must have  $\bar{\omega} = \bar{\omega}_*(\theta, \mathbb{V}^k) = \phi^*(\theta, \mathbb{V}_+^k) = \phi^*(\theta, (\mathbb{V}^{\lfloor \frac{k}{2} \rfloor})^2)$ , which implies the CAD (3.49) is a symmetric OCAD for  $\mathbb{V}^k$ .  $\square$

*Remark 3.28.* Notice that  $\phi(p; \theta)$  satisfies  $\phi(\alpha p; \theta) = \phi(p; \theta)$  for any  $\alpha > 0$ . Thus, by normalization with  $\langle p \rangle_\Omega = 1$ , Problem 3.21 can be equivalently cast into

$$(3.50) \quad \begin{aligned} & \max_{p \in \mathbb{V}^k} (1 + \theta) \langle p \rangle_\Omega^x + (1 - \theta) \langle p \rangle_\Omega^y \\ & \text{subject to: } p(x, y) \geq 0 \quad \forall (x, y) \in \Omega, \\ & \quad \langle p \rangle_\Omega = 1. \end{aligned}$$

Obviously, this problem (3.50) is a convex semi-infinite optimization problem, which actually falls into the category of polynomial optimization, and its solution is very difficult to obtain. Lasserre [13] proposed the semidefinite relaxation method to numerically solve polynomial optimization problems like (3.50), by relaxing the problem into a sequence of semidefinite programming (SDP) problems with increasing complexity. See [14, 15] for a comprehensive introduction of polynomial optimization and the semidefinite relaxation method.

Due to the challenges in solving (3.50), it seems difficult to seek 2D OCADs directly based on the optimality criterion #1. Fortunately, we find an explicit analytical formula for  $\phi^*(\theta, (\mathbb{V}^{\lfloor \frac{k}{2} \rfloor})^2) := \inf_{q \in \mathbb{V}^{\lfloor \frac{k}{2} \rfloor}} \phi(q^2; \theta)$  with  $k \in \mathbb{N}_+$ , as derived below. This will inspire us to understand, construct, and verify 2D OCADs via the above optimality criteria #3 and #4.

Define  $D := \dim \mathbb{V}^{\lfloor \frac{k}{2} \rfloor}$ . Denote the monomial basis of  $\mathbb{V}^{\lfloor \frac{k}{2} \rfloor}$  by  $\mathbf{b}(x, y) := (b_1(x, y), \dots, b_D(x, y))^\top$ . Define three  $D \times D$  symmetric matrices  $\mathbf{M}_\Omega$ ,  $\mathbf{M}_\Omega^x$ , and  $\mathbf{M}_\Omega^y$  by

$$(3.51) \quad [\mathbf{M}_\Omega]_{ij} = \langle b_i b_j \rangle_\Omega, \quad [\mathbf{M}_\Omega^x]_{ij} = \langle b_i b_j \rangle_\Omega^x, \quad [\mathbf{M}_\Omega^y]_{ij} = \langle b_i b_j \rangle_\Omega^y, \quad i, j = 1, \dots, D.$$

For any polynomial  $q \in \mathbb{V}^{\lfloor \frac{k}{2} \rfloor} \setminus \{0\}$ , it has a unique expansion:

$$q(x, y) = \sum_{i=1}^D q_i b_i(x, y) = \mathbf{q}^\top \mathbf{b}(x, y).$$

With the matrices defined in (3.51), one can express  $\langle q^2 \rangle_\Omega$ ,  $\langle q^2 \rangle_\Omega^x$  and  $\langle q^2 \rangle_\Omega^y$  in quadratic forms:

$$(3.52) \quad \langle q^2 \rangle_\Omega = \mathbf{q}^\top \mathbf{M}_\Omega \mathbf{q}, \quad \langle q^2 \rangle_\Omega^x = \mathbf{q}^\top \mathbf{M}_\Omega^x \mathbf{q}, \quad \langle q^2 \rangle_\Omega^y = \mathbf{q}^\top \mathbf{M}_\Omega^y \mathbf{q}.$$

If  $\mathbf{q} \neq \mathbf{0}$  or equivalently  $q \neq 0$ , then  $\langle q^2 \rangle_\Omega > 0$ ,  $\langle q^2 \rangle_\Omega^x \geq 0$ , and  $\langle q^2 \rangle_\Omega^y \geq 0$ . Thus, the symmetric matrix  $\mathbf{M}_\Omega$  is positive definite, and the matrices  $\mathbf{M}_\Omega^x$  and  $\mathbf{M}_\Omega^y$  are positive semi-definite so that the matrix

$$\mathbf{M}_\theta := (1 + \theta)\mathbf{M}_\Omega^x + (1 - \theta)\mathbf{M}_\Omega^y$$

is positive semi-definite for any  $\theta \in [-1, 1]$ .

**Theorem 3.29.** *For any  $\theta \in [-1, 1]$ , it holds that*

$$(3.53) \quad \phi^* \left( \theta, (\mathbb{V}^{\lfloor \frac{k}{2} \rfloor})^2 \right) = \phi(q_*^2; \theta) = \frac{1}{\left\| \mathbf{M}_\Omega^{-\frac{1}{2}} \mathbf{M}_\theta \mathbf{M}_\Omega^{-\frac{1}{2}} \right\|_2},$$

namely, where  $\|\cdot\|_2$  denotes the 2-norm of matrix, and the critical positive polynomial

$$(3.54) \quad p_*(x, y) = q_*^2(x, y) \quad \text{with} \quad q_*(x, y) := \widehat{\mathbf{q}}_\theta^\top \mathbf{M}_\Omega^{-\frac{1}{2}} \mathbf{b}(x, y)$$

where  $\widehat{\mathbf{q}}_\theta$  is an eigenvector corresponding to the spectral radius of  $\mathbf{M}_\Omega^{-\frac{1}{2}} \mathbf{M}_\theta \mathbf{M}_\Omega^{-\frac{1}{2}}$ . In other words,  $\phi^* \left( \theta, (\mathbb{V}^{\lfloor \frac{k}{2} \rfloor})^2 \right)$  is the smallest real root of the following polynomial

$$\mathcal{F}_\theta(\phi) := \det(\mathbf{M}_\Omega - \phi \mathbf{M}_\theta).$$

*Proof.* For any  $q \in \mathbb{V}^{\lfloor \frac{k}{2} \rfloor} \setminus \{0\}$ , denote by  $\mathbf{q}$  the associated expansion coefficients. Noting that  $\mathbf{M}_\Omega$  is positive definite, we define  $\widehat{\mathbf{q}} := \mathbf{M}_\Omega^{\frac{1}{2}} \mathbf{q} \neq \mathbf{0}$ . It follows from (3.52) that

$$\phi(q^2; \theta) = \frac{\mathbf{q}^\top \mathbf{M}_\Omega \mathbf{q}}{\mathbf{q}^\top (\theta \mathbf{M}_\Omega^x + (1 - \theta) \mathbf{M}_\Omega^y) \mathbf{q}} = \frac{\mathbf{q}^\top \mathbf{M}_\Omega \mathbf{q}}{\mathbf{q}^\top \mathbf{M}_\theta \mathbf{q}} = \frac{\|\widehat{\mathbf{q}}\|^2}{\widehat{\mathbf{q}}^\top \mathbf{M}_\Omega^{-\frac{1}{2}} \mathbf{M}_\theta \mathbf{M}_\Omega^{-\frac{1}{2}} \widehat{\mathbf{q}}}.$$

Therefore,

$$\begin{aligned} \phi^* \left( \theta, (\mathbb{V}^{\lfloor \frac{k}{2} \rfloor})^2 \right) &= \inf_{0 \neq q \in \mathbb{V}^{\lfloor \frac{k}{2} \rfloor}} \phi(q^2; \theta) = \inf_{\mathbf{0} \neq \mathbf{q} \in \mathbb{R}^D} \frac{\mathbf{q}^\top \mathbf{M}_\Omega \mathbf{q}}{\mathbf{q}^\top \mathbf{M}_\theta \mathbf{q}} = \inf_{\mathbf{0} \neq \widehat{\mathbf{q}} \in \mathbb{R}^D} \frac{\|\widehat{\mathbf{q}}\|^2}{\widehat{\mathbf{q}}^\top \mathbf{M}_\Omega^{-\frac{1}{2}} \mathbf{M}_\theta \mathbf{M}_\Omega^{-\frac{1}{2}} \widehat{\mathbf{q}}} \\ &= \left( \sup_{\mathbf{0} \neq \widehat{\mathbf{q}} \in \mathbb{R}^D} \frac{\widehat{\mathbf{q}}^\top \mathbf{M}_\Omega^{-\frac{1}{2}} \mathbf{M}_\theta \mathbf{M}_\Omega^{-\frac{1}{2}} \widehat{\mathbf{q}}}{\|\widehat{\mathbf{q}}\|^2} \right)^{-1} = \frac{1}{\left\| \mathbf{M}_\Omega^{-\frac{1}{2}} \mathbf{M}_\theta \mathbf{M}_\Omega^{-\frac{1}{2}} \right\|_2} = \phi(q_*^2; \theta). \end{aligned}$$

It implies  $\phi^* \left( \theta, (\mathbb{V}^{\lfloor \frac{k}{2} \rfloor})^2 \right)^{-1}$  is the largest eigenvalue of  $\mathbf{M}_\Omega^{-\frac{1}{2}} \mathbf{M}_\theta \mathbf{M}_\Omega^{-\frac{1}{2}}$ , consequently, is the largest root of characteristic polynomial

$$\det \left[ \lambda \mathbf{I} - \mathbf{M}_\Omega^{-\frac{1}{2}} \mathbf{M}_\theta \mathbf{M}_\Omega^{-\frac{1}{2}} \right] = 0$$

which is equivalent to

$$\det [\lambda \mathbf{M}_\Omega - \mathbf{M}_\theta] = 0.$$

Thus,  $\phi^* \left( \theta, (\mathbb{V}^{\lfloor \frac{k}{2} \rfloor})^2 \right)$  is the smallest real root of

$$\det [\mathbf{M}_\Omega - \phi \mathbf{M}_\theta] = 0.$$

The proof is completed.  $\square$

**3.7. More critical findings and geometric insights.** Based on extensive numerical experiments, we achieve two interesting findings, which are critical for further understanding, constructing, and verifying the 2D OCADs.

First, we discover that, for  $\mathbb{V}^k$  being either  $\mathbb{Q}^k$  or  $\mathbb{P}^k$ , the inequality (3.46) should be an equality.

**Conjecture 3.1.** *For  $\mathbb{V}^k$  being either  $\mathbb{Q}^k$  or  $\mathbb{P}^k$  with  $k \in \mathbb{N}_+$ , it holds that*

$$(3.55) \quad \bar{\omega}_*(\theta, \mathbb{V}^k) = \phi^*(\theta, \mathbb{V}_+^k) \quad \forall \theta \in [-1, 1],$$

and there always exists a critical positive polynomial for  $\phi^*(\theta, \mathbb{V}_+^k)$ .

Furthermore, we observe that there exists a critical positive polynomial in the squared form.

**Conjecture 3.2.** *For  $\mathbb{V}^k$  being either  $\mathbb{Q}^k$  or  $\mathbb{P}^k$  with  $k \in \mathbb{N}_+$ , it holds that*

$$\phi^*(\theta, \mathbb{V}_+^k) = \phi^*(\theta, (\mathbb{V}^{\lfloor \frac{k}{2} \rfloor})^2) := \inf_{q \in \mathbb{V}^{\lfloor \frac{k}{2} \rfloor}} \phi(q^2; \theta) \quad \forall \theta \in [-1, 1],$$

and there exists a critical positive polynomial  $p^* = q_*^2$  with  $q_* \in \mathbb{V}^{\lfloor \frac{k}{2} \rfloor} \setminus \{0\}$ .

We can show that for all the 2D OCADs found in this paper, the above two conjectures are true. More specifically, we will prove these two conjectures for the spaces  $\mathbb{Q}^k$  with any  $k \in \mathbb{N}_+$ , and for the spaces  $\mathbb{P}^k$  with  $1 \leq k \leq 7$ . Numerical evidence has demonstrated the validity of these conjectures for  $\mathbb{P}^k$  spaces with higher  $k \in \{8, 9, \dots, 15\}$ , although a rigorous analytical proof is not available yet. It is worth noting that if the optimality criteria in Theorems 3.25 to 3.27 work, then Conjecture 3.1 and 3.2 will get proved immediately.

For a given space  $\mathbb{V}^k$ , we define the following region

$$(3.56) \quad \mathbb{B}_\omega^* := \{(\bar{\omega}_1, \bar{\omega}_2) \in [0, 1]^2 : \langle p \rangle_\Omega - 2\bar{\omega}_1 \langle p \rangle_\Omega^x - 2\bar{\omega}_2 \langle p \rangle_\Omega^y \geq 0 \ \forall p \in \mathbb{V}_+^k\}.$$

**Theorem 3.30.** *For any given space  $\mathbb{V}^k$ , we have  $\mathbb{B}_\omega \subseteq \mathbb{B}_\omega^*$ . If Conjecture 3.1 holds true, then we further have  $\mathbb{B}_\omega = \mathbb{B}_\omega^*$ .*

*Proof.* For any  $(\bar{\omega}_1, \bar{\omega}_2) \in \mathbb{B}_\omega$ , there is a symmetric CAD with  $(\bar{\omega}_1, \bar{\omega}_2)$  as the boundary weights:

$$\langle p \rangle_\Omega = 2\bar{\omega}_1 \langle p \rangle_\Omega^x + 2\bar{\omega}_2 \langle p \rangle_\Omega^y + \sum_s \omega_s \overline{p(x^{(s)}, y^{(s)})}.$$

It follows that

$$\langle p \rangle_\Omega - 2\bar{\omega}_1 \langle p \rangle_\Omega^x - 2\bar{\omega}_2 \langle p \rangle_\Omega^y = \sum_s \overline{\omega_s p(x^{(s)}, y^{(s)})} \geq 0 \quad \forall p \in \mathbb{V}_+^k,$$

so that  $(\bar{\omega}_1, \bar{\omega}_2) \in \mathbb{B}_\omega^*$ . Hence  $\mathbb{B}_\omega \subseteq \mathbb{B}_\omega^*$ . On the other hand, if  $(\bar{\omega}_1, \bar{\omega}_2) \in \mathbb{B}_\omega^*$ , we define  $\bar{\omega}_1 = \frac{1}{2}\bar{\omega}(1 + \theta)$  and  $\bar{\omega}_2 = \frac{1}{2}\bar{\omega}(1 - \theta)$  with  $\theta \in [-1, 1]$ . Then  $\langle p \rangle_\Omega - \bar{\omega}[(1 + \theta)\langle p \rangle_\Omega^x + (1 - \theta)\langle p \rangle_\Omega^y] \geq 0$  for all  $p \in \mathbb{V}_+^k$ , which yields  $\bar{\omega} \leq \inf_{p \in \mathbb{V}_+^k} \phi(p; \theta) = \phi^*(\theta, \mathbb{V}_+^k) = \bar{\omega}_*(\theta, \mathbb{V}^k)$  if Conjecture 3.1 holds true. Thanks to the convexity of  $\mathbb{B}_\omega$ , we know that  $(\bar{\omega}_1, \bar{\omega}_2)$  is the boundary weights of a feasible symmetric CAD. That is,  $(\bar{\omega}_1, \bar{\omega}_2) \in \mathbb{B}_\omega$ , and  $\mathbb{B}_\omega = \mathbb{B}_\omega^*$ .  $\square$

Based on Theorem 3.30 and the OCADs found in Sections 4 and 5 later, we can visualize the region  $\mathbb{B}_\omega$  for several  $\mathbb{Q}^k$  and  $\mathbb{P}^k$  spaces, as shown in Figures 2 to 4. Based on the visualization results, we have the following important observations and insights from the geometric point of view:

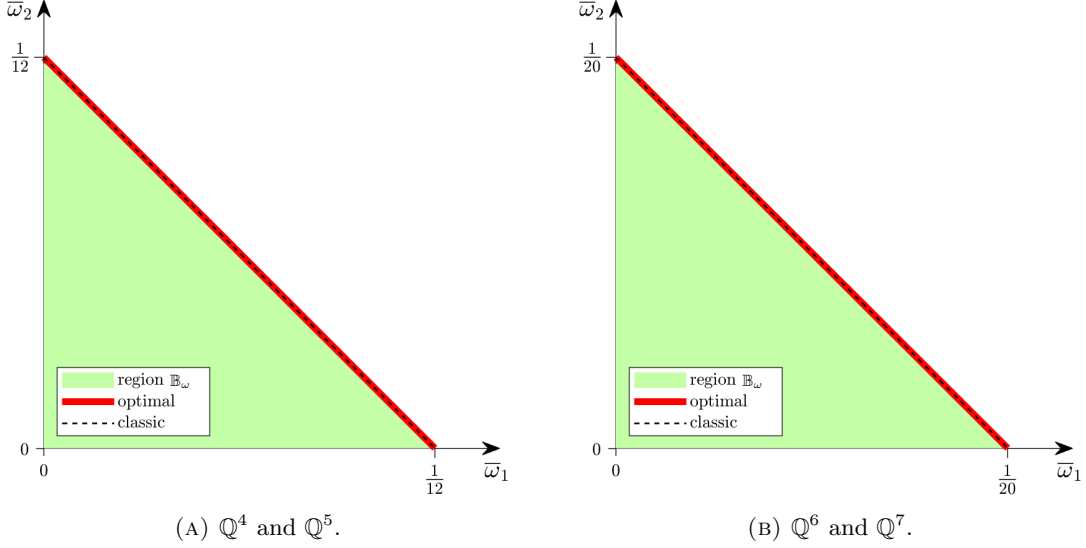


FIGURE 3. Geometric illustration of the region  $\mathbb{B}_\omega$ , the boundary weights of the classic CAD, the boundary weights of the OCAD for  $\mathbb{Q}^k$  spaces: the boundary weights of the classic CAD lies on  $\partial\mathbb{B}$  and coincide with the boundary weights of the OCAD.

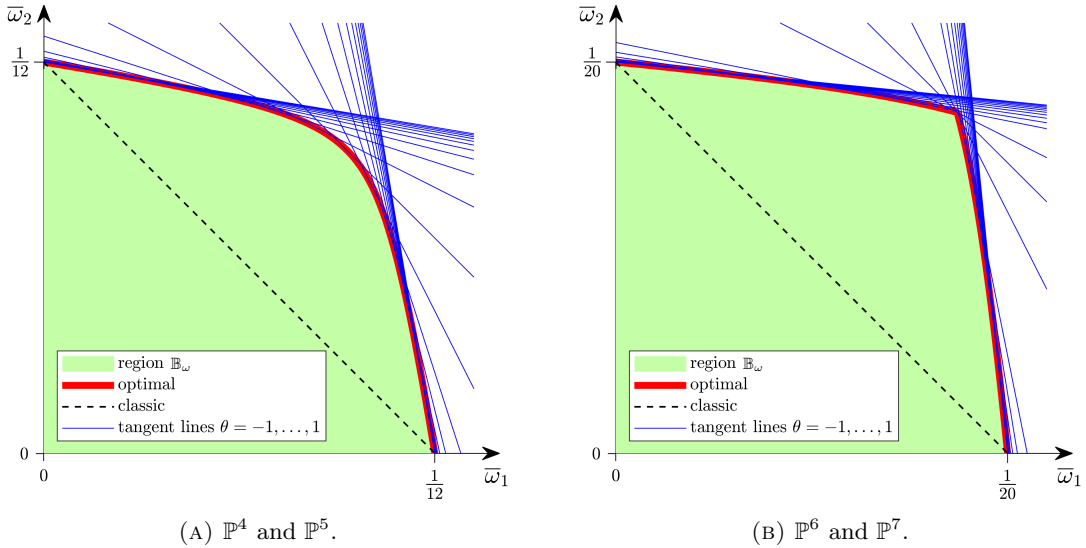


FIGURE 4. Geometric illustration of the region  $\mathbb{B}_\omega$ , the boundary weights of the classic CAD, the boundary weights of the OCAD for  $\mathbb{P}^k$  spaces. We also plot the straight lines  $\langle p^* \rangle_\Omega = 2\bar{\omega}_1 \langle p^* \rangle_\Omega^x + 2\bar{\omega}_2 \langle p^* \rangle_\Omega^y$  with  $p^*$  denoting the critical positive polynomial for different  $\theta = -1, -0.9, \dots, 1$ , which are exactly tangent to  $\partial\mathbb{B}_\omega$ .

- The region  $\mathbb{B}_\omega$  is compact, confirming the theoretical result in Lemma 3.3.
- The region  $\mathbb{B}_\omega$  is symmetric with respect to the line  $\bar{\omega}_1 = \bar{\omega}_2$ , validating the analysis in Lemma 3.17.
- The region  $\mathbb{B}_\omega$  is convex, confirming the theoretical result in Lemma 3.5. Any line segment connected two points in  $\mathbb{B}_\omega$  represents a convex combination of two feasible CADs. Consequently, the classic CAD is actually a convex combination of the two OCADs at  $\theta = \pm 1$ , as it will be proved in Remark 5.3.

- For the  $\mathbb{Q}^k$  spaces, we see from Figure 3 that the region  $\mathbb{B}_\omega$  is triangular in shape. Moreover, the boundary weights of the classic CAD lie on  $\partial\mathbb{B}_\omega$  and coincide with the boundary weights of OCAD, inferring the classic CAD is optimal for the  $\mathbb{Q}^k$  spaces as it will be proved in Section 4.
- For the  $\mathbb{P}^k$  spaces, we see from Figure 4 that the boundary weights of the classic CAD lie inside  $\mathbb{B}_\omega$  rather than on  $\partial\mathbb{B}_\omega$ , which implies that the classic CAD is feasible but indeed not optimal in general (except in the special cases of  $\theta = \pm 1$ ).
- Figure 4 displays the straight lines  $\langle p^* \rangle_\Omega = 2\bar{\omega}_1 \langle p^* \rangle_\Omega^x + 2\bar{\omega}_2 \langle p^* \rangle_\Omega^y$  with  $p^*$  denoting the critical positive polynomial for different  $\theta = -1, -0.9, \dots, 1$ . We find that these lines are exactly tangent to  $\partial\mathbb{B}_\omega$ . This finding is consistent with Theorem 3.30 and is closely related to the geometric quasilinearization proposed in [28] for convex regions.
- As shown in Figures 2b and 4, the region boundary  $\partial\mathbb{B}_\omega$  corresponding to OCADs is generally smooth, except at  $\theta = 0$  (namely,  $\bar{\omega}_1 = \bar{\omega}_2$ ) for  $\mathbb{P}^2, \mathbb{P}^3, \mathbb{P}^6$  and  $\mathbb{P}^7$  (more generally for  $\mathbb{P}^{4k+2}$  and  $\mathbb{P}^{4k+3}$  with  $k \in \mathbb{N}$ ). At the nonsmooth point on  $\partial\mathbb{B}_\omega$ , the tangent lines are clearly not unique. This indicates in these special cases, the OCADs and the critical positive polynomials (normalized with  $\langle p^* \rangle_\Omega = 1$ ) are both not unique (see Remarks 5.8 and 5.11).

#### 4. 2D OCAD FOR $\mathbb{Q}^k$ SPACES

With the help of Theorem 3.26, we now prove that the classic 2D CAD (1.14) is optimal for  $\mathbb{Q}^k$  with  $k \in \mathbb{N}_+$ . The 2D OCAD for  $\mathbb{P}^k$  is much more difficult and will be explored carefully in Section 5.

Recall that the classic CAD (1.14) is symmetric. It can be transformed onto the reference cell  $\Omega = [-1, 1]^2$  as

$$(4.1) \quad \begin{aligned} \langle p \rangle_\Omega &= \omega_1^{\text{GL}} [(1 + \theta) \langle p \rangle_\Omega^x + (1 - \theta) \langle p \rangle_\Omega^y] \\ &+ \frac{1 + \theta}{2} \sum_{\ell=2}^{L-1} \sum_{q=1}^Q \omega_\ell^{\text{GL}} \omega_q^{\text{G}} p(x_\ell^{\text{GL}}, y_q^{\text{G}}) + \frac{1 - \theta}{2} \sum_{\ell=2}^{L-1} \sum_{q=1}^Q \omega_\ell^{\text{GL}} \omega_q^{\text{G}} p(x_q^{\text{G}}, y_\ell^{\text{GL}}), \end{aligned}$$

where  $\{x_\ell^{\text{GL}}\}$  and  $\{y_\ell^{\text{GL}}\}$  denote the  $L$ -point Gauss–Lobatto quadrature nodes in the internal  $[-1, 1]$ ,  $\{x_q^{\text{G}}\}$  and  $\{y_q^{\text{G}}\}$  are the  $Q$ -point Gauss quadrature nodes in the internal  $[-1, 1]$ .

**Theorem 4.1.** *For any  $\theta \in [-1, 1]$  and the spaces  $\mathbb{Q}^k$  with any  $k \in \mathbb{N}_+$ , the classic 2D CAD (4.1) with  $L = \lceil \frac{k+3}{2} \rceil$  and  $Q \geq \frac{k+1}{2}$  is an OCAD, and Conjectures 3.1 and 3.2 hold true with*

$$(4.2) \quad \bar{\omega}_*(\theta, \mathbb{Q}^k) = \phi^*(\theta, \mathbb{Q}_+^k) = \phi^*(\theta, (\mathbb{Q}^{\lfloor \frac{k}{2} \rfloor})^2) = \omega_1^{\text{GL}} = \frac{1}{L(L-1)}.$$

*Proof.* Consider the polynomial

$$(4.3) \quad p^*(x, y) = q_*^2(x, y) \quad \text{with} \quad q_*(x, y) := \prod_{\ell=2}^{L-1} (x - x_\ell^{\text{GL}}) \cdot \prod_{\ell=2}^{L-1} (y - y_\ell^{\text{GL}}),$$

which vanishes at all the internal nodes of CAD (4.1). Besides, the degrees of  $q_*$  in  $x$  and  $y$  are both

$$L - 2 = \left\lceil \frac{k+3}{2} \right\rceil - 2 = \left\lceil \frac{k-1}{2} \right\rceil \leq \left\lfloor \frac{k}{2} \right\rfloor,$$

so that  $q_* \in \mathbb{Q}^{\lfloor \frac{k}{2} \rfloor}$  and  $p^* \in \mathbb{Q}^k$ . According to Theorem 3.26, we have (4.2),  $p^*$  is a critical positive polynomial for  $\phi^*(\theta, \mathbb{Q}_+^k)$ , and the classic CAD (4.1) is an OCAD for the space  $\mathbb{Q}^k$ .  $\square$

The internal nodes of the classic CAD (4.1) and the critical positive polynomial  $p^*$  are illustrated in Figure 5. Note that  $p^*$  lies in the space  $\mathbb{Q}^k$ , but does not belong to the space  $\mathbb{P}^k$ . Thus, the above proof does not imply that the CAD (4.1) is an OCAD for  $\mathbb{P}^k$ . As it will be shown in Section 5, solving the 2D OCAD problem for  $\mathbb{P}^k$  is much more complicated and challenging.

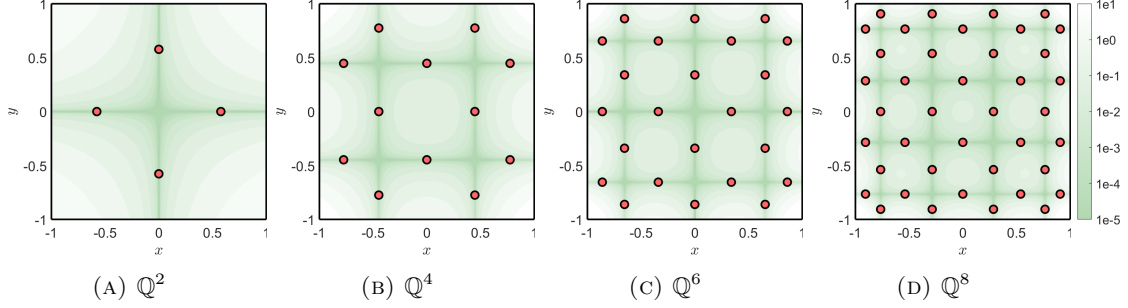


FIGURE 5. Internal nodes of the CAD (4.1) for polynomial spaces  $\mathbb{Q}^k$ ,  $k = 2, 4, 6, 8$ , with  $L = \lceil \frac{k+3}{2} \rceil$  and  $Q = \lceil \frac{k+1}{2} \rceil$ . In the background, each corresponding critical positive polynomial (4.3) is shown in the logarithmic scale.

## 5. 2D SYMMETRIC OCAD FOR $\mathbb{P}^k$ SPACES

In this section, we discuss the construction of the symmetric OCAD for  $\mathbb{P}^k$  with  $k \in \mathbb{N}_+$ . When  $k = 1$ , the following CAD on the reference cell  $\Omega = [-1, 1]^2$  is obviously the symmetric OCAD for  $\mathbb{P}^1$ :

$$\langle p \rangle_\Omega = \frac{1}{2} [(1 + \theta) \langle p \rangle_\Omega^x + (1 - \theta) \langle p \rangle_\Omega^y],$$

which is also the OCAD for  $\mathbb{Q}^1$ . However, when  $k \geq 2$ , the classic CAD (4.1) is generally not optimal for  $\mathbb{P}^k$ . Recently, the OCADs were found in [4] for  $\mathbb{P}^2$  and  $\mathbb{P}^3$ . For  $\mathbb{P}^k$  with higher degrees  $k \geq 4$ , the OCADs remain unknown yet, and their exploration is highly nontrivial and becomes our goal.

We will start our exploration of symmetric OCADs for three special  $\theta \in \{-1, 1, 0\}$  in Sections 5.1 and 5.2, and then study the symmetric OCADs for general  $\theta \in [-1, 1]$  in Section 5.3. The OCADs for the special  $\theta \in \{-1, 1, 0\}$  will also be helpful for establishing the near-optimal or quasi-optimal CADs for general  $\theta \in [-1, 1]$ ; see Section 6.

### 5.1. Symmetric OCAD for $\mathbb{P}^k$ and $\theta = \pm 1$ .

**Theorem 5.1.** *In case of  $\theta = -1$ , the following symmetric 2D CAD with  $L = \lceil \frac{k+3}{2} \rceil$  and  $Q \geq \frac{k+1}{2}$  is an OCAD on  $\Omega$  for  $\mathbb{P}^k$  with any  $k \in \mathbb{N}_+$ .*

$$(5.1) \quad \langle p \rangle_\Omega = 2\omega_1^{\text{GL}} \langle p \rangle_\Omega^y + \sum_{\ell=2}^{L-1} \sum_{q=1}^Q \omega_\ell^{\text{GL}} \omega_q^{\text{G}} p(x_q^{\text{G}}, y_\ell^{\text{GL}}).$$

In this case, Conjectures 3.1 and 3.2 hold true with

$$(5.2) \quad \bar{\omega}_*(-1, \mathbb{P}^k) = \phi^*(-1, \mathbb{P}_+^k) = \phi^*(-1, (\mathbb{P}^{\lfloor \frac{k}{2} \rfloor})^2) = \omega_1^{\text{GL}} = \frac{1}{L(L-1)}.$$

*Proof.* Consider the polynomial

$$(5.3) \quad p^*(x, y) = q_*^2(x, y) \quad \text{with} \quad q_*(x, y) := \prod_{\ell=2}^{L-1} (y - y_\ell^{\text{GL}}),$$

which vanishes at all the internal nodes of CAD (5.1). Besides, the degree of  $q_*$  in  $x$  is 0, and the degree of  $q_*$  in  $y$  is  $(L-2) = \lceil \frac{k-1}{2} \rceil \leq \lfloor \frac{k}{2} \rfloor$  so that  $q_* \in \mathbb{P}^{\lfloor \frac{k}{2} \rfloor}$ . According to Theorem 3.26, we have (5.2),  $p^*$  is a critical positive polynomial  $\phi^*(-1, \mathbb{P}_+^k)$ , and the CAD (4.1) is an OCAD for  $\mathbb{P}^k$  and  $\theta = -1$ .  $\square$

Based on Lemma 3.18 and Remark 3.19, we immediately obtain an OCAD for  $\theta = 1$ .

**Theorem 5.2.** *In case of  $\theta = 1$ , the following symmetric 2D CAD with  $L = \lceil \frac{k+3}{2} \rceil$  and  $Q \geq \frac{k+1}{2}$  is an OCAD on  $\Omega$  for  $\mathbb{P}^k$  with any  $k \in \mathbb{N}_+$ .*

$$(5.4) \quad \langle p \rangle_\Omega = 2\omega_1^{\text{GL}} \langle p \rangle_\Omega^x + \sum_{\ell=2}^{L-1} \sum_{q=1}^Q \omega_\ell^{\text{GL}} \omega_q^{\text{G}} p(x_\ell^{\text{GL}}, y_q^{\text{G}}).$$

In this case, Conjectures 3.1 and 3.2 hold true with

$$(5.5) \quad \bar{\omega}_*(1, \mathbb{P}^k) = \phi^*(1, \mathbb{P}_+^k) = \phi^*(1, (\mathbb{P}^{\lfloor \frac{k}{2} \rfloor})^2) = \omega_1^{\text{GL}} = \frac{1}{L(L-1)}.$$

*Remark 5.3.* Note that

$$(5.6) \quad \text{CAD (4.1)} = \frac{1+\theta}{2} \times \text{CAD (5.1)} + \frac{1-\theta}{2} \times \text{CAD (5.4)},$$

which implies the classic CAD (4.1) is actually a convex combination of the above two OCADs (5.1) and (5.4). In the special cases of  $\theta = \pm 1$ , the above OCADs (5.1) and (5.4) for  $\mathbb{P}^k$  coincide with the classic CAD (4.1), which is also optimal for  $\mathbb{Q}^k$ . However, unfortunately, in the cases of  $\theta \in (-1, 1)$ , the classic CAD (4.1) is no longer optimal for  $\mathbb{P}^k$ .

**5.2. Fully symmetric OCAD for  $\mathbb{P}^k$  and  $\theta = 0$ .** In this subsection, we focus on the case of  $\theta = 0$ , namely,  $a_1/\Delta x = a_2/\Delta y$ . In this case, there is a symmetric OCAD for  $\mathbb{P}^k$  in the form of

$$\langle p \rangle_\Omega = \bar{\omega}_*(0, \mathbb{P}^k) [\langle p \rangle_\Omega^x + \langle p \rangle_\Omega^y] + \sum_s \omega_s \overline{p(x^{(s)}, y^{(s)})}.$$

Then, according to Lemma 3.18 and Remark 3.19, the following symmetric CAD is also optimal for  $\mathbb{P}^k$  and  $\theta = 0$ :

$$\langle p \rangle_\Omega = \bar{\omega}_*(0, \mathbb{P}^k) [\langle p \rangle_\Omega^x + \langle p \rangle_\Omega^y] + \sum_s \omega_s \overline{p(y^{(s)}, x^{(s)})}.$$

Taking an average of the above two OCADs leads to a new fully symmetric OCAD:

$$(5.7) \quad \langle p \rangle_\Omega = \bar{\omega}_*(0, \mathbb{P}^k) [\langle p \rangle_\Omega^x + \langle p \rangle_\Omega^y] + \sum_s \frac{\omega_s}{2} \left[ \overline{p(x^{(s)}, y^{(s)})} + \overline{p(y^{(s)}, x^{(s)})} \right],$$

whose internal nodes are symmetric not only with respect to the  $x$ - and  $y$ -axes, but also with respect to  $x = y$  and  $x = -y$ . Such full symmetry is very helpful for finding the OCAD (5.7).

In order to precisely describe such fully symmetric structures, we can invoke the invariance with respect to the following full symmetric group of transformations:

$$(5.8) \quad \mathcal{G}_f := \left\{ \begin{array}{llll} (x, y) \mapsto (x, y), & (x, y) \mapsto (-x, y), & (x, y) \mapsto (x, -y), & (x, y) \mapsto (-x, -y) \\ (x, y) \mapsto (y, x), & (x, y) \mapsto (-y, x), & (x, y) \mapsto (y, -x), & (x, y) \mapsto (-y, -x) \end{array} \right\}.$$

Clearly, the reference cell  $\Omega = [-1, 1]^2$  is  $\mathcal{G}_f$ -invariant, namely,  $g(\Omega) = \Omega$  for all  $g \in \mathcal{G}_f$ . In addition, the space  $\mathbb{P}^k$  is  $\mathcal{G}_f$ -invariant, namely,

$$(5.9) \quad g(p) := p(g(x, y)) \in \mathbb{P}^k \quad \forall g \in \mathcal{G}_f.$$

**Definition 5.4.** ( $\mathcal{G}_f$ -invariant subspace) The polynomial space

$$\mathbb{P}^k(\mathcal{G}_f) := \{p \in \mathbb{P}^k : g(p) = p \ \forall g \in \mathcal{G}_f\}$$

is called the  $\mathcal{G}_f$ -invariant subspace of  $\mathbb{P}^k$ .

The OCAD in the form of (5.7) is called fully symmetric as its internal nodes form a  $\mathcal{G}_f$ -invariant set. The fully symmetric structure is helpful for reducing the feasibility requirement in condition (i) of Definition 1.3, as shown in the following lemma.

**Lemma 5.5.** *If a fully symmetric CAD (5.7) is feasible for the  $\mathcal{G}_f$ -invariant subspace  $\mathbb{P}^k(\mathcal{G}_f)$ , then it is feasible for  $\mathbb{P}^k$ .*

*Proof.* The proof is similar to that of Lemma 3.10 and is thus omitted.  $\square$



*Remark 5.6.* Note that the dimension of the subspace  $\mathbb{P}^k(\mathcal{G}_f)$  is typically much smaller than the dimension of  $\mathbb{P}^k$ . For example, for  $\mathbb{P}^3 = \text{span}\{1, x, y, x^2, xy, y^2, x^3, x^2y, xy^2, y^3\}$ , we have  $\mathbb{P}^3(\mathcal{G}_f) = \text{span}\{1, x^2 + y^2\}$ , and  $\dim \mathbb{P}^3(\mathcal{G}_f) = 2 \ll \dim \mathbb{P}^3 = 10$ . In general, by the invariant theory [8], the basis  $\mathbb{P}^k(\mathcal{G}_f)$  for  $k \in \mathbb{N}_+$  can be represented using  $x^2 + y^2$  and  $x^2y^2$ :

$$\mathbb{P}^k(\mathcal{G}_f) = \text{span} \left\{ (x^2y^2)^\alpha (x^2 + y^2)^\beta \mid 4\alpha + 2\beta \leq k, \alpha, \beta \in \mathbb{N} \right\}.$$

For example, for  $k = 2, 4, 6, 8$ , we have the following basis of  $\mathbb{P}^k(\mathcal{G}_f)$

$$\mathbb{P}^2(\mathcal{G}_f) = \text{span}\{1, x^2 + y^2\},$$

$$\mathbb{P}^4(\mathcal{G}_f) = \text{span}\{1, x^2 + y^2, (x^2 + y^2)^2, x^2y^2\},$$

$$\mathbb{P}^6(\mathcal{G}_f) = \text{span}\{1, x^2 + y^2, (x^2 + y^2)^2, x^2y^2, (x^2 + y^2)^3, (x^2 + y^2)x^2y^2\},$$

$$\mathbb{P}^8(\mathcal{G}_f) = \text{span}\{1, x^2 + y^2, (x^2 + y^2)^2, x^2y^2, (x^2 + y^2)^3, (x^2 + y^2)x^2y^2, (x^2 + y^2)^4, (x^2 + y^2)^2x^2y^2, x^4y^4\}.$$

It is clear that  $\dim \mathbb{P}^k(\mathcal{G}_f) \ll \dim \mathbb{P}^k = \frac{(k+2)(k+1)}{2}$ . Therefore, Lemma 5.5 greatly simplifies the feasibility requirement and will be very useful for seeking fully symmetric OCADs.

As shown in the following theorems, we have successfully found out the fully symmetric OCADs in the form of (5.7) for  $\theta = 0$  and  $\mathbb{P}^k$  spaces with  $2 \leq k \leq 7$ . With the help of Lemma 5.5, we will provide a general algorithm to numerically compute the fully symmetric OCADs (5.7) for  $\theta = 0$  and  $\mathbb{P}^k$  with higher  $k \geq 8$ .

**Theorem 5.7** (OCAD for  $\theta = 0$ ,  $\mathbb{P}^2$  and  $\mathbb{P}^3$ ). *In case of  $\theta = 0$ , the following fully symmetric CAD is an OCAD on  $\Omega$  for the spaces  $\mathbb{P}^2$  and  $\mathbb{P}^3$ :*

$$(5.10) \quad \langle p \rangle_\Omega = \frac{1}{4} [\langle p \rangle_\Omega^x + \langle p \rangle_\Omega^y] + \frac{1}{2} p(0, 0).$$

*In this case, Conjectures 3.1 and 3.2 hold true for  $2 \leq k \leq 3$  with*

$$(5.11) \quad \bar{\omega}_*(0, \mathbb{P}^k) = \phi^*(0, \mathbb{P}_+^k) = \phi^*(0, (\mathbb{P}^1)^2) = \frac{1}{4}, \quad k = 2, 3.$$

*Proof.* It can be verified that the fully symmetric CAD (5.10) is feasible for the  $\mathcal{G}_f$ -invariant subspace  $\mathbb{P}^2(\mathcal{G}_f) = \mathbb{P}^3(\mathcal{G}_f) = \text{span}\{1, x^2 + y^2\}$ . Thus, by Lemma 5.5, it is feasible for  $\mathbb{P}^2$  and  $\mathbb{P}^3$ . Both polynomials

$$(5.12) \quad p_1^*(x, y) = x^2 \quad \text{and} \quad p_2^*(x, y) = y^2$$

vanish at the internal node  $(0, 0)$ . Additionally, both  $p_1^*$  and  $p_2^*$  belong to  $(\mathbb{P}^1)^2$ . By Theorem 3.26, the fully symmetric CAD (5.10) is optimal for  $\mathbb{P}^2$  and  $\mathbb{P}^3$  spaces, and both  $p_1^*$  and  $p_2^*$  are the corresponding critical positive polynomials.  $\square$

*Remark 5.8.* As shown in (5.12), the critical positive polynomials for either  $\phi^*(0, \mathbb{P}_+^2)$  or  $\phi^*(0, \mathbb{P}_+^3)$  are not unique. In fact, there are infinitely many critical positive polynomials in this case, for example,  $(x + ty)^2$  for any  $t \in \mathbb{R}$ ,  $\alpha_1 x^2 + \alpha_2 y^2$  for any  $\alpha_1, \alpha_2 \in \mathbb{R}_+$ , as discussed in Lemma 3.23.

**Theorem 5.9** (OCAD for  $\theta = 0$ ,  $\mathbb{P}^4$  and  $\mathbb{P}^5$ ). *In case of  $\theta = 0$ , the following fully symmetric CAD is an OCAD on  $\Omega$  for the spaces  $\mathbb{P}^4$  and  $\mathbb{P}^5$ :*

$$(5.13) \quad \langle p \rangle_\Omega = \left( 2 - \frac{\sqrt{14}}{2} \right) [\langle p \rangle_\Omega^x + \langle p \rangle_\Omega^y] + \frac{5\sqrt{14} - 15}{7} p \left( \sqrt{\frac{7 - \sqrt{14}}{15}}, \sqrt{\frac{7 - \sqrt{14}}{15}} \right) \\ + \frac{\sqrt{14} - 3}{7} \left[ p \left( \sqrt{\frac{14 - 2\sqrt{14}}{15}}, 0 \right) + p \left( 0, \sqrt{\frac{14 - 2\sqrt{14}}{15}} \right) \right].$$

*In this case, Conjectures 3.1 and 3.2 hold true for  $4 \leq k \leq 5$  with*

$$(5.14) \quad \bar{\omega}_*(0, \mathbb{P}^k) = \phi^*(0, \mathbb{P}_+^k) = \phi^*(0, (\mathbb{P}^2)^2) = 2 - \frac{\sqrt{14}}{2}, \quad k = 4, 5.$$

*Proof.* It can be verified that the fully symmetric CAD (5.13) is feasible for the  $\mathcal{G}_f$ -invariant subspace  $\mathbb{P}^4(\mathcal{G}_f) = \mathbb{P}^5(\mathcal{G}_f) = \text{span}\{1, x^2 + y^2, (x^2 + y^2)^2, x^2y^2\}$ . Thus, by Lemma 5.5, it is feasible for  $\mathbb{P}^4$  and  $\mathbb{P}^5$ . The polynomial

$$(5.15) \quad p^*(x, y) = q_\star^2(x, y) \quad \text{with} \quad q_\star(x, y) := x^2 + y^2 - \frac{14 - 2\sqrt{14}}{15}$$

vanishes at all the internal nodes. By Theorem 3.26, the fully symmetric CAD (5.13) is optimal for  $\mathbb{P}^4$  and  $\mathbb{P}^5$ , and  $p^*$  is the corresponding critical positive polynomial.  $\square$

**Theorem 5.10** (OCAD for  $\theta = 0$ ,  $\mathbb{P}^6$  and  $\mathbb{P}^7$ ). *In case of  $\theta = 0$ , the following fully symmetric CAD is an OCAD on  $\Omega$  for the spaces  $\mathbb{P}^6$  and  $\mathbb{P}^7$ :*

$$(5.16) \quad \langle p \rangle_\Omega = \left(1 - \frac{\sqrt{30}}{6}\right) [\langle p \rangle_\Omega^x + \langle p \rangle_\Omega^y] + \frac{875\sqrt{30} - 3125}{4563} p \left( \sqrt{\frac{3}{5} - \frac{\sqrt{30}}{25}}, \sqrt{\frac{3}{5} - \frac{\sqrt{30}}{25}} \right) \\ + \frac{343\sqrt{30} - 1225}{4563} \left[ p \left( \sqrt{\frac{6}{7} - \frac{2\sqrt{30}}{35}}, 0 \right) + p \left( 0, \sqrt{\frac{6}{7} - \frac{2\sqrt{30}}{35}} \right) \right] + \frac{1012 - 40\sqrt{30}}{4563} p(0, 0).$$

In this case, Conjectures 3.1 and 3.2 hold true for  $6 \leq k \leq 7$  with

$$(5.17) \quad \bar{\omega}_\star(0, \mathbb{P}^k) = \phi^\star(0, \mathbb{P}_+^k) = \phi^\star(0, (\mathbb{P}^3)^2) = 1 - \frac{\sqrt{30}}{6}, \quad k = 6, 7.$$

*Proof.* It can be verified that the fully symmetric CAD (5.16) is feasible for the  $\mathcal{G}_f$ -invariant subspace  $\mathbb{P}^6(\mathcal{G}_f) = \mathbb{P}^7(\mathcal{G}_f) = \text{span}\{1, x^2 + y^2, (x^2 + y^2)^2, x^2y^2, (x^2 + y^2)^3, (x^2 + y^2)x^2y^2\}$ . Thus, by Lemma 5.5, it is feasible for  $\mathbb{P}^6$  and  $\mathbb{P}^7$ . Both polynomials

$$(5.18) \quad p_1^\star(x, y) = y^2 \left(15x^2 + 35y^2 + 2\sqrt{30} - 30\right)^2 \quad \text{and} \quad p_2^\star(x, y) = x^2 \left(35x^2 + 15y^2 + 2\sqrt{30} - 30\right)^2$$

vanish at all the internal nodes of CAD (5.16). Additionally, both  $p_1^\star$  and  $p_2^\star$  belong to  $(\mathbb{P}^3)^2$ , thus belong to  $\mathbb{P}_+^6$  and  $\mathbb{P}_+^7$ . By Theorem 3.26, the fully symmetric CAD (5.16) is optimal for  $\mathbb{P}^6$  and  $\mathbb{P}^7$ , and both  $p_1^\star$  and  $p_2^\star$  are the corresponding critical positive polynomials.  $\square$

*Remark 5.11.* One can add  $p_1^\star$  and  $p_2^\star$  in (5.12) (or (5.18)), resulting in a new critical positive polynomial, which is  $\mathcal{G}_f$ -invariant. In Figure 6, we plot the internal nodes and the critical polynomial with such a symmetry for  $\mathbb{P}^2$  to  $\mathbb{P}^7$  spaces. We observe that the internal nodes of our OCADs are much fewer than those of the classic CAD (4.1).

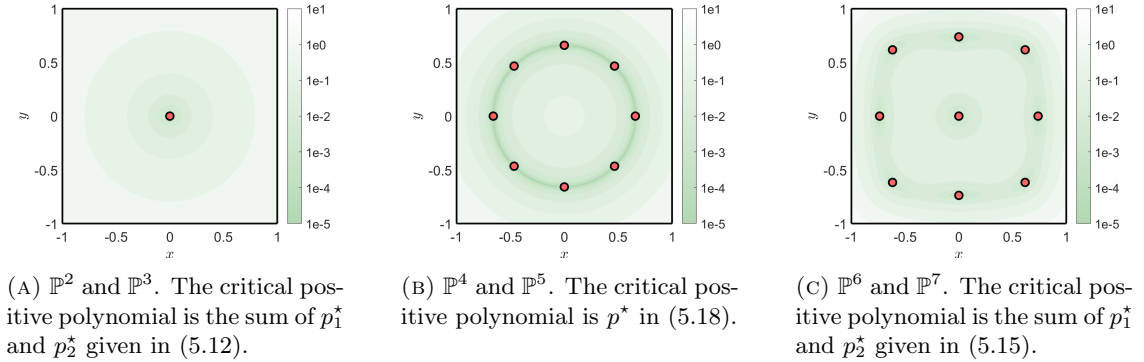


FIGURE 6. Internal nodes of the fully symmetric OCADs for  $\theta = 0$  and  $\mathbb{P}^k$  spaces with  $2 \leq k \leq 7$ . The background also displays the corresponding critical positive polynomials.

As the degree  $k$  increases, it becomes more and more difficult to find the analytical form of the fully symmetric OCADs, even in the special case of  $\theta = 0$ . We propose the following general theorem, based on which we can numerically seek the fully symmetric OCADs for  $\mathbb{P}^k$  spaces with  $k \geq 8$  (Appendix C).

**Theorem 5.12.** *For any given  $k \in \mathbb{N}_+$ , let  $q_*(x, y) \in \mathbb{P}^{\lfloor \frac{k}{2} \rfloor}$  be the polynomial defined in (3.54). If there exist  $\{(\omega_s, x^{(s)}, y^{(s)}) : \omega_s > 0, 0 \leq y^{(s)} \leq x^{(s)} \leq 1\}_{s=1}^S$  satisfying the following system*

$$(5.19) \quad \begin{cases} q_*(x^{(s)}, y^{(s)}) = 0, \\ \langle g_i \rangle_\Omega = 2\phi^*(0, (\mathbb{P}^{\lfloor \frac{k}{2} \rfloor})^2) \langle g_i \rangle_\Omega^x + \sum_{s=1}^S \omega_s g_i(x^{(s)}, y^{(s)}), \quad 1 \leq i \leq \dim(\mathbb{P}^k(\mathcal{G}_f)) \end{cases}$$

with  $\{g_i\}$  being a basis of  $\mathbb{P}^k(\mathcal{G}_f)$ , then the following CAD

$$(5.20) \quad \langle p \rangle_\Omega = \phi^*(0, (\mathbb{P}^{\lfloor \frac{k}{2} \rfloor})^2) [\langle p \rangle_\Omega^x + \langle p \rangle_\Omega^y] + \sum_{s=1}^S \frac{\omega_s}{2} [\overline{p(x^{(s)}, y^{(s)})} + \overline{p(y^{(s)}, x^{(s)})}]$$

is a fully symmetric OCAD for  $\theta = 0$  and  $\mathbb{P}^k$ . Furthermore, in this case, Conjectures 3.1 and 3.2 hold true with

$$(5.21) \quad \bar{\omega}_*(0, \mathbb{P}^k) = \phi^*(0, \mathbb{P}_+^k) = \phi^*(0, (\mathbb{P}^{\lfloor \frac{k}{2} \rfloor})^2) = \phi(q_*^2; 0),$$

and  $q_*^2(x, y)$  is the critical positive polynomial for  $\phi^*(0, \mathbb{P}_+^k)$ .

*Proof.* Due to the symmetry of  $g_i \in \mathbb{P}^k(\mathcal{G}_f)$ , it satisfies

$$g_i(x^{(s)}, y^{(s)}) = \overline{g_i(x^{(s)}, y^{(s)})} = \overline{g_i(y^{(s)}, x^{(s)})} \quad 1 \leq s \leq S.$$

and  $\langle g_i \rangle_\Omega^x = \langle g_i \rangle_\Omega^y$ . Thus, (5.19) implies

$$(5.22) \quad \langle g_i \rangle_\Omega = \phi^*(0, (\mathbb{P}^{\lfloor \frac{k}{2} \rfloor})^2) [\langle g_i \rangle_\Omega^x + \langle g_i \rangle_\Omega^y] + \sum_{s=1}^S \frac{\omega_s}{2} [\overline{g_i(x^{(s)}, y^{(s)})} + \overline{g_i(y^{(s)}, x^{(s)})}]$$

for all  $1 \leq i \leq \dim(\mathbb{P}^k(\mathcal{G}_f))$ . Since  $\{g_i\}$  are a basis of  $\mathbb{P}^k(\mathcal{G}_f)$ , the decomposition (5.20) holds for any  $g \in \mathbb{P}^k(\mathcal{G}_f)$ . Thanks to Lemma 5.5, the fully symmetric CAD (5.20) is feasible for  $\mathbb{P}^k$ . Next, we verify the optimality of the CAD (5.20). Because  $\{(\omega_s, x^{(s)}, y^{(s)})\}_{s=1}^S$  satisfy (5.19), the polynomial  $q_*^2 \in \mathbb{P}^k$  vanishes at all the internal nodes of the CAD (5.20). By Theorem 3.26, the CAD (5.20) is optimal for  $\theta = 0$  and  $\mathbb{P}^k$ , and  $q_*^2(x, y)$  is the critical positive polynomial for  $\phi^*(0, \mathbb{P}_+^k)$ .  $\square$

When  $k \geq 8$ , it become very difficult to find the analytical solution to the system (5.19) or to rigorously prove the existence of its solution. Nevertheless, we can always construct the fully symmetric OCAD (5.22) by numerically solving the equations (5.19) using an iterative method. The readers are referred to Appendix C for the fully symmetric OCADs we found for  $\mathbb{P}^k$  spaces with  $8 \leq k \leq 15$ .

**5.3. Symmetric OCADs for  $\mathbb{P}^k$  and general  $\theta \in [-1, 1]$ .** In this subsection, we discuss the symmetric OCADs for  $\mathbb{P}^k$  and general  $\theta \in [-1, 1]$ . Seeking OCADs for general  $\theta$  is much more difficult than it for the three special cases in the previous subsections. As shown in the following theorems, we have successfully found out the analytical formulas of the symmetric OCADs for  $\mathbb{P}^k$  spaces with  $k \leq 7$ , which cover the widely used polynomial spaces. We will also provide a general algorithm to numerically compute the symmetric OCADs for general  $\theta \in [-1, 1]$  and  $\mathbb{P}^k$  with higher degree  $k \geq 8$ .

**Theorem 5.13** (OCAD for  $\mathbb{P}^2$  and  $\mathbb{P}^3$ ). *For any  $\theta \in [-1, 1]$ , the 2D symmetric OCAD on  $\Omega$  for  $\mathbb{P}^2$  and  $\mathbb{P}^3$  spaces is given by*

$$(5.23) \quad \langle p \rangle_\Omega = \bar{\omega}_* \left[ (1 + \theta) \langle p \rangle_\Omega^x + (1 - \theta) \langle p \rangle_\Omega^y \right] + \omega_1 \overline{p(x^{(1)}, y^{(1)})}$$

with

$$(5.24) \quad \bar{\omega}_* = \frac{1}{4 + 2|\theta|}, \quad \omega_1 = \frac{1 + |\theta|}{2 + |\theta|}, \quad (x^{(1)}, y^{(1)}) = \begin{cases} \left( \sqrt{\frac{2|\theta|}{3 + 3|\theta|}}, 0 \right) & \text{if } \theta \in [-1, 0], \\ \left( 0, \sqrt{\frac{2|\theta|}{3 + 3|\theta|}} \right) & \text{if } \theta \in [0, 1]. \end{cases}$$

Moreover, Conjectures 3.1 and 3.2 hold true for all  $\theta \in [-1, 1]$  and  $2 \leq k \leq 3$  with

$$(5.25) \quad \bar{\omega}_*(\theta, \mathbb{P}^k) = \phi^*(\theta, \mathbb{P}_+^k) = \phi^*(\theta, (\mathbb{P}^1)^2) = \frac{1}{4 + 2|\theta|}, \quad k = 2, 3.$$

*Proof.* It is easy to verify that the symmetric CAD (5.23) is feasible for the  $\mathcal{G}_s$ -invariant subspace  $\mathbb{P}^2(\mathcal{G}_s) = \mathbb{P}^3(\mathcal{G}_s) = \text{span}\{1, x^2, y^2\}$ . Thus by Lemma 3.10, it is feasible for  $\mathbb{P}^2$  and  $\mathbb{P}^3$  spaces. In case of  $\theta \in [-1, 0]$ , the nonnegative polynomial  $p^*(x, y) = y^2$  belong to  $(\mathbb{P}^1)^2$ , thus is in both  $\mathbb{P}_+^2$  and  $\mathbb{P}_+^3$ . Furthermore,  $p^*$  vanishes at all the internal nodes given in (5.24). By Theorem 3.26, the symmetric CAD (5.23) is optimal for both  $\mathbb{P}^2$  and  $\mathbb{P}^3$  spaces when  $\theta \in [-1, 0]$ , and (5.25) holds for all  $\theta \in [-1, 0]$  and  $2 \leq k \leq 3$ . By Lemma 3.18, the CAD (5.23) is also optimal when  $\theta \in [0, 1]$ . The proof is completed.  $\square$

*Remark 5.14.* For comparison, Table 2 illustrates our symmetric OCAD (5.23) and the classic CAD (4.1). We clearly see that the OCAD (5.23) involves much fewer internal nodes than the classic CAD. It is worth mentioning that the symmetric OCAD (5.23) is consistent with the OCAD derived in our previous paper [4], where only the OCAD for  $\mathbb{P}^2$  and  $\mathbb{P}^3$  spaces was found.

**Theorem 5.15** (OCAD for  $\mathbb{P}^4$  and  $\mathbb{P}^5$ ). *For any  $\theta \in [-1, 1]$ , the 2D symmetric OCAD on  $\Omega$  for  $\mathbb{P}^4$  and  $\mathbb{P}^5$  spaces is given by*

$$(5.26) \quad \langle p \rangle_\Omega = \bar{\omega}_* [(1 + \theta) \langle p \rangle_\Omega^x + (1 - \theta) \langle p \rangle_\Omega^y] + \omega_1 \overline{p(x^{(1)}, y^{(1)})} + \omega_2 \overline{p(x^{(2)}, y^{(2)})}$$

with

$$(5.27a) \quad \bar{\omega}_* = \left[ \frac{14}{3} + \frac{2}{3} \sqrt{78\theta^2 + 46} \cos \left( \frac{1}{3} \arccos \frac{1476\theta^2 - 244}{(78\theta^2 + 46)^{\frac{3}{2}}} \right) \right]^{-1},$$

$$(5.27b) \quad \omega_1 = \frac{5(1 - 4\bar{\omega}_* + 2|\theta|\bar{\omega}_*)^2}{9(1 - 6\bar{\omega}_* + 4|\theta|\bar{\omega}_*)}, \quad \omega_2 = 1 - 2\bar{\omega}_* - \omega_1,$$

$$(5.27c) \quad (x^{(1)}, y^{(1)}) = \begin{cases} \left( \sqrt{\frac{3(1 - 6\bar{\omega}_* + 4|\theta|\bar{\omega}_*)}{5(1 - 4\bar{\omega}_* + 2|\theta|\bar{\omega}_*)}}, \sqrt{\frac{1 - 6\bar{\omega}_*}{3(1 - 4\bar{\omega}_* + 2|\theta|\bar{\omega}_*)}} \right) & \text{if } \theta \in [-1, 0], \\ \left( \sqrt{\frac{1 - 6\bar{\omega}_*}{3(1 - 4\bar{\omega}_* + 2|\theta|\bar{\omega}_*)}}, \sqrt{\frac{3(1 - 6\bar{\omega}_* + 4|\theta|\bar{\omega}_*)}{5(1 - 4\bar{\omega}_* + 2|\theta|\bar{\omega}_*)}} \right) & \text{if } \theta \in [0, 1], \end{cases}$$

$$(5.27d) \quad (x^{(2)}, y^{(2)}) = \begin{cases} \left( 0, \sqrt{\frac{1 - 4\bar{\omega}_* - 2|\theta|\bar{\omega}_* - 3\omega_1(y^{(1)})^2}{3\omega_2}} \right) & \text{if } \theta \in [-1, 0], \\ \left( \sqrt{\frac{1 - 4\bar{\omega}_* - 2|\theta|\bar{\omega}_* - 3\omega_1(x^{(1)})^2}{3\omega_2}}, 0 \right) & \text{if } \theta \in [0, 1]. \end{cases}$$

Moreover, Conjectures 3.1 and 3.2 hold true for all  $\theta \in [-1, 1]$  and  $4 \leq k \leq 5$ .

For better readability, we put the proof of Theorem 5.15 in Appendix A. The weights and nodes (5.27a)–(5.27d) are illustrated in Figure 7, which clearly verifies the feasibility conditions (ii) and (iii) in Definition 1.3.

*Remark 5.16.* For comparison, Table 2 illustrates our symmetric OCAD (5.26) and the classic CAD (4.1). We clearly see that the OCAD (5.26) involves much fewer internal nodes than the classic CAD.

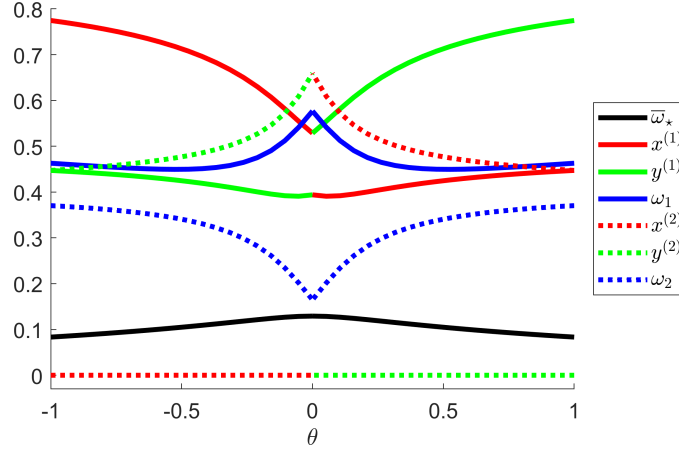


FIGURE 7. The boundary weight  $\bar{\omega}_*$ , internal weights  $\{\omega_s\}$  and internal nodes  $(x^{(s)}, y^{(s)})$  of the symmetric OCAD (5.26) for  $\theta \in [-1, 1]$ .

We have also found out the 2D symmetric OCAD (5.28) for  $\mathbb{P}^6$  and  $\mathbb{P}^7$  spaces, whose discovery is highly nontrivial; see Theorem 5.17.

**Theorem 5.17.** *For any  $\theta \in [-1, 1]$ , the 2D symmetric OCAD on  $\Omega$  for  $\mathbb{P}^6$  and  $\mathbb{P}^7$  spaces is given by*

$$(5.28) \quad \langle p \rangle_\Omega = \bar{\omega}_* [(1 + \theta) \langle p \rangle_\Omega^x + (1 - \theta) \langle p \rangle_\Omega^y] + \sum_{s=1}^4 \omega_s p(x^{(s)}, y^{(s)}).$$

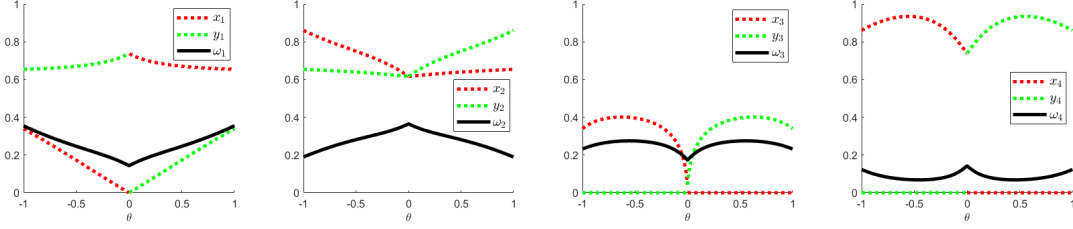
The boundary weight is given by

$$(5.29) \quad \bar{\omega}_* = \left[ 2|\theta| + \frac{20}{3} + \frac{2}{3} \sqrt{126\theta^2 + 96|\theta| + 94} \cos \left( \frac{1}{3} \arccos \frac{864|\theta|^3 + 2916\theta^2 + 288|\theta| - 532}{(126\theta^2 + 96|\theta| + 94)^{\frac{3}{2}}} \right) \right]^{-1}.$$

The coordinates and the weights of internal nodes # 1 and # 2 are given by

$$(5.30) \quad (x^{(1)}, y^{(1)}, \omega_1) = \begin{cases} \left( \sqrt{\frac{m_{22} - \sqrt{\frac{(1-\beta_1)\beta_2}{\beta_1}}}}{m_{02}}}, \sqrt{\frac{m_{04} + \sqrt{\frac{(1-\beta_1)\beta_3}{\beta_1}}}}{m_{02}}}, \frac{\beta_1 m_{02}}{(y^{(1)})^2} \right), & \text{if } \theta \in [-1, 0], \\ \left( \sqrt{\frac{m_{40} + \sqrt{\frac{(1-\beta_1)\beta_2}{\beta_1}}}}{m_{20}}}, \sqrt{\frac{m_{22} - \sqrt{\frac{(1-\beta_1)\beta_3}{\beta_1}}}}{m_{20}}}, \frac{\beta_1 m_{20}}{(x^{(1)})^2} \right), & \text{if } \theta \in [0, 1], \end{cases}$$

$$(5.31) \quad (x^{(2)}, y^{(2)}, \omega_2) = \begin{cases} \left( \sqrt{\frac{m_{22} + \sqrt{\frac{\beta_1\beta_2}{1-\beta_1}}}}{m_{02}}}, \sqrt{\frac{m_{04} - \sqrt{\frac{\beta_1\beta_3}{1-\beta_1}}}}{m_{02}}}, \frac{(1-\beta_1)m_{02}}{(y^{(2)})^2} \right), & \text{if } \theta \in [-1, 0], \\ \left( \sqrt{\frac{m_{40} - \sqrt{\frac{\beta_1\beta_2}{1-\beta_1}}}}{m_{20}}}, \sqrt{\frac{m_{22} + \sqrt{\frac{\beta_1\beta_3}{1-\beta_1}}}}{m_{20}}}, \frac{(1-\beta_1)m_{20}}{(x^{(2)})^2} \right), & \text{if } \theta \in [0, 1] \end{cases}$$

FIGURE 8. The weights and the internal nodes of the OCAD (5.28) for  $\theta \in [-1, 1]$ .

with

$$(5.32) \quad (\beta_1, \beta_2, \beta_3) = \begin{cases} \left( 1 - \frac{m_{22}^2}{m_{42}m_{02}} + \frac{\sqrt{30}+2}{36}\theta^2, m_{42}m_{02} - m_{22}^2, m_{06}m_{02} - m_{04}^2 \right) & \text{if } \theta \in [-1, 0], \\ \left( 1 - \frac{m_{22}^2}{m_{24}m_{02}} + \frac{\sqrt{30}+2}{36}\theta^2, m_{60}m_{20} - m_{40}^2, m_{24}m_{20} - m_{22}^2 \right) & \text{if } \theta \in [0, 1], \end{cases}$$

and

$$m_{ij} = \frac{1}{(i+1)(j+1)} - \bar{\omega}_* \left[ \frac{1+\theta}{1+j} + \frac{1-\theta}{1+i} \right], \quad i, j = 0, 2, 4, 6, \quad i+j \leq 6.$$

The weights and the coordinates of internal nodes # 3 and # 4 are given by

$$(5.33) \quad \omega_3 = \frac{m_0}{2} \left( 1 + \frac{\beta_4}{\sqrt{\beta_4^2 + 4}} \right), \quad \omega_4 = \frac{m_0}{2} \left( 1 - \frac{\beta_4}{\sqrt{\beta_4^2 + 4}} \right),$$

(5.34)

$$(x_3, y_3, x_4, y_4) = \begin{cases} \left( \left( \sqrt{\frac{m_2}{m_0} - \frac{\sqrt{\omega_4}}{\omega_3} \frac{\sqrt{m_4 m_0 - m_2^2}}{m_0}}, 0, \sqrt{\frac{m_2}{m_0} + \frac{\sqrt{\omega_3}}{\omega_4} \frac{\sqrt{m_4 m_0 - m_2^2}}{m_0}}, 0 \right) & \text{if } \theta \in [-1, 0], \\ \left( 0, \sqrt{\frac{m_2}{m_0} - \frac{\sqrt{\omega_4}}{\omega_3} \frac{\sqrt{m_4 m_0 - m_2^2}}{m_0}}, 0, \sqrt{\frac{m_2}{m_0} + \frac{\sqrt{\omega_3}}{\omega_4} \frac{\sqrt{m_4 m_0 - m_2^2}}{m_0}} \right) & \text{if } \theta \in [0, 1] \end{cases}$$

with

$$\beta_4 = \frac{m_6 m_0^2 - 3m_4 m_2 m_0 + 2m_2^3}{(m_4 m_0 - m_2^2)^{3/2}},$$

$$m_k = \begin{cases} m_{k0} - \omega_1 (x^{(1)})^k - \omega_2 (x^{(2)})^k, & \text{if } \theta \in [-1, 0], \\ m_{0k} - \omega_1 (y^{(1)})^k - \omega_2 (y^{(2)})^k, & \text{if } \theta \in [0, 1], \end{cases} \quad k = 0, 2, 4, 6.$$

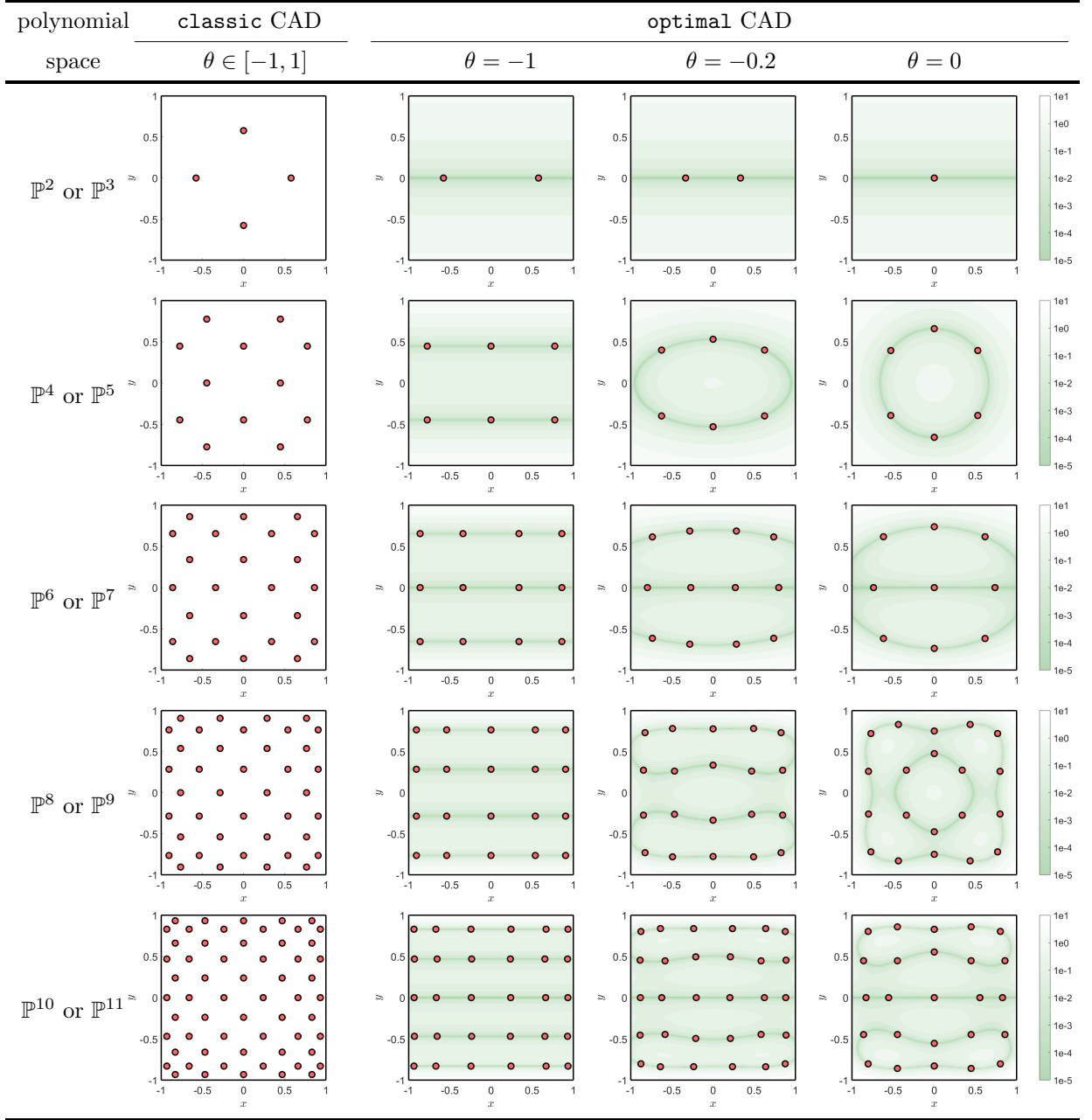
Moreover, Conjectures 3.1 and 3.2 hold true for all  $\theta \in [-1, 1]$  and  $6 \leq k \leq 7$ .

For better readability, we put the proof of Theorem 5.17 in Appendix B. The weights and nodes (5.29)–(5.34) are illustrated in Figure 8, which clearly verifies the feasibility conditions (ii) and (iii) in Definition 1.3.

*Remark 5.18.* For comparison, Table 2 illustrates our symmetric OCAD (5.28) and the classic CAD (4.1). We clearly see that the OCAD (5.28) involves much fewer internal nodes than the classic CAD. As  $\theta \rightarrow 0$ , the symmetric OCAD (5.28) converges to the fully symmetric OCAD in (5.16), for which the critical positive polynomial is not unique (as it was explained in Figure 4b due to the non-smoothness of  $\partial\mathbb{B}_\omega$ ).

We have derived the explicit formulas of OCADs for  $\mathbb{P}^2$  to  $\mathbb{P}^7$  spaces. However, for  $\mathbb{P}^k$  spaces with  $k \geq 8$ , seeking the analytical form of the OCADs for general  $\theta \in [-1, 1]$  is very challenging (if not impossible). In the following, we propose a systematic approach to numerically construct OCADs for higher  $k \geq 8$ .

TABLE 2. Internal nodes of the OCADs (for  $\theta = -1, -0.2, 0$ ) and the classic CAD for  $\mathbb{P}^k$ ,  $k = 2, \dots, 11$ . The critical polynomials of the OCADs are also displayed.



**Theorem 5.19.** For any given  $k \in \mathbb{N}_+$  and  $\theta \in [-1, 1]$ , let  $q_\star(x, y) \in \mathbb{P}^{\lfloor \frac{k}{2} \rfloor}$  be the polynomial defined in (3.54). If there exist  $\{(\omega_s, x^{(s)}, y^{(s)}) : \omega_s > 0, x^{(s)}, y^{(s)} \in [0, 1]\}_{s=1}^S$  satisfying the following system

$$(5.35) \quad \begin{cases} q_\star(x^{(s)}, y^{(s)}) = 0, \\ \langle g_i \rangle_\Omega = \phi^\star(\theta, (\mathbb{P}^{\lfloor \frac{k}{2} \rfloor})^2) \left[ (1 + \theta) \langle g_i \rangle_\Omega^x + (1 - \theta) \langle g_i \rangle_\Omega^y \right] + \sum_{s=1}^S \omega_s \overline{g_i(x^{(s)}, y^{(s)})}, \quad 1 \leq i \leq \dim(\mathbb{P}^k(\mathcal{G}_s)) \end{cases}$$

with  $\{g_i\}$  being a basis of  $\mathbb{P}^k(\mathcal{G}_s)$ , then the following symmetric CAD

$$(5.36) \quad \langle p \rangle_\Omega = \phi^*(\theta, (\mathbb{P}^{\lfloor \frac{k}{2} \rfloor})^2) \left[ (1 + \theta) \langle p \rangle_\Omega^x + (1 - \theta) \langle p \rangle_\Omega^y \right] + \sum_{s=1}^S \overline{\omega_s p(x^{(s)}, y^{(s)})}$$

is an OCAD for  $\mathbb{P}^k$  and  $\theta \in [-1, 1]$ . Furthermore, in this case, Conjectures 3.1 and 3.2 hold true with

$$(5.37) \quad \bar{\omega}_*(\theta, \mathbb{P}^k) = \phi^*(\theta, \mathbb{P}_+^k) = \phi^*(\theta, (\mathbb{P}^{\lfloor \frac{k}{2} \rfloor})^2) = \phi(q_*^2; \theta),$$

and  $q_*^2(x, y)$  is the critical positive polynomial for  $\phi^*(\theta, \mathbb{P}_+^k)$ .

*Proof.* Since  $\{g_i\}$  are a basis of  $\mathbb{P}^k(\mathcal{G}_s)$ , the decomposition (5.36) holds for any  $g \in \mathbb{P}^k(\mathcal{G}_s)$ . Thanks to Lemma 3.10, the symmetric CAD (5.36) is feasible for  $\mathbb{P}^k$ . Because the non-negative polynomial  $q_*^2 \in \mathbb{P}^{\lfloor \frac{k}{2} \rfloor}$  vanishes at all the internal nodes of (5.36), the CAD (5.36) is optimal for  $\mathbb{P}^k$  according to Theorem 3.26. Moreover,  $\bar{\omega}_*(\theta, \mathbb{P}^k) = \phi^*(\theta, (\mathbb{P}^{\lfloor \frac{k}{2} \rfloor})^2)$ , which implies the validity of Conjectures 3.1 and 3.2.  $\square$

Yet, when  $k \geq 8$ , we cannot find the analytical solution to the system (5.35) nor rigorously prove the existence of its solution. Based on Theorem 5.19, we propose the following algorithm for constructing the OCAD (5.22) by numerically solving the equations (5.35).

**Algorithm 5.20.** For  $\theta \in (-1, 1)$  and  $k \geq 8$ , the symmetric OCAD for  $\mathbb{P}^k$  space can be obtained via the following steps:

- (1) Calculate the value of  $\phi^*(\theta, (\mathbb{P}^{\lfloor \frac{k}{2} \rfloor})^2)$  according (3.53).
- (2) Find the polynomial  $q_*(x, y)$  according to (3.54).
- (3) Solve the system (5.35) to obtain  $\{\omega_s, x^{(s)}, y^{(s)}\}$ .
- (4) Obtain the OCAD for  $\mathbb{P}^k$  space in the form of (5.36).

For  $\theta = \pm 1$  and any  $k \in \mathbb{N}_+$ , the symmetric OCADs for  $\mathbb{P}^k$  were given in Theorems 5.1 and 5.2.

*Remark 5.21.* According to Lemma 3.15, the symmetric OCAD for  $\mathbb{P}^{2k}$  space is also a symmetric OCAD for  $\mathbb{P}^{2k+1}$ . According to Lemma 3.18 and Remark 3.19, given the OCAD for  $\mathbb{P}^{2k}$  space and  $\theta \in [-1, 0]$ , we immediately obtain the corresponding symmetric OCAD for  $\theta \in [0, 1]$  via (3.45). As such, we only need to seek the symmetric OCAD for  $\mathbb{P}^{2k}$  space ( $k \geq 4$ ) and  $\theta \in [-1, 0]$  via Algorithm 5.20.

In Step (3) of Algorithm 5.20, numerically solving the nonlinear algebraic equations (5.35) is a nontrivial task. This is typically based on an iterative algorithm (we use the MATLAB built-in function `fsolve`), which requires us to provide a good initial guess sufficiently close to the true solution so as to ensure the convergence. We choose the initial guess as follows. Given  $k \in \mathbb{N}_+$  and  $\theta \in [-1, 0]$ , we first partition the interval  $[-1, \theta]$  into  $-1 = \theta_0 < \theta_1 < \dots < \theta_j < \dots < \theta_J = \theta$ , and then perform Algorithm 5.20 from  $\theta_0$  to  $\theta_J$  sequentially. For each  $j \in \{1, \dots, J\}$ , the initial guess of solving the system (5.35) corresponding  $\theta_j$  is given by the final numerical solution to the system (5.35) corresponding to  $\theta_{j-1}$ . It is worth noting that, at the beginning of this process, the exact solution to the system (5.35) corresponding to  $\theta_0 = -1$  was already analytically given in Theorem 5.1.

For example, we apply the above-mentioned strategy to find the OCADs for  $\mathbb{P}^k$  spaces ( $8 \leq k \leq 11$ ) with  $\theta = -1, -0.8, \dots, -0.2, 0$ . The residual of each iteration is plotted in Figure 9, indicating the fast convergence of the iterations to machine accuracy. The internal nodes of the found OCADs (for  $\theta = -1, -0.2, 0$ ) are illustrated in Table 2.

## 6. 2D QUASI-OPTIMAL CAD FOR $\mathbb{P}^k$ SPACES

As discussed in Remark 5.3, the classic CAD (4.1) is optimal for only  $\theta = \pm 1$  but not optimal for general  $\theta \in (-1, 1)$ . Recall that the classic CAD (4.1) is actually convex combinations of the two special OCADs (5.1) and (5.4) for  $\theta = \pm 1$ . For the OCADs (5.1) and (5.4), the corresponding boundary weights are repetitively  $(0, \bar{\omega}_*(-1, \mathbb{P}^k))$  and  $(\bar{\omega}_*(1, \mathbb{P}^k), 0)$ , which are two vertexes on  $\partial \mathbb{B}_\omega$ . See Figure 10 for an illustration. The boundary weights of the classic CAD (4.1) form a straight line segment between the two vertexes  $(0, \bar{\omega}_*(-1, \mathbb{P}^k))$  and  $(\bar{\omega}_*(1, \mathbb{P}^k), 0)$ . Any



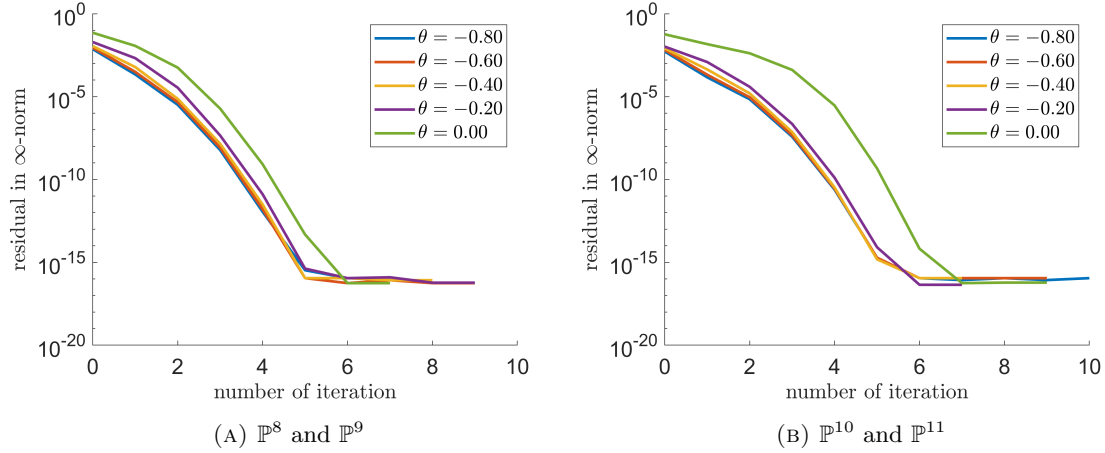


FIGURE 9. Fast convergence of the iterations for solving system (5.35) using the MATLAB built-in function `fsolve` with the proposed initial-guess strategy.

straight line segment in the region  $\mathbb{B}_\omega$  represents convex combinations of two feasible CADs. As observed from Figure 10a for  $\mathbb{P}^2$  and  $\mathbb{P}^3$ , the boundary weights of OCAD for all  $\theta \in [-1, 1]$  lie on  $\partial\mathbb{B}_\omega$ , forming two line segments that connect three vertexes  $(0, \bar{\omega}_\star(-1, \mathbb{P}^k))$ ,  $(\bar{\omega}_\star(1, \mathbb{P}^k), 0)$ , and  $(\frac{1}{2}\bar{\omega}_\star(0, \mathbb{P}^k), \frac{1}{2}\bar{\omega}_\star(0, \mathbb{P}^k))$ . This intuitively reveals that the general OCAD (5.23) for  $\mathbb{P}^2$  and  $\mathbb{P}^3$  with  $\theta \in [-1, 1]$  is actually convex combinations of three special OCADs for  $\theta \in \{-1, 0, 1\}$ . However, as shown in Figures 10b to 10d, for  $\mathbb{P}^k$  with higher  $k \geq 4$ , the part of  $\partial\mathbb{B}_\omega$  related to OCAD weights becomes curved, namely, it is no longer formed by straight edges. In spite of this, we discover that some convex combinations of three special OCADs for  $\theta \in \{-1, 0, 1\}$  will still provide a feasible CAD, which is very close to the OCAD and thus named as “*quasi-optimal CAD*” in the following.

In order to define the quasi-optimal CAD, let us denote the symmetric OCAD for  $\mathbb{P}^k$  and  $\theta = 0$  by

$$(6.1) \quad \langle p \rangle_\Omega = \bar{\omega}_{\star,0} [\langle p \rangle_\Omega^x + \langle p \rangle_\Omega^y] + \sum_{s=1}^{S_0} \omega_0^{(s)} p(x_0^{(s)}, y_0^{(s)}) \quad \forall p \in \mathbb{P}^k,$$

where  $\bar{\omega}_{\star,0} := \bar{\omega}_\star(0, \mathbb{P}^k)$ . The values of  $\bar{\omega}_{\star,0}$ , internal weights  $\{\omega_0^{(s)}\}$ , and nodes  $\{(x_0^{(s)}, y_0^{(s)})\}$  can be obtained via Sections 5.2 and 5.3.

**Theorem 6.1** (Quasi-optimal CAD). *The following symmetric CAD is feasible for  $\mathbb{P}^k$ :*

$$\langle p \rangle_\Omega = \begin{cases} \tau \cdot [\text{OCAD in (5.1) for } \theta = -1] + (1 - \tau) \cdot [\text{OCAD in (6.1) for } \theta = 0] & \text{if } \theta \in [-1, 0], \\ \tau \cdot [\text{OCAD in (5.3) for } \theta = 1] + (1 - \tau) \cdot [\text{OCAD in (6.1) for } \theta = 0] & \text{if } \theta \in [0, 1], \end{cases}$$

which can be equivalently written as

$$(6.2) \quad \langle p \rangle_\Omega = \bar{\omega}_\star^q [(1 + \theta)\langle p \rangle_\Omega^x + (1 - \theta)\langle p \rangle_\Omega^y] + \tau \sum_{\ell=2}^{L-1} \sum_{q=1}^Q \omega_\ell^{\text{GL}} \omega_q^{\text{G}} p(x_{\ell q}^q, y_{\ell q}^q) + (1 - \tau) \sum_{s=1}^{S_0} \omega_0^{(s)} \overline{p(x_0^{(s)}, y_0^{(s)})}$$

with

$$\tau = \frac{\bar{\omega}_{\star,0} |\theta|}{\bar{\omega}_{\star,0} |\theta| + \omega_1^{\text{GL}} (1 - |\theta|)}, \quad \bar{\omega}_\star^q = \frac{\bar{\omega}_{\star,0} \omega_1^{\text{GL}}}{\bar{\omega}_{\star,0} |\theta| + \omega_1^{\text{GL}} (1 - |\theta|)},$$

and

$$(x_{\ell q}^q, y_{\ell q}^q) = \begin{cases} (x_q^{\text{G}}, y_\ell^{\text{GL}}), & \text{if } \theta \in [-1, 0], \\ (x_\ell^{\text{GL}}, y_q^{\text{G}}), & \text{if } \theta \in [0, 1]. \end{cases}$$

*Proof.* The quasi-optimal CAD (6.2) is either the convex combination of the two special OCADs for  $\theta = -1$  and  $\theta = 0$  (if  $\theta \in [-1, 0]$ ) or the convex combination of the two special OCADs for

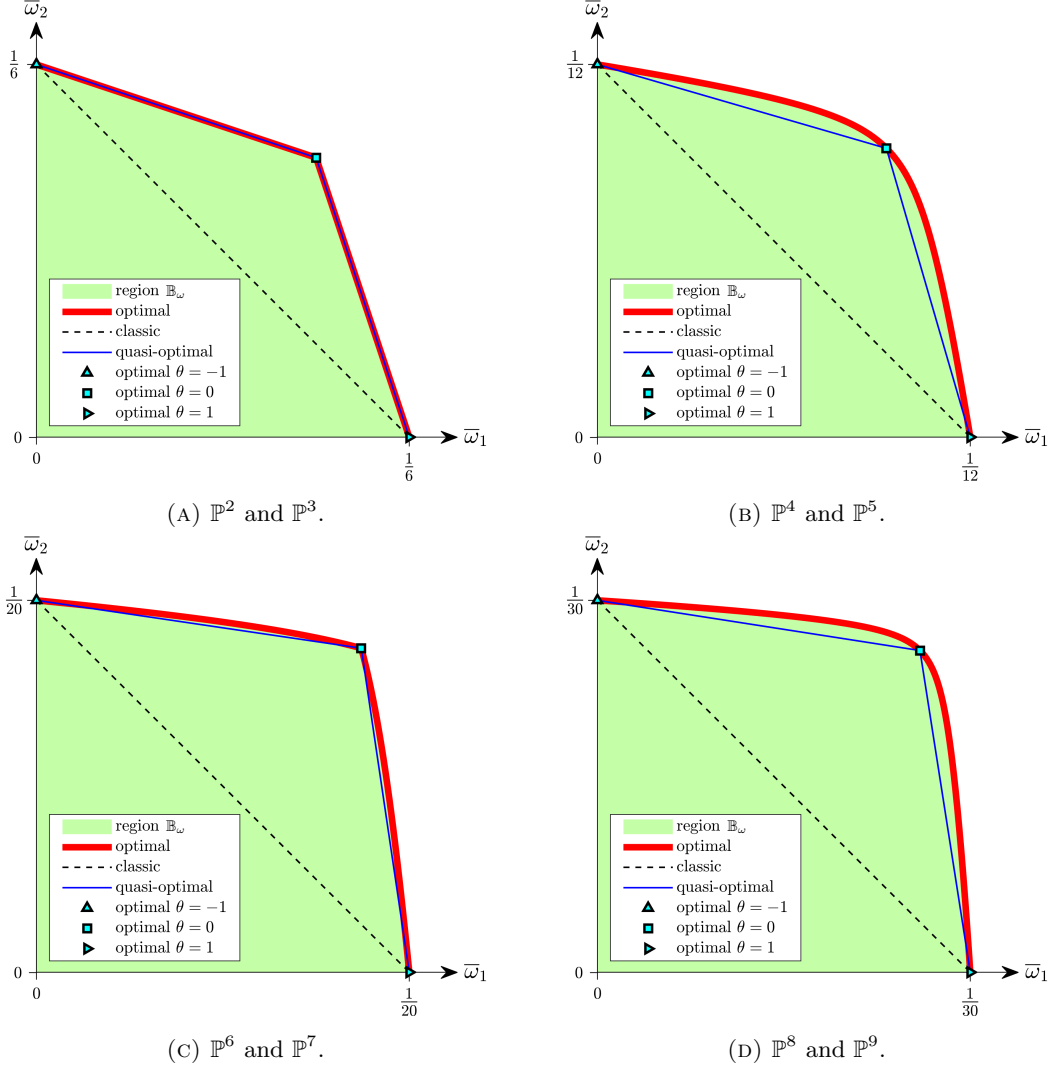


FIGURE 10. Geometric illustration and comparison of the optimal, classic, quasi-optimal CADs for their boundary weights in the region  $\mathbb{B}_\omega$ .

$\theta = 1$  and  $\theta = 0$  (if  $\theta \in [0, 1]$ ). Consequently, the quasi-optimal CAD (6.2) is feasible, according to Lemma 3.5.  $\square$

For comparison, Figure 10 illustrates the boundary weights of the optimal, classic, quasi-optimal CADs in the region  $\mathbb{B}_\omega$ . One can see that the classic CAD is notably far from the OCAD, especially when  $\theta$  is near 0, while the quasi-optimal CAD is much closer to the OCAD. In particular, the quasi-optimal CAD exactly coincides with the OCAD for  $\mathbb{P}^2$  and  $\mathbb{P}^3$ .

To quantitatively analyze how close the quasi-optimal CAD is to the OCAD for  $\mathbb{P}^k$  with  $k \geq 4$ , we define the  $\bar{\omega}$ -ratio as follow.

**Definition 6.2** ( $\bar{\omega}$ -ratio). For a feasible symmetric CAD

$$\langle p \rangle_\Omega = \bar{\omega} [(1 + \theta) \langle p \rangle_\Omega^x + (1 - \theta) \langle p \rangle_\Omega^y] + \sum_s \omega_s \overline{p(x^{(s)}, y^{(s)})} \quad \forall p \in \mathbb{P}^k,$$

the ratio of its weight  $\bar{\omega}$  to the OCAD weight  $\bar{\omega}_*(\theta, \mathbb{P}^k)$  is called the  $\bar{\omega}$ -ratio.

In particular, the  $\bar{\omega}$ -ratio of the classic CAD (4.1) for  $\mathbb{P}^k$  is given by

$$(6.3) \quad \frac{\omega_1^{\text{GL}}}{\bar{\omega}_*} = \frac{1}{\left\lceil \frac{k+3}{2} \right\rceil \left\lceil \frac{k+1}{2} \right\rceil \bar{\omega}_*(\theta, \mathbb{P}^k)},$$

and  $\bar{\omega}$ -ratio of the quasi-optimal CAD (6.2) for  $\mathbb{P}^k$  is given by

$$(6.4) \quad \frac{\bar{\omega}_*^{\text{Q}}}{\bar{\omega}_*} = \frac{\bar{\omega}_{*,0}}{\bar{\omega}_{*,0}|\theta| + \omega_1^{\text{GL}}(1-|\theta|)} \times \frac{\omega_1^{\text{GL}}}{\bar{\omega}_*}.$$

For  $\mathbb{P}^2$  and  $\mathbb{P}^3$ , the quasi-optimal CAD (6.2) is OCAD, so that  $\frac{\bar{\omega}_*^{\text{Q}}}{\bar{\omega}_*} = 1$ . For  $\mathbb{P}^k$  with higher  $k \geq 4$ , Figure 11 gives a comparison of the optimal, classic, quasi-optimal CADs in terms of their boundary weights and  $\bar{\omega}$ -ratios. One can see that the  $\bar{\omega}$ -ratio of the classic CAD (4.1) can reach as low as 57% ~ 65%, and

$$\omega_1^{\text{GL}} \geq 57\% \bar{\omega}_*.$$

Consequently, using OCAD to replace the classic CAD would help to notably improve the BP CFL condition. From Figure 11, we also clearly observe that  $\bar{\omega}_*^{\text{Q}}$  is very close to  $\bar{\omega}_*$ , and the  $\bar{\omega}$ -ratio of the quasi-optimal CAD (6.2) is always above 95% (overall much higher than that of the classic CAD (4.1)), namely,

$$\bar{\omega}_*^{\text{Q}} \geq 95\% \bar{\omega}_*.$$

In other words,  $\bar{\omega}^{\text{Q}}$  is only less than 5% lower than  $\bar{\omega}_*$ . Since the construction of quasi-optimal CAD (6.2) only requires the special OCAD for  $\theta \in \{-1, 0, 1\}$ , and thus is much easier than the construction of OCAD for all  $\theta \in [-1, 1]$ . Therefore, the quasi-optimal CAD (6.2) is a good alternative for OCAD.

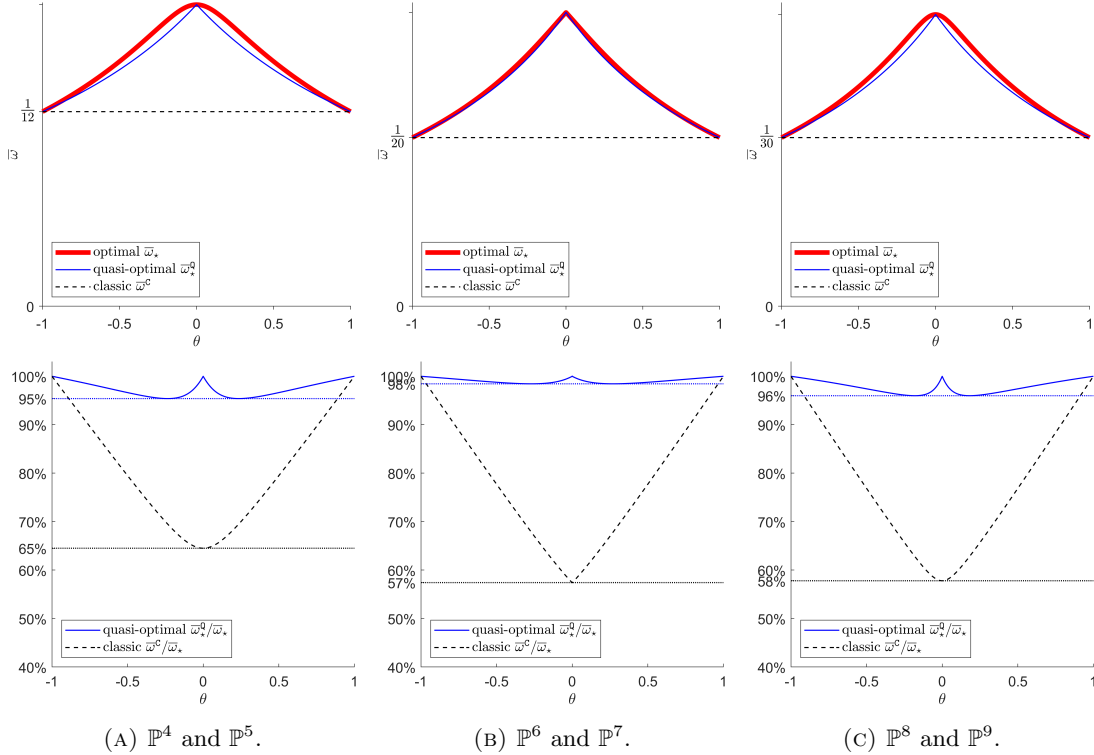


FIGURE 11. Comparison of the optimal, classic, quasi-optimal CADs in terms of their boundary weights (top row) and  $\bar{\omega}$ -ratios (bottom row).

## 7. BP SCHEMES BASED ON OCAD AND QUASI-OPTIMAL CAD FOR HYPERBOLIC SYSTEMS

In this section, we apply the proposed OCAD and quasi-optimal CAD to designing efficient BP schemes for hyperbolic systems of conservation laws. Since we have proved that the existing classic CAD (1.14) by Zhang and Shu [36, 37] is already optimal in 1D and for  $\mathbb{Q}^k$  spaces in 2D, this section is only focused on the  $\mathbb{P}^k$ -based BP DG schemes in 2D.

Consider the  $(k+1)$ th-order  $\mathbb{P}^k$ -based DG scheme with the forward Euler time discretization<sup>2</sup> for the 2D hyperbolic conservation laws

$$(7.1) \quad \frac{\partial}{\partial t} u + \frac{\partial}{\partial x} f_1(u) + \frac{\partial}{\partial y} f_2(u) = 0 \quad (x, y, t) \in \mathbb{R} \times \mathbb{R} \times \mathbb{R}^+.$$

Following the Zhang–Shu framework [36, 37], in order to design a BP DG scheme, we only need to ensure the cell averages within the region  $G$ . As long as the BP property of the updated cell averages is guaranteed, one may employ a simple BP limiter to enforce the pointwise bounds of the piecewise DG polynomial solutions without affecting the high-order accuracy [36, 37]. On a rectangular cell  $\Omega_{ij} := [x_{i-\frac{1}{2}}, x_{i+\frac{1}{2}}] \times [y_{j-\frac{1}{2}}, y_{j+\frac{1}{2}}]$ , the evolution equation of cell averages for the  $(k+1)$ th-order DG scheme reads

$$(7.2) \quad \begin{aligned} \bar{u}_{ij}^{n+1} = \bar{u}_{ij}^n - \frac{\Delta t}{\Delta x} \sum_{q=1}^Q \omega_q^G \left[ \hat{f}_1(u_{i+\frac{1}{2},q}^-, u_{i+\frac{1}{2},q}^+) - \hat{f}_1(u_{i-\frac{1}{2},q}^-, u_{i-\frac{1}{2},q}^+) \right] \\ - \frac{\Delta t}{\Delta y} \sum_{q=1}^Q \omega_q^G \left[ \hat{f}_2(u_{q,j+\frac{1}{2}}^-, u_{q,j+\frac{1}{2}}^+) - \hat{f}_2(u_{q,j-\frac{1}{2}}^-, u_{q,j-\frac{1}{2}}^+) \right], \end{aligned}$$

where  $Q$  is typically taken as  $k+1$  such that the Gauss quadrature has sufficient high-order accuracy, and the limiting values at the cell interfaces are computed by

$$(7.3) \quad u_{i-\frac{1}{2},q}^+ = p_{ij}(x_{i-\frac{1}{2}}, y_{j,q}^G), \quad u_{i+\frac{1}{2},q}^- = p_{ij}(x_{i+\frac{1}{2}}, y_{j,q}^G),$$

$$(7.4) \quad u_{q,j-\frac{1}{2}}^+ = p_{ij}(x_{i,q}^G, y_{j-\frac{1}{2}}), \quad u_{q,j+\frac{1}{2}}^- = p_{ij}(x_{i,q}^G, y_{j+\frac{1}{2}})$$

with  $p_{ij}(x, y) \in \mathbb{P}^k$  denoting the DG solution polynomial on  $\Omega_{ij}$  at time level  $n$  satisfying

$$\bar{u}_{ij}^n = \frac{1}{\Delta x \Delta y} \int_{x_{i-\frac{1}{2}}}^{x_{i+\frac{1}{2}}} \int_{y_{j-\frac{1}{2}}}^{y_{j+\frac{1}{2}}} p_{ij}(x, y) dy dx.$$

In (7.2), we take the numerical fluxes  $\hat{f}_1$  and  $\hat{f}_2$  as the BP numerical fluxes with which the corresponding 1D three-point first-order schemes are BP, i.e., for any  $u_1, u_2, u_3 \in G$  it holds that

$$(7.5) \quad u_2 - \frac{\Delta t}{\Delta x} \left( \hat{f}_1(u_2, u_3) - \hat{f}_1(u_1, u_2) \right) \in G, \quad u_2 - \frac{\Delta t}{\Delta y} \left( \hat{f}_2(u_2, u_3) - \hat{f}_2(u_1, u_2) \right) \in G$$

under a suitable CFL condition  $\max\{a_1 \Delta t / \Delta x, a_2 \Delta t / \Delta y\} \leq c_0$ , where  $a_1$  and  $a_2$  denote the maximum characteristic speeds in  $x$ - and  $y$ -directions, and  $c_0$  is the maximum allowable CFL number for the 1D first-order schemes. For example, typically  $c_0 = 1$  for the Lax–Friedrichs flux [37, 12], and  $c_0 = \frac{1}{2}$  for the HLL and HLLC fluxes [12].

We now discuss the BP conditions for the scheme (7.2) based on a 2D feasible symmetric CAD for  $\mathbb{P}^k$  in the form of

$$(7.6) \quad \langle p \rangle_\Omega = \bar{\omega} \left[ (1 + \theta) \langle p \rangle_\Omega^x + (1 - \theta) \langle p \rangle_\Omega^y \right] + \sum_{s=1}^S \overline{\omega_s p(x^{(s)}, y^{(s)})} \quad \forall p \in \mathbb{P}^k$$

with  $\theta$  defined in (3.34). Given a feasible CAD (7.6) on the reference cell  $\Omega = [-1, 1]^2$ , we should first transfer it onto  $\Omega_{ij}$  as

$$(7.7) \quad \langle p \rangle_{\Omega_{ij}} = \bar{\omega} \left[ (1 + \theta) \langle p \rangle_{\Omega_{ij}}^x + (1 - \theta) \langle p \rangle_{\Omega_{ij}}^y \right] + \sum_{s=1}^S \overline{\omega_s p(x_{ij}^{(s)}, y_{ij}^{(s)})} \quad \forall p \in \mathbb{P}^k$$

<sup>2</sup>All our discussions are also valid for high-order strong-stability-preserving (SSP) time discretizations [9], which are convex combinations of forward Euler step.

with the weights unchanged and the nodes  $\{(x_{ij}^{(s)}, y_{ij}^{(s)})\}$  given by the inverse transformation of (3.14).

**Theorem 7.1** (BP via general symmetric CAD). *Suppose that there is a 2D feasible symmetric CAD in the form of (7.6). If the DG solution polynomial  $p_{ij}(x, y)$  satisfies for all  $i$  and  $j$  that*

$$(7.8) \quad u_{i-\frac{1}{2},q}^+ \in G, \quad u_{i+\frac{1}{2},q}^- \in G, \quad u_{q,j-\frac{1}{2}}^+ \in G, \quad u_{q,j+\frac{1}{2}}^- \in G, \quad q = 1, \dots, Q,$$

and

$$(7.9) \quad \Pi_{ij} := \frac{1}{1-2\bar{\omega}} \sum_{s=1}^S \overline{\omega_s p_{ij}(x_{ij}^{(s)}, y_{ij}^{(s)})} \in G,$$

then the high-order scheme (7.2) preserves  $\bar{u}_{ij}^{n+1} \in G$  under the BP CFL condition

$$(7.10) \quad \Delta t \left( \frac{a_1}{\Delta x} + \frac{a_2}{\Delta y} \right) \leq \bar{\omega} c_0.$$

*Proof.* Applying the symmetric CAD (7.7) to  $\bar{u}_{ij}^n = \langle p_{ij} \rangle_{\Omega_{ij}}$  gives

$$(7.11) \quad \bar{u}_{ij}^n = \hat{\omega}_1 \sum_{q=1}^Q \omega_q^G \left( u_{i-\frac{1}{2},q}^+ + u_{i+\frac{1}{2},q}^- \right) + \hat{\omega}_2 \sum_{q=1}^Q \omega_q^G \left( u_{q,j-\frac{1}{2}}^+ + u_{q,j+\frac{1}{2}}^- \right) + (1-2\bar{\omega})\Pi_{ij}$$

where the Gauss quadrature and (7.9) have been used, and

$$\hat{\omega}_1 := \frac{\bar{\omega}(1+\theta)}{2} = \frac{\bar{\omega}a_1/\Delta x}{a_1/\Delta x + a_2/\Delta y}, \quad \hat{\omega}_2 := \frac{\bar{\omega}(1-\theta)}{2} = \frac{\bar{\omega}a_2/\Delta x}{a_1/\Delta x + a_2/\Delta y}.$$

Under the assumption of (7.8) and (7.9), it holds that  $\bar{u}_{ij}^n \in G$ . Substituting the decomposition (7.11) into (7.2), one can rewrite the scheme (7.2) as

$$(7.12) \quad \bar{u}_{ij}^{n+1} = \sum_{q=1}^Q \omega_q^G \hat{\omega}_1 (H_{i+\frac{1}{2},q}^- + H_{i-\frac{1}{2},q}^+) + \sum_{q=1}^Q \omega_q^G \hat{\omega}_2 (H_{q,j+\frac{1}{2}}^- + H_{q,j-\frac{1}{2}}^+) + (1-2\bar{\omega})\Pi_{ij}$$

with

$$\begin{aligned} H_{i+\frac{1}{2},q}^- &= u_{i+\frac{1}{2},q}^- - \frac{\Delta t}{\hat{\omega}_1 \Delta x} \left( \hat{f}_1(u_{i+\frac{1}{2},q}^-, u_{i+\frac{1}{2},q}^+) - \hat{f}_1(u_{i-\frac{1}{2},q}^+, u_{i+\frac{1}{2},q}^-) \right), \\ H_{i-\frac{1}{2},q}^+ &= u_{i-\frac{1}{2},q}^+ - \frac{\Delta t}{\hat{\omega}_1 \Delta x} \left( \hat{f}_1(u_{i-\frac{1}{2},q}^+, u_{i+\frac{1}{2},q}^-) - \hat{f}_1(u_{i-\frac{1}{2},q}^-, u_{i-\frac{1}{2},q}^+) \right), \\ H_{q,j+\frac{1}{2}}^- &= u_{q,j+\frac{1}{2}}^- - \frac{\Delta t}{\hat{\omega}_2 \Delta y} \left( \hat{f}_2(u_{q,j+\frac{1}{2}}^-, u_{q,j+\frac{1}{2}}^+) - \hat{f}_2(u_{q,j-\frac{1}{2}}^+, u_{q,j+\frac{1}{2}}^-) \right), \\ H_{q,j-\frac{1}{2}}^+ &= u_{q,j-\frac{1}{2}}^+ - \frac{\Delta t}{\hat{\omega}_2 \Delta y} \left( \hat{f}_2(u_{q,j-\frac{1}{2}}^+, u_{q,j+\frac{1}{2}}^-) - \hat{f}_2(u_{q,j-\frac{1}{2}}^-, u_{q,j-\frac{1}{2}}^+) \right), \end{aligned}$$

which have the same form as the 1D three-point first-order schemes (7.5) and thus satisfy

$$H_{i+\frac{1}{2},q}^- \in G, \quad H_{i-\frac{1}{2},q}^+ \in G, \quad H_{q,j+\frac{1}{2}}^- \in G, \quad H_{q,j-\frac{1}{2}}^+ \in G,$$

under the CFL type conditions

$$(7.13) \quad a_1 \Delta t \leq c_0 \hat{\omega}_1 \Delta x, \quad a_2 \Delta t \leq c_0 \hat{\omega}_2 \Delta y.$$

Because (7.12) is a convex combination form, by the convexity of  $G$  we conclude that  $\bar{u}_{ij}^{n+1} \in G$  under the CFL conditions (7.13), which are exactly equivalent to (7.10). The proof is completed.  $\square$

*Remark 7.2* (Classic CAD). If the Zhang–Shu classic CAD is considered, then the BP CFL condition (7.10) becomes

$$(7.14) \quad \Delta t \left( \frac{a_1}{\Delta x} + \frac{a_2}{\Delta y} \right) \leq \omega_1^{\text{GL}} c_0.$$

*Remark 7.3* (BP Limiter). The condition (7.9) is satisfied if  $p_{ij}(x, y) \in G$  for all  $(x, y) \in \mathbb{S}_{ij}$ . In general, the DG solution polynomial may not automatically meet the conditions (7.8) and (7.9), which should be enforced by a BP limiter. For the scalar conservation law with the maximum principle (1.2) and  $G = [U_{\min}, U_{\max}]$ , the BP limiter [36] is given by

$$(7.15) \quad \tilde{p}_{ij}(x, y) = \delta(p_{ij}(x, y) - \bar{u}_{ij}^n) + \bar{u}_{ij}^n, \quad \delta = \min \left\{ \left| \frac{U_{\max} - \bar{u}_{ij}^n}{p_{ij}^{\max} - \bar{u}_{ij}^n} \right|, \left| \frac{U_{\min} - \bar{u}_{ij}^n}{p_{ij}^{\min} - \bar{u}_{ij}^n} \right|, 1 \right\},$$

where

$$p_{ij}^{\max} = \max_{(x, y) \in \Theta_{ij}} p_{ij}(x, y), \quad p_{ij}^{\min} = \min_{(x, y) \in \Theta_{ij}} p_{ij}(x, y), \quad \Theta_{ij} = \{(x_{i \pm \frac{1}{2}}, y_{j, q}^G), (x_{i, q}^G, y_{j \pm \frac{1}{2}})\}_{q=1}^Q \cup \mathbb{S}_{ij}.$$

One can verify that the limited DG solution polynomial  $\tilde{p}_{ij}$  satisfies the desired conditions (7.8) and (7.9). Similar local scaling BP limiters have also been designed for the Euler equations [37] and many other hyperbolic systems [20, 16, 22, 26]. It is worth noting that the internal nodes of the OCAD are much fewer than those of the classic CAD (see Table 2). When the local scaling BP limiter is performed at the internal nodes in all computational cells, using our OCAD also reduces the computational cost in the BP limiting procedure.

*Remark 7.4* (Simplified BP Limiter). One can also use a simplified BP limiter [38] to enforce the conditions (7.8) and (7.9), without using the internal nodes  $\mathbb{S}_{ij}$  of the CAD. In fact, according to (7.11),  $\Pi_{ij}$  can also be represented as

$$(7.16) \quad \Pi_{ij} = \frac{\bar{u}_{ij}^n - \bar{\omega} \left[ \frac{1+\theta}{2} \sum_{q=1}^Q \omega_q^G \left( u_{i-\frac{1}{2}, q}^+ + u_{i+\frac{1}{2}, q}^- \right) + \frac{1-\theta}{2} \sum_{q=1}^Q \omega_q^G \left( u_{q, j-\frac{1}{2}}^+ + u_{q, j+\frac{1}{2}}^- \right) \right]}{1 - 2\bar{\omega}}.$$

For example, for the scalar conservation law with  $G = [U_{\min}, U_{\max}]$ , the simplified BP limiter is given by (7.15) with

$$(7.17) \quad p_{ij}^{\max} = \max \left\{ p_{ij}(x_{i \pm \frac{1}{2}}, y_{j, q}^G), p_{ij}(x_{i, q}^G, y_{j \pm \frac{1}{2}}), \Pi_{ij} \right\},$$

$$(7.18) \quad p_{ij}^{\min} = \min \left\{ p_{ij}(x_{i \pm \frac{1}{2}}, y_{j, q}^G), p_{ij}(x_{i, q}^G, y_{j \pm \frac{1}{2}}), \Pi_{ij} \right\},$$

where  $\Pi_{ij}$  is computed by (7.16). *A remarkable advantage of using the simplified BP limiter is that it only involves the boundary weight of CAD and does not require the information of internal CAD nodes in the resulting BP schemes. As we have seen, finding the internal CAD nodes is difficult. Therefore, using the simplified BP limiter to construct BP schemes effectively avoids such difficulty.*

As direct consequences of Theorem 7.1, we have the following conclusions.

**Theorem 7.5** (BP via OCAD). *Consider the OCAD for the  $\mathbb{P}^k$ -based DG scheme. If for all  $i$  and  $j$  the (limited) DG solution polynomial  $\tilde{p}_{ij}(x, y)$  satisfies*

$$(7.19) \quad \tilde{u}_{i-\frac{1}{2}, q}^+ \in G, \quad \tilde{u}_{i+\frac{1}{2}, q}^- \in G, \quad \tilde{u}_{q, j-\frac{1}{2}}^+ \in G, \quad \tilde{u}_{q, j+\frac{1}{2}}^- \in G, \quad q = 1, \dots, Q,$$

and

$$(7.20) \quad \Pi_{ij} := \frac{\bar{u}_{ij}^n - \bar{\omega}_*(\theta, \mathbb{P}^k) \left[ \frac{1+\theta}{2} \sum_{q=1}^Q \omega_q^G \left( \tilde{u}_{i-\frac{1}{2}, q}^+ + \tilde{u}_{i+\frac{1}{2}, q}^- \right) + \frac{1-\theta}{2} \sum_{q=1}^Q \omega_q^G \left( \tilde{u}_{q, j-\frac{1}{2}}^+ + \tilde{u}_{q, j+\frac{1}{2}}^- \right) \right]}{1 - 2\bar{\omega}_*(\theta, \mathbb{P}^k)} \in G,$$

then the high-order scheme (7.2) with the BP limiter preserves  $\bar{u}_{ij}^{n+1} \in G$  under the BP CFL condition

$$(7.21) \quad \Delta t \left( \frac{a_1}{\Delta x} + \frac{a_2}{\Delta y} \right) \leq \bar{\omega}_* c_0.$$

**Theorem 7.6** (BP via quasi-optimal CAD). *Consider the quasi-optimal CAD for the  $\mathbb{P}^k$ -based DG scheme. If for all  $i$  and  $j$  the (limited) DG solution polynomial  $\tilde{p}_{ij}(x, y)$  satisfies (7.19) and (7.22)*

$$\Pi_{ij} := \frac{\bar{u}_{ij}^n - \bar{\omega}_*^Q \left[ \frac{1+\theta}{2} \sum_{q=1}^Q \omega_q^G \left( \tilde{u}_{i-\frac{1}{2}, q}^+ + \tilde{u}_{i+\frac{1}{2}, q}^- \right) + \frac{1-\theta}{2} \sum_{q=1}^Q \omega_q^G \left( \tilde{u}_{q, j-\frac{1}{2}}^+ + \tilde{u}_{q, j+\frac{1}{2}}^- \right) \right]}{1 - 2\bar{\omega}_*^Q} \in G,$$

then the high-order scheme (7.2) with the BP limiter preserves  $\bar{u}_{ij}^{n+1} \in G$  under the BP CFL condition

$$(7.23) \quad \Delta t \left( \frac{a_1}{\Delta x} + \frac{a_2}{\Delta y} \right) \leq \bar{\omega}_*^q c_0$$

with  $\bar{\omega}_*^q = \frac{\bar{\omega}_{*,0} \omega_1^{\text{GL}}}{\bar{\omega}_{*,0} |\theta| + \omega_1^{\text{GL}} (1 - |\theta|)}$  and  $\bar{\omega}_{*,0} := \bar{\omega}_*(0, \mathbb{P}^k)$ .

*Remark 7.7* (Comparison of CFL conditions). The standard CFL condition for linear stability of the  $\mathbb{P}^k$ -based DG method with a  $(k+1)$ -stage  $(k+1)$ -order Runge–Kutta (RK) time discretization [3] is given by the following empirical formula

$$(7.24) \quad \Delta t \left( \frac{a_1}{\Delta x} + \frac{a_2}{\Delta y} \right) \leq \frac{1}{2k+1}.$$

Table 1 gives a comparison of different CFL numbers in the special case of  $a_1 \Delta y = a_2 \Delta x$  (i.e.  $\theta = 0$ ) and  $c_0 = 1$ . It indicates that the optimal BP CFL condition (7.21) of the DG schemes (with the BP limiter) is much weaker than the classic BP CFL condition (7.14) via the Zhang–Shu classic CAD. Moreover, if  $c_0 = 1$ , the optimal BP CFL condition (7.21) is typically weaker than the standard CFL condition (7.24) except for  $k = 8$ . In practice, one may need to consider both the BP CFL and linearly stable CFL conditions to fully ensure the stability of the DG method. Under this consideration, the standard CFL condition with OCAD is sufficient to guarantee the BP property when  $c_0 = 1$ , while if  $c_0 = \frac{1}{2}$  the optimal BP CFL condition (7.21) dominates but it is still much weaker than classic BP CFL condition (7.14); see Figure 12 for further illustration.

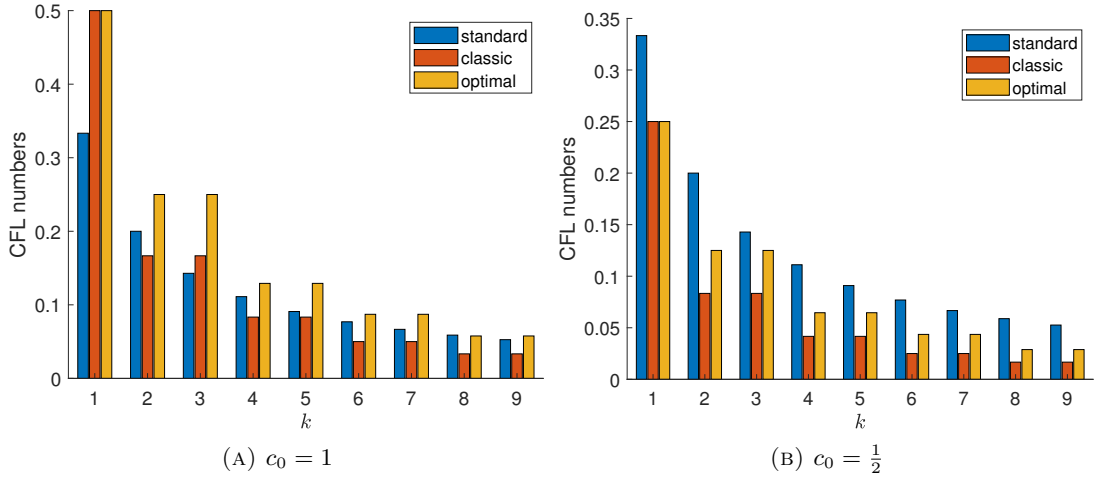


FIGURE 12. Comparison of standard linearly stable CFL number  $\frac{1}{2k+1}$ , classic BP CFL number  $\omega_1^{\text{GL}} c_0$ , and optimal BP CFL number  $\bar{\omega}_* c_0$ , in the case of  $a_1 \Delta y = a_2 \Delta x$  for  $\mathbb{P}^k$ -based DG methods with  $1 \leq k \leq 9$ .

*Remark 7.8* (Easy implementation). It is worth emphasizing that one only requires a slight and local modification to an existing code to enjoy the above-mentioned advantages of our OCADs or quasi-optimal CADs. Specifically, one only needs to slightly modify the BP limiting procedure, and then the theoretical BP CFL condition is notably improved.

*Remark 7.9*. The above analysis only considered the forward Euler time discretization. Because a high-order SSP time discretization can be viewed as a convex combination of the forward Euler method, our analysis and conclusions are also valid if the high-order SSP time discretization is employed.

## 8. NUMERICAL EXPERIMENTS

This section tests the accuracy, efficiency, and robustness of the 2D high-order BP DG schemes designed via the proposed OCAD and quasi-optimal CAD, which are respectively referred to as the “**optimal** approach” and “**quasi-optimal** approach” for short. For comparison, we also present the results of the 2D high-order BP DG schemes designed via the Zhang–Shu classic CAD (1.14), which are referred to as the “**classic** approach” for short. We employ the three-stage third-order SSP Runge–Kutta method [9] for time discretization, except for the accuracy tests in Example 1 where the  $(k + 1)$ th-order SSP multi-step method is used for the  $\mathbb{P}^k$ -based DG scheme to match the temporal and spatial accuracy. The time step-size is taken as that indicated by the theoretical BP CFL condition, or that indicated by linear stability, whichever is smaller, namely,

$$\Delta t = C_{\text{SSP}} \frac{\min\{\bar{\omega}c_0, \frac{1}{2k+1}\}}{\frac{a_1}{\Delta x} + \frac{a_2}{\Delta y}},$$

where  $C_{\text{SSP}}$  denotes the SSP coefficient of the adopted time discretization method,  $\bar{\omega} = \bar{\omega}_*$  for the **optimal** approach,  $\bar{\omega} = \bar{\omega}_*^{\text{q}}$  for the **quasi-optimal** approach, and  $\bar{\omega} = \omega_1^{\text{GL}}$  for the **classic** approach, respectively. While the CAD is independent of the choice of BP numerical fluxes, we adopt the global Lax–Friedrichs flux with  $c_0 = 1$  in all our numerical tests. All the schemes are implemented using C++ language with double precision on a Linux server with Intel(R) Xeon(R) Platinum 8268 CPU @ 2.90GHz 2TB RAM.

**8.1. Example 1: Linear convection equation.** In order to examine the convergence, we first consider the 2D linear convection equation

$$u_t + u_x + u_y = 0, \quad (x, y, t) \in [-1, 1] \times [-1, 1] \times \mathbb{R}^+$$

with periodic boundary conditions and initial data  $u(x, y, 0) = \sin(\pi(x + y))$ . The exact solution  $u(x, y, t) = \sin(\pi(x + y - 2t))$  satisfies a maximum principle with the invariant region  $G = [-1, 1]$ . We simulate this problem until  $t = 0.5$ . Tables 3 to 6 list the  $\ell^2$  numerical errors and the corresponding convergence rates for the  $\mathbb{P}^k$ -based BP DG method with  $k \in \{2, 4, 6, 8\}$  at different grid resolutions of  $N \times N$  cells with  $\Delta x = \Delta y = 2/N$ . The CPU time of all these simulations is presented in these tables. The results show the expected  $(k + 1)$ th-order convergence is achieved by the  $\mathbb{P}^k$  BP DG method, while the BP limiter does not destroy the accuracy. Moreover, the **optimal** approach admits a larger time step and thus uses much less CPU time than the **classic** approach, while the numerical errors of the two approaches are very close. This confirms the advantage in efficiency of using OCAD over the classic CAD.

TABLE 3. Example 1:  $\ell^2$  errors at  $t = 0.5$  and corresponding convergence rates for  $\mathbb{P}^2$ -based BP DG methods with a four-step third-order multi-step method whose SSP coefficient is  $\frac{1}{3}$ . The CPU time is measured and shown in seconds.

N	optimal approach			classic approach		
	$\ell^2$ error	Order	CPU(s)	$\ell^2$ error	Order	CPU(s)
	$\Delta t = \frac{1}{30} \Delta x$			$\Delta t = \frac{1}{36} \Delta x$		
20	5.37e-4	-	0.52	5.39e-4	-	0.67
40	5.94e-5	3.18	2.50	5.96e-5	3.18	3.37
80	7.30e-6	3.02	14.62	7.31e-6	3.03	21.88
160	9.11e-7	3.00	103.20	9.11e-7	3.00	132.39
320	1.14e-7	3.00	517.60	1.14e-7	3.00	695.42
640	1.42e-8	3.00	2870.80	1.42e-8	3.00	3858.67



TABLE 4. Same as Table 3 except for  $\mathbb{P}^4$ -based BP DG methods with a ten-step fifth-order multi-step method whose SSP coefficient is about 0.282.

$N$	optimal approach			classic approach		
	$\ell^2$ error	Order	CPU(s)	$\ell^2$ error	Order	CPU(s)
	$\Delta t = \frac{0.282}{18} \Delta x$			$\Delta t = \frac{0.282}{24} \Delta x$		
20	6.98e-7	-	4.30	6.78e-7	-	6.95
40	2.11e-8	5.05	25.62	2.11e-8	5.00	35.66
60	2.78e-9	5.00	70.72	2.78e-9	5.00	108.96
80	6.61e-10	5.00	142.74	6.61e-10	5.00	211.88
100	2.17e-10	5.00	225.72	2.17e-10	5.00	343.83
120	8.70e-11	5.00	354.57	8.70e-11	5.00	542.14

TABLE 5. Same as Table 3 except for  $\mathbb{P}^6$ -based BP DG methods with an eighteen-step seventh-order multi-step method whose SSP coefficient is about 0.217.

$N$	optimal approach			classic approach		
	$\ell^2$ error	Order	CPU(s)	$\ell^2$ error	Order	CPU(s)
	$\Delta t = \frac{0.217}{26} \Delta x$			$\Delta t = \frac{0.217}{40} \Delta x$		
4	1.37e-4	-	0.58	1.57e-4	-	1.12
8	1.98e-7	9.44	2.35	3.12e-7	8.98	4.07
12	1.17e-8	6.97	5.18	1.37e-8	7.72	9.49
16	1.59e-9	6.94	10.21	1.59e-9	7.48	18.97
20	3.40e-10	6.91	16.91	3.40e-10	6.91	30.92
24	9.69e-11	6.88	24.99	9.69e-11	6.88	44.33

TABLE 6. Same as Table 3 except for  $\mathbb{P}^8$ -based BP DG methods with a 22-step ninth-order multi-step method whose SSP coefficient is 0.1.

$N$	optimal approach			classic approach		
	$\ell^2$ error	Order	CPU(s)	$\ell^2$ error	Order	CPU(s)
	$\Delta t = \frac{0.005767}{2} \Delta x \approx \frac{0.1}{34.68} \Delta x$			$\Delta t = \frac{0.1}{60} \Delta x$		
4	2.12e-7	-	3.38	2.29e-7	-	7.78
6	5.36e-9	9.08	7.18	5.38e-9	9.25	15.17
8	4.00e-10	9.02	12.91	4.00e-10	9.04	28.41
10	5.41e-11	8.97	22.99	5.41e-11	8.96	47.77
12	1.04e-11	9.03	32.06	1.04e-11	9.03	68.85
14	2.61e-12	9.00	44.91	2.62e-12	8.97	92.61

8.2. **Example 2: Inviscid Burgers' equation.** In this example [36], we consider the inviscid Burgers' equation

$$(8.1) \quad u_t + \left(\frac{u^2}{2}\right)_x + \left(\frac{u^2}{2}\right)_y = 0, \quad (x, y, t) \in [-1, 1] \times [-1, 1] \times \mathbb{R}^+.$$

The initial condition is taken as  $u(x, y, 0) = \sin(\pi(x + y))$ , and the periodic boundary conditions are adopted. The exact solution also obeys the maximum principle with  $G = [-1, 1]$ . The exact solution is smooth up to  $t = \frac{1}{2\pi} \approx 0.159$ , and later a stationary shock wave develops. Figure 13 shows the numerical solutions at  $t = 0.23$  and the snapshots cut along  $y = x$ , obtained by using

$\mathbb{P}^2, \mathbb{P}^4, \mathbb{P}^6$ -based BP DG methods. We see the shock is well captured, with only the BP limiter and without using any non-oscillatory limiters. One can observe that the **optimal** approach and the **classic** approach give very similar results, and the shock is equally well resolved by both approaches. However, the CPU time of the **optimal** approach is much less than that of the **classic** approach, as shown in Table 7.

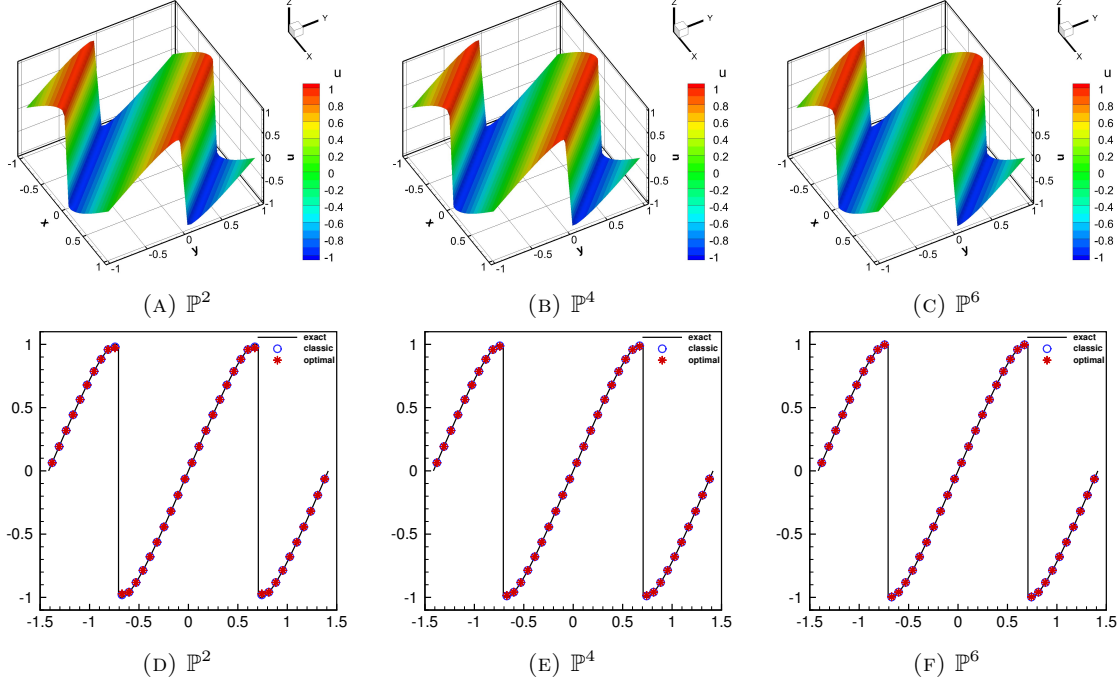


FIGURE 13. Example 2: the numerical solutions at  $t = 0.23$  obtained by the  $\mathbb{P}^2, \mathbb{P}^4, \mathbb{P}^6$ -based BP DG methods. Top: the surface of the solutions with **optimal** approach. Bottom: Comparison of the solutions cut along  $y = x$ . The spatial mesh size is  $\Delta x = \Delta y = \frac{2}{40}$ .

TABLE 7. CPU time in seconds for simulating Example 2 up to  $t = 0.23$ .

Mesh	CAD	$\mathbb{P}^2$	$\mathbb{P}^4$	$\mathbb{P}^6$
$40 \times 40$	<b>optimal</b> approach	1.098	1.988	39.015
	<b>classic</b> approach	1.350	2.598	59.180
$80 \times 80$	<b>optimal</b> approach	7.081	12.945	214.307
	<b>classic</b> approach	8.321	16.272	323.648

**8.3. Example 3: Compressible Euler equations.** In this example, we simulate the interaction of a shock and a vortex with low density and low pressure, by solving the two-dimensional compressible Euler equations, which can be formulated in the form of (7.1) with

$$(8.2) \quad u = \begin{pmatrix} \rho \\ m_1 \\ m_2 \\ E \end{pmatrix}, \quad f_1(u) = \begin{pmatrix} m_1 \\ m_1 v_1 + P \\ m_2 v_1 \\ (E + p)v_1 \end{pmatrix}, \quad f_2(u) = \begin{pmatrix} m_2 \\ m_1 v_2 \\ m_2 v_2 + P \\ (E + p)v_2 \end{pmatrix}.$$

Here  $\rho$  is the density,  $(m_1, m_2) = \rho(v_1, v_2)$  denotes the momentum vector with  $(v_1, v_2)$  being the velocity field,  $P$  is the pressure, and  $E = \frac{1}{2}\rho(v_1^2 + v_2^2) + \frac{P}{\gamma-1}$  denotes the total energy. The

adiabatic index  $\gamma$  is taken as 1.4. The density and the internal energy should be positive, yielding the invariant region

$$G = \left\{ u = (\rho, m_1, m_2, E)^\top : \rho(u) > 0, \rho e(u) := E - \frac{m_1^2 + m_2^2}{2\rho} > 0 \right\},$$

which is a convex set [37] because  $\rho e(u)$  is a concave function of  $u$ .

The setup of our the shock-vortex interaction problem is similar to [11] except for that the present case involves very low density and low pressure. The computational domain is taken as  $[0, 2] \times [0, 1]$ . A shock of Mach number  $M = 1.1$  is positioned at  $x = 0.5$  plane and perpendicular to the  $x$ -axis. Its left state is  $(\rho_l, v_{1,l}, v_{2,l}, P_l) = (1, 1.1\sqrt{\gamma}, 0, 1)$  while the right state can be obtained through the Rankine-Hugoniot condition:

$$\frac{\rho_r}{\rho_l} = \frac{(\gamma + 1)M^2}{2 + (\gamma - 1)M^2}, \quad \frac{P_r}{P_l} = 1 + \frac{2\gamma}{\gamma + 1}(M^2 + 1), \quad \frac{v_{1,r}}{v_{1,l}} = \frac{2 + (\gamma - 1)M^2}{(\gamma + 1)M^2}, \quad v_{2,r} = 0.$$

Initially, an isentropic vortex is imposed and centered at  $(x_c, y_c) = (0.25, 0.5)$  on the mean flow left to the shock. The perturbations to the velocity  $(\delta v_1, \delta v_2)$ , temperature  $T_l = P_l/\rho_l$ , and entropy  $S_l = \ln(P_l/\rho_l^\gamma)$  associated with the vortex are denoted by

$$(\delta v_1, \delta v_2) = \frac{\varepsilon}{r_c} e^{\alpha(1-\tau^2)} (\bar{y}, -\bar{x}), \quad \delta T = -\frac{(\gamma - 1)\varepsilon^2}{4\alpha\gamma} e^{2\alpha(1-\tau^2)}, \quad \delta S = 0,$$

where  $\tau = \frac{r}{r_c}$ ,  $(\bar{x}, \bar{y}) = (x - x_c, y - y_c)$ ,  $r^2 = \bar{x}^2 + \bar{y}^2$ . Here  $\varepsilon$  is the strength of the vortex,  $\alpha = 0.204$  controls the decay rate of the vortex, and  $r_c = 0.4$  is the critical radius. Different from [11], we take the vortex strength as  $\varepsilon = 1.378106$ , so that the lowest density and lowest pressure are  $4.7 \times 10^{-15}$  and  $8.8 \times 10^{-21}$ , respectively. Figures 14 and 15 give the numerical solutions obtained by the  $\mathbb{P}^2$ -based and  $\mathbb{P}^4$ -based DG methods, respectively, on the uniform mesh of  $450 \times 225$  cells. We can see that flow structures are well captured by all the BP DG schemes. The results of the **optimal** and **quasi-optimal** approaches are comparable to those of the **classic** approach. However, the **optimal** and **quasi-optimal** approaches allow larger time steps, with which the CPU time is much less, as shown in Table 8.

For all the three approaches, we use the simplified BP limiter [38] as detailed in Remark 8.1. Without the BP limiter, the DG code would break down because of nonphysical solutions. Due to the presence of strong shocks in this and next examples, the WENO limiter [17] is also used, right before the BP limiter, within some adaptively detected troubled cells to suppress potential numerical oscillations.

TABLE 8. CPU time in minutes of simulating Example 3 up to  $t = 0.6$ .

	optimal approach	quasi-optimal approach	classic approach
$\mathbb{P}^2$	169.29	169.45	201.45
$\mathbb{P}^4$	1299.55	1327.45	1772.26

*Remark 8.1* (Simplified BP limiter for Euler equations). As discussed in Remark 7.4 for the scalar conservation laws, in this example we use the simplified BP limiter, which modifies the DG polynomial  $p_{ij}(x, y) = (\rho_{ij}(x, y), \mathbf{m}_{ij}(x, y), E_{ij}(x, y))$  to  $\tilde{p}_{ij}(x, y)$  as follows.

- First, modify the density to enforce its positivity via

$$\hat{\rho}_{ij}(x, y) = \theta_1(\rho_{ij}(x, y) - \bar{\rho}_{ij}) + \bar{\rho}_{ij} \quad \text{with} \quad \theta_1 := \min \left\{ \left| \frac{\bar{\rho}_{ij} - \epsilon_1}{\bar{\rho}_{ij} - \rho_{\min, ij}} \right|, 1 \right\},$$

where  $\epsilon_1$  is a small positive number introduced for avoiding the effect of round-off error and can be taken as  $\epsilon_1 = \min\{10^{-13}, \bar{\rho}_{ij}\}$ .  $\rho_{\min, ij} = \min\{\rho(u_{i \pm \frac{1}{2}, j}^\mp), \rho(u_{i, j \pm \frac{1}{2}}^\mp), \rho(\Pi_{ij})\}$ . Here  $\Pi_{ij}$  is defined by (7.16) with  $\bar{\omega}$  taken as  $\bar{\omega}_*$  for the **optimal** approach, taken as  $\bar{\omega}_*^q$  for the **quasi-optimal** approach, and taken as  $\omega_1^{\text{GL}}$  for the **classic** approach, respectively.

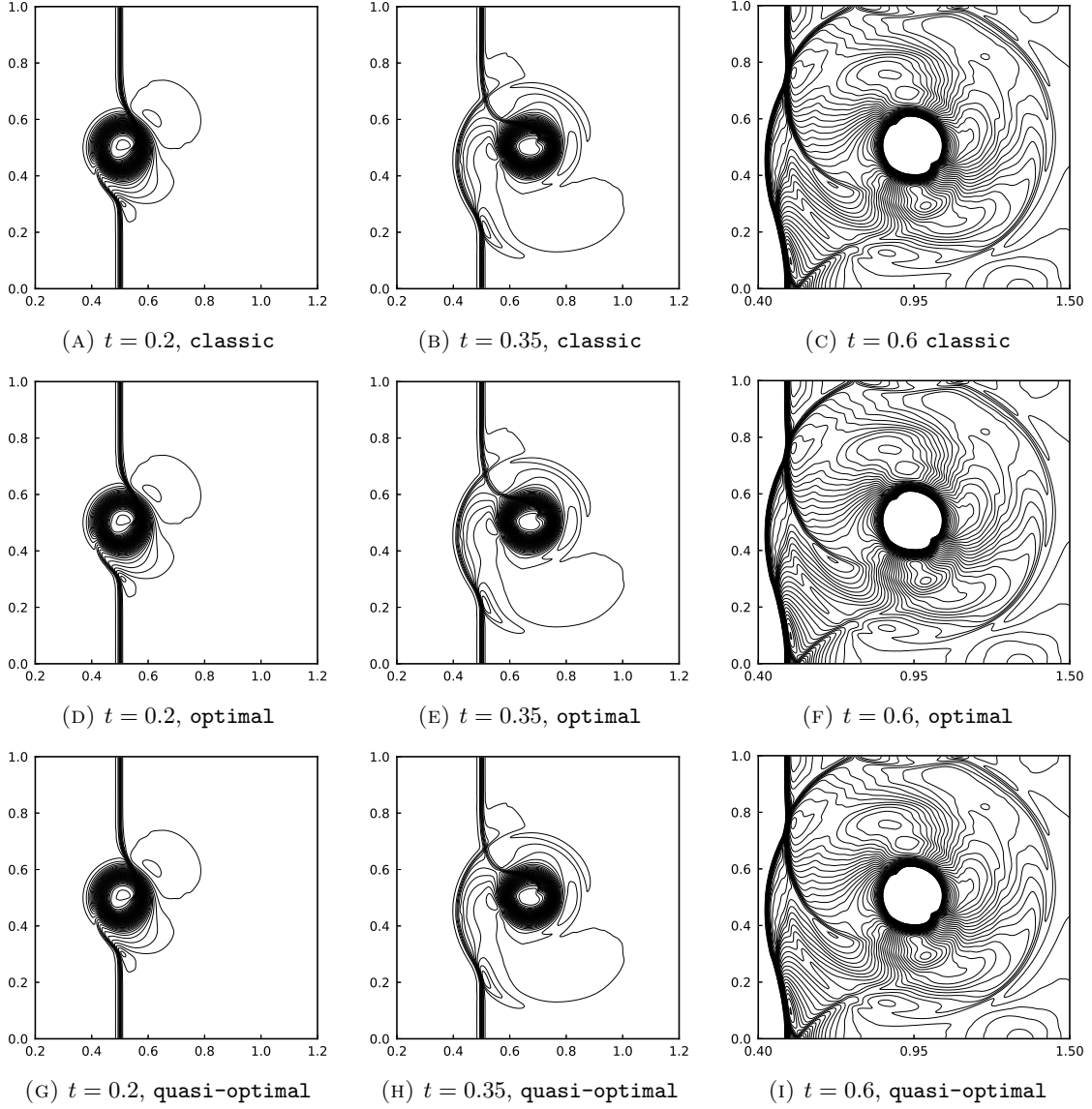


FIGURE 14. Example 3: The contour plots of pressure obtained by the  $\mathbb{P}^2$ -based BP DG methods (designed with three different CADs) at  $t = 0.2$ ,  $t = 0.35$ , and  $t = 0.6$  (from left to right). 50 contour lines: from 0.005 to 1.33 for  $t = 0.2$ ; from 0.01 to 1.402 for  $t = 0.35$ ; from 1.03 to 1.39:  $t = 0.6$ .

- Modify  $\hat{p}_{ij}(x, y) =: (\hat{\rho}_{ij}(x, y), \mathbf{m}_{ij}(x, y), E_{ij}(x, y))$  to  $\tilde{p}_{ij}(x, y)$  to enforce the positivity of  $\rho e$  by

$$\tilde{p}_{ij}(x, y) = \theta_2(\hat{p}_{ij}(x, y) - \bar{u}_{ij}) + \bar{u}_{ij} \quad \text{with} \quad \theta_2 := \min \left\{ \left| \frac{\rho e(\bar{u}_{ij}) - \epsilon_2}{\rho e(\bar{u}_{ij}) - \hat{\rho} e_{\min, ij}} \right|, 1 \right\},$$

where  $\epsilon_2$  is a small positive number introduced for avoiding the effect of round-off error and can be taken as  $\epsilon_1 = \min\{10^{-13}, \rho e(\bar{u}_{ij})\}$ , and

$$\hat{\rho} e_{\min, ij} = \min\{\rho e(\hat{u}_{i \pm \frac{1}{2}, j}^\mp), \rho e(\hat{u}_{i, j \pm \frac{1}{2}}^\mp), \rho e(\hat{\Pi}_{ij})\},$$

which are computed via (7.3), (7.4), and (7.16) but based on  $\tilde{p}_{ij}(x, y)$ .

**8.4. Example 4: 2D Riemann problem of relativistic hydrodynamics.** In this example, we simulate a 2D Riemann problem [29] with large Lorentz factor, low density, and low pressure

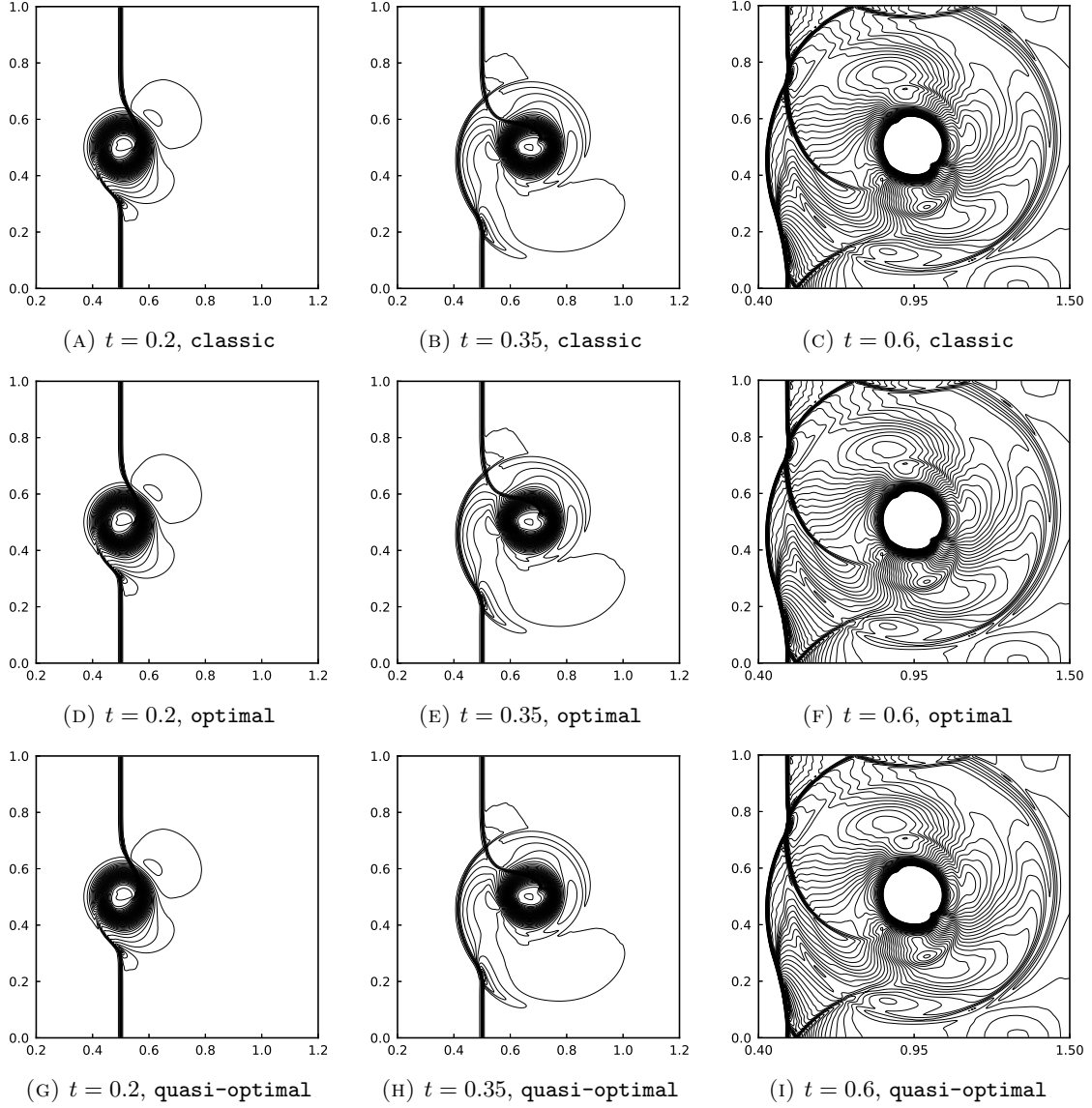


FIGURE 15. Same as Figure 14 except for  $\mathbb{P}^4$ -based BP DG methods, which are designed with three different CADs.

for special relativistic hydrodynamics, whose governing equations take the form of (7.1) with

$$(8.3) \quad u = \begin{pmatrix} D \\ m_1 \\ m_2 \\ E \end{pmatrix}, \quad f_1(u) = \begin{pmatrix} Dv_1 \\ m_1v_1 + P \\ m_2v_1 \\ m_1 \end{pmatrix}, \quad f_2(u) = \begin{pmatrix} Dv_2 \\ m_1v_2 \\ m_2v_2 + P \\ m_2 \end{pmatrix}.$$

Here  $D = \rho W$  is the density with  $\rho$  being the rest-mass density,  $(m_1, m_2) = \rho h W^2 (v_1, v_2)$  denotes the momentum vector with  $(v_1, v_2)$  being the velocity,  $E = \rho h W^2 - P$  is the total energy with  $P$  being the pressure,  $W = (1 - v_1^2 - v_2^2)^{\frac{1}{2}}$  denotes the Lorentz factor, and  $h = 1 + \frac{\gamma P}{(\gamma-1)\rho}$  is the specific enthalpy with  $\gamma$  being the adiabatic index. Normalized units are used here such that the speed of light equals one. For the relativistic hydrodynamic system (8.3), the density and pressure should be positive, and the magnitude of velocity should be smaller than the speed of light. As

proved in [29], these constraints form an invariant region which can be equivalently expressed as

$$G = \left\{ u = (D, m_1, m_2, E)^\top : D(u) > 0, q(u) := E - \sqrt{D^2 + m_1^2 + m_2^2} > 0 \right\},$$

where  $q(u)$  is a concave function of  $u$  so that  $G$  is a convex set [29].

The initial conditions of this 2D Riemann problem [29] are given by

$$(\rho, u, v, p) = \begin{cases} (0.1, 0, 0, 20), & x > 0.5, y > 0.5, \\ (0.00414329639576, 0.9946418833556542, 0, 0.05), & x < 0.5, y > 0.5, \\ (0.01, 0, 0, 0.05), & x < 0.5, y < 0.5, \\ (0.00414329639576, 0, 0.9946418833556542, 0.05), & x > 0.5, y < 0.5. \end{cases}$$

The adiabatic index  $\gamma$  is taken as  $5/3$ , and outflow conditions are specified on the boundary of the computational domain  $[0, 1]^2$ . Figure 16 displays the contours of density logarithm  $\ln \rho$ , obtained by using the BP DG methods designed with three different CADs, on the mesh of  $400 \times 400$  uniform cells at  $t = 0.4$ . It is seen that two moving shocks and two stationary contact discontinuities interact each other, forming a mushroom-like structure expanding to the left-bottom region. The results of three different approaches are consistent and agree well with those computed in [29]. Table 9 presents the CPU time in minutes for optimal, quasi-optimal and classic approaches, demonstrating the efficiency of using optimal and quasi-optimal approaches with larger time steps. We also observe that the maximum wave speeds in  $x$ - and  $y$ -directions are very close so that the quasi-optimal CAD is very close to OCAD in the simulation, since the exact solution of this problem is symmetric with respect to  $y = x$ .

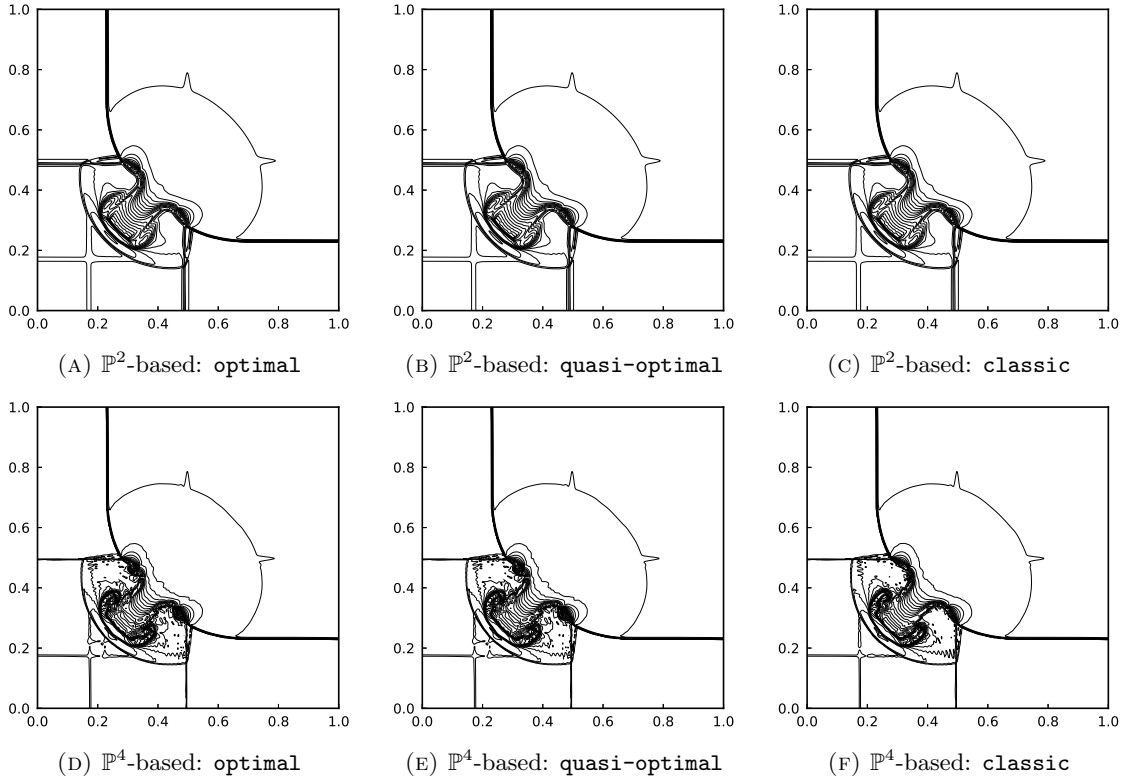


FIGURE 16. Example 4: The density logarithm  $\ln \rho$  with 25 equally spaced contour lines from  $-9.5$  to  $-2.38$  at  $t = 0.4$ .

TABLE 9. CPU time in minutes of simulating Example 4 up to  $t = 0.4$ .

	optimal approach	quasi-optimal approach	classic approach
$\mathbb{P}^2$	292.28	298.75	358.83
$\mathbb{P}^4$	1623.67	1597.97	2103.50

8.5. **Example 5: Axisymmetric jet of relativistic hydrodynamics.** In the last example, we simulate a challenging astrophysical jet problem [34, 29] by solving the axisymmetric relativistic hydrodynamic equations, which can be written in the cylindrical coordinates  $(r, z)$  as

$$(8.4) \quad \frac{\partial}{\partial t} u + \frac{\partial}{\partial r} f_1(u) + \frac{\partial}{\partial z} f_2(u) = s(u)$$

with  $u$ ,  $f_1(u)$ , and  $f_2(u)$  defined as (8.3), and

$$s(u) = -\frac{1}{r}(Dv_1, m_1v_1, m_2v_1, m_1).$$

The adiabatic index is taken as  $5/3$ . The computational domain is set as  $[0, 15] \times [0, 45]$ , which is divided into  $240 \times 720$  uniform cells. Initially, the domain is full of the static uniform medium with

$$(\rho, v_1, v_2, P) = (0.01, 0.0, 0.0, 0.000170304823218172071).$$

A high-speed relativistic jet with state

$$(\rho_b, v_{1,b}, v_{2,b}, P_b) = (0.01, 0.0, 0.99, 0.000170304823218172071)$$

is injected in  $z$ -direction through nozzle ( $r \leq 1$ ) of the bottom boundary ( $z = 0$ ). In other words, the fixed inflow condition  $(\rho_b, v_{1,b}, v_{2,b}, P_b)$  is applied on  $\{r \leq 1, z = 0\}$  of the bottom boundary. The symmetrical condition is specified on the left boundary  $r = 0$ , outflow conditions are applied on other boundaries. For this jet, the classical Mach number is 6, and the corresponding relativistic Mach number is about 41.95.

TABLE 10. CPU time in hours of simulating Example 5 up to  $t = 100$ .

	optimal approach	quasi-optimal approach	classic approach
$\mathbb{P}^2$	45.8	50.12	59.72
$\mathbb{P}^4$	297.26	334.59	414.19

The high speed and low pressure make this test very challenging. Without using the BP technique, the simulation with a DG code would break down quickly. Figure 17 displays the schlieren images of rest-mass density logarithm  $\ln \rho$  in the domain  $[-15, 15] \times [0, 45]$  by respectively using the **optimal**, **quasi-optimal**, and **classic** approaches at  $t = 100$ . The results demonstrate the excellent robustness for all the three approaches. One can see the turbulent structures are produced, and the jet dynamics and morphology agree well with those simulated in [34, 29]. Table 10 also displays the CPU time in this test, further confirming the notable advantage of the **optimal** and **quasi-optimal** approaches in efficiency.

## 9. CONCLUSIONS

In this paper, we have presented the first systematic analysis of the OCAD problem for constructing efficient high-order BP numerical methods within Zhang-Shu framework. We have proved that the classic 1D CAD originally proposed by Zhang and Shu is optimal for general  $\mathbb{P}^k$  spaces of an arbitrary  $k \in \mathbb{N}_+$ . We have also established the general theory for studying the 2D OCAD problem on Cartesian meshes. Based on the proposed theory, we have proved that the classic 2D CAD (1.14) is optimal for general  $\mathbb{Q}^k$  spaces of an arbitrary  $k \in \mathbb{N}_+$ .

Unfortunately, the classic CAD is not optimal for the widely used 2D  $\mathbb{P}^k$  spaces. As the polynomial degree  $k$  increases, seeking the genuine OCAD is more and more difficult. We have

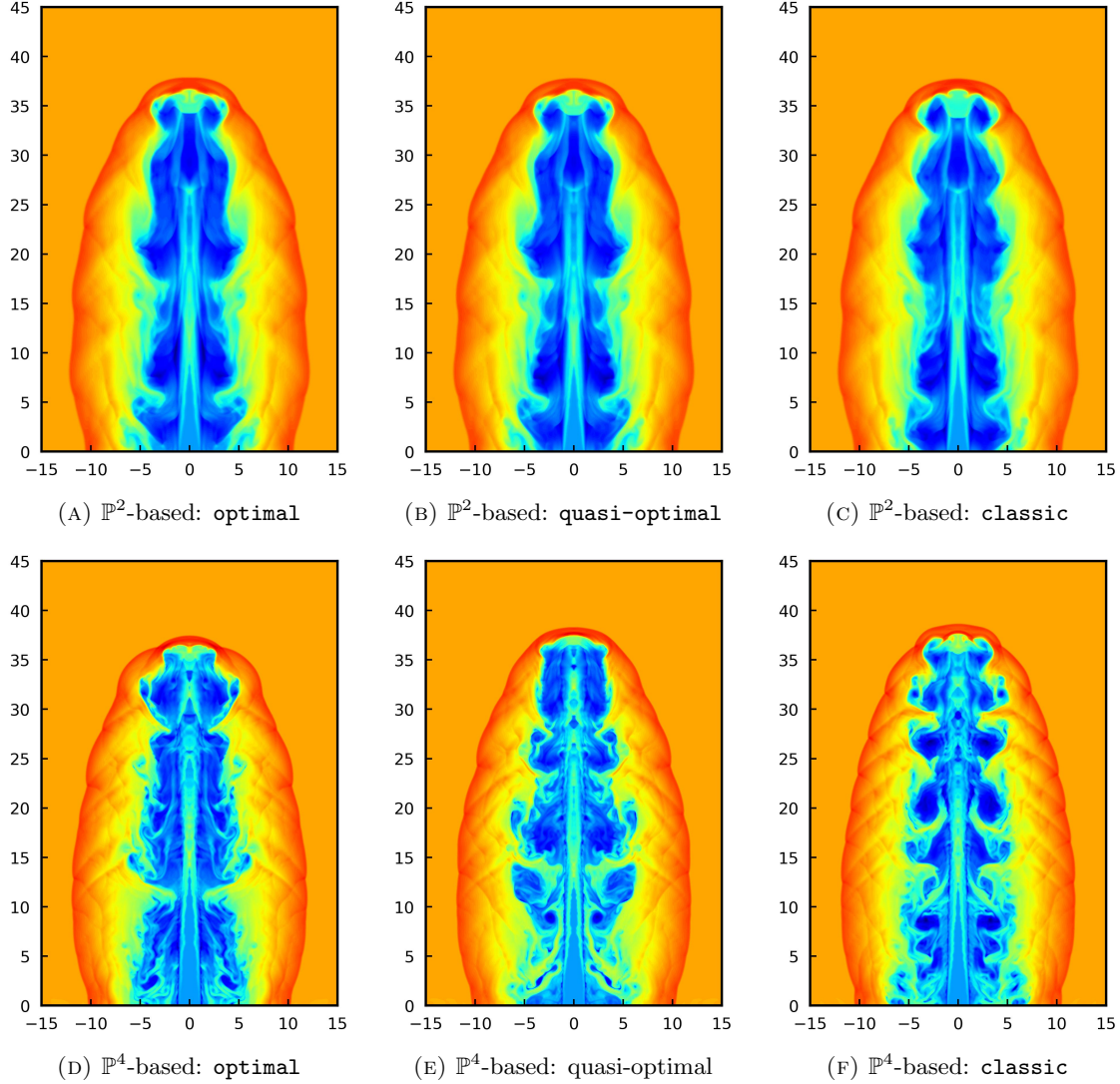


FIGURE 17. Example 5: The rest-mass density logarithm  $\ln \rho$  at  $t = 100$ .

developed a systematic approach to find the genuinely optimal CADs for the 2D  $\mathbb{P}^k$  spaces. We have derived the analytical formulas of OCADs for  $\mathbb{P}^k$  spaces with  $k \leq 7$ . A general algorithm has also been proposed to construct the OCADs for  $\mathbb{P}^k$  spaces with  $k \geq 8$ . Based on some geometric insights, we have also proposed a more practical quasi-optimal CAD, which can be easily constructed via a convex combination of the OCADs in three special cases. We have demonstrated that our quasi-optimal CAD can achieve a near-optimal BP CFL condition, which is very close (at least 95%) to the optimal one. The discovery of OCADs and quasi-optimal CADs is highly nontrivial yet meaningful, as it leads to an improvement of high-order BP schemes for a large class of hyperbolic or convection-dominated equations, at the little cost of only a slight and local modification to the implementation code. The remarkable advantages in efficiency have been confirmed by several numerical examples covering four hyperbolic partial differential equations.

The presented theory on OCAD is highly nontrivial and involves novel techniques from several branches of mathematics. For example, we have proved the existence of OCAD by using Carathéodory's theorem from *convex geometry*, and we have simplified the 2D OCAD problem to a symmetric OCAD problem based on *the invariant theory of symmetric group*. Most notably, we have discovered that the symmetric OCAD problem is closely related to polynomial optimization



of a positive linear functional on the positive polynomial cone, by which we have established four useful criteria for examining the optimality of a feasible CAD. Some geometric insights have also been provided to interpret our critical findings. Our future work will include exploring OCADs and quasi-optimal CADs on unstructured meshes and 3D meshes.

#### APPENDIX A. PROOF OF THEOREM 5.15

The proof of Theorem 5.15 is given as follows.

*Proof.* We only need to prove the result for  $\theta \in [-1, 0]$ , as the conclusion for  $\theta \in [0, 1]$  then directly follows from Lemma 3.18 and Remark 3.19.

The proof for  $\theta \in [-1, 0]$  consists of the following three steps.

**Step 1: Verify the feasibility condition (i) in Definition 1.3.** Thanks to Lemma 5.5, we only need to verify that the symmetric CAD (5.26) is feasible for the  $\mathcal{G}_s$ -invariant subspace  $\mathbb{P}^4(\mathcal{G}_s) = \mathbb{P}^5(\mathcal{G}_s) = \text{span}\{1, x^2, y^2, x^4, x^2y^2, y^4\}$ . In other words, it suffices to verify the correctness of the following equations:

$$\begin{aligned} 1 &= \frac{1}{1} \cdot \bar{\omega}_*(1 + \theta) + \frac{1}{1} \cdot \bar{\omega}_*(1 - \theta) + \omega_1 + \omega_2, \\ \frac{1}{3} &= \frac{1}{1} \cdot \bar{\omega}_*(1 + \theta) + \frac{1}{3} \cdot \bar{\omega}_*(1 - \theta) + \omega_1(x^{(1)})^2, \\ \frac{1}{3} &= \frac{1}{3} \cdot \bar{\omega}_*(1 + \theta) + \frac{1}{1} \cdot \bar{\omega}_*(1 - \theta) + \omega_1(y^{(1)})^2 + \omega_2(y^{(2)})^2, \\ \frac{1}{5} &= \frac{1}{1} \cdot \bar{\omega}_*(1 + \theta) + \frac{1}{5} \cdot \bar{\omega}_*(1 - \theta) + \omega_1(x^{(1)})^4, \\ \frac{1}{9} &= \frac{1}{3} \cdot \bar{\omega}_*(1 + \theta) + \frac{1}{3} \cdot \bar{\omega}_*(1 - \theta) + \omega_1(x^{(1)})^2(y^{(1)})^2, \\ \frac{1}{5} &= \frac{1}{5} \cdot \bar{\omega}_*(1 + \theta) + \frac{1}{1} \cdot \bar{\omega}_*(1 - \theta) + \omega_1(y^{(1)})^4 + \omega_2(y^{(2)})^4, \end{aligned}$$

which are equivalent to

$$(A.1a) \quad 1 - 2\bar{\omega}_* = \omega_1 + \omega_2,$$

$$(A.1b) \quad \frac{1}{3} - \frac{2}{3}\bar{\omega}_*\theta - \frac{4}{3}\bar{\omega}_* = \omega_1(x^{(1)})^2,$$

$$(A.1c) \quad \frac{1}{3} + \frac{2}{3}\bar{\omega}_*\theta - \frac{4}{3}\bar{\omega}_* = \omega_1(y^{(1)})^2 + \omega_2(y^{(2)})^2,$$

$$(A.1d) \quad \frac{1}{5} - \frac{4}{5}\bar{\omega}_*\theta - \frac{6}{5}\bar{\omega}_* = \omega_1(x^{(1)})^4,$$

$$(A.1e) \quad \frac{1}{9} - \frac{2}{3}\bar{\omega}_* = \omega_1(x^{(1)})^2(y^{(1)})^2,$$

$$(A.1f) \quad \frac{1}{5} + \frac{4}{5}\bar{\omega}_*\theta - \frac{6}{5}\bar{\omega}_* = \omega_1(y^{(1)})^4 + \omega_2(y^{(2)})^4.$$

It is easy to check that the formulas of  $\omega_1, \omega_2, (x^{(1)}, y^{(1)})$  and  $(x^{(2)}, y^{(2)})$ , given in (5.27b)–(5.27d), always automatically satisfy the equations (A.1a)–(A.1e). The remaining task is to verify (A.1f). Submitting the formulas of  $\omega_1, \omega_2, y^{(1)}$  and  $y^{(2)}$  into (A.1f), we can equivalently reformulate (A.1f) into

$$\frac{1}{5} + \frac{4}{5}\bar{\omega}_*\theta - \frac{6}{5}\bar{\omega}_* = \frac{36\theta^3\bar{\omega}_*^3 - 30\theta^2\bar{\omega}_*^3 + 17\theta^2\bar{\omega}_*^2 - 72\theta\bar{\omega}_*^3 + 18\theta\bar{\omega}_*^2 + 66\bar{\omega}_*^3 - 59\bar{\omega}_*^2 + 14\bar{\omega}_* - 1}{45\theta^2\bar{\omega}_*^2 + 18\theta\bar{\omega}_*^2 + 36\theta\bar{\omega}_* - 63\bar{\omega}_*^2 + 72\bar{\omega}_* - 9},$$

which is equivalent to a cubic equation of  $\bar{\omega}_*$ :

$$(A.2) \quad 12(1 - \theta^2)\bar{\omega}_*^3 + (26\theta^2 - 50)\bar{\omega}_*^2 + 14\bar{\omega}_* - 1 = 0.$$

Now we only need to verify that  $\bar{\omega}_*$  defined (5.27a) satisfies (A.2). In fact, the following cubic equation

$$(A.3) \quad 12(1 - \theta^2) + (26\theta^2 - 50)\mu + 14\mu^2 - \mu^3 = 0$$

has the following positive zero

$$\mu = \frac{14}{3} + \frac{2}{3}\sqrt{78\theta^2 + 46} \cos \left[ \frac{1}{3} \arccos \frac{1476\theta^2 - 244}{(78\theta^2 + 46)^{\frac{3}{2}}} \right] = \frac{1}{\bar{\omega}_*}.$$

This implies that  $\bar{\omega}_*$  defined (5.27a) satisfies (A.2). In summary, we have completed the verification of the feasibility condition (i) for the symmetric CAD (5.26).

**Step 2: Verify the feasibility conditions (ii) and (iii) in Definition 1.3.** The plots of  $\bar{\omega}_*$ ,  $x^{(1)}$ ,  $x^{(2)}$ ,  $y^{(1)}$ ,  $y^{(2)}$ ,  $\omega^{(1)}$ ,  $\omega^{(2)}$  are displayed in Figure 7, which clearly shows that

$$\bar{\omega}_* > 0, \quad \omega^{(1)} > 0, \quad \omega^{(2)} > 0, \quad (x^{(s)}, y^{(s)}) \in [0, 1]^2, \quad s = 1, 2.$$

**Step 3: Verify the optimality of the symmetric CAD (5.26).** Consider

$$(A.4) \quad p^*(x, y) = q_*^2(x, y) \quad \text{with} \quad q_*(x, y) := \left( (y^{(2)})^2 - (y^{(1)})^2 \right) x^2 + (x^{(1)})^2 y^2 - (x^{(1)})^2 (y^{(2)})^2,$$

which vanishes at all the internal nodes of symmetric CAD (5.26). Moreover,  $q_*(x, y) \in \mathbb{P}^2$ . Thus,  $p^*(x, y)$  is an element of  $(\mathbb{P}^2)^2$  and belongs to  $\mathbb{P}_+^4$  and  $\mathbb{P}_+^5$ . According to Theorem 3.26,  $p^*(x, y)$  is the critical positive polynomial for both  $\phi^*(\theta, \mathbb{P}_+^4)$  and  $\phi^*(\theta, \mathbb{P}_+^5)$ . Moreover, Conjectures 3.1 and 3.2 hold true for all  $\theta \in [-1, 1]$  and  $4 \leq k \leq 5$  with

$$\bar{\omega}_*(\theta, \mathbb{P}^k) = \phi^*(\theta, \mathbb{P}_+^k) = \phi^*(\theta, (\mathbb{P}^2)^2), \quad k = 4, 5.$$

In summary, we have proved that (5.26) is an OCAD for  $\mathbb{P}^4$  and  $\mathbb{P}^5$  in the case of  $\theta \in [-1, 0]$ . By Lemmas 3.17 and 3.18, it can be proved that (5.26) is also an OCAD in case of  $\theta \in [0, 1]$ . The proof is completed.  $\square$

## APPENDIX B. PROOF OF THEOREM 5.17

The proof of Theorem 5.17 is given as follows.

*Proof.* We only need to prove the result for  $\theta \in [-1, 0]$ , as the conclusion for  $\theta \in [0, 1]$  then directly follows from Lemma 3.18 and Remark 3.19.

In the case of  $\theta \in [-1, 0]$ , we have  $y_3 = y_4 = 0$  and the formulas in (5.29), (5.30) and (5.31) imply that the following moment equations are true:

$$(B.1) \quad \begin{aligned} m_{02} &= \sum_{s=1}^4 \omega_s y_s^2, & m_{04} &= \sum_{s=1}^4 \omega_s y_s^4, & m_{06} &= \sum_{s=1}^4 \omega_s y_s^6, \\ m_{22} &= \sum_{s=1}^4 \omega_s x_s^2 y_s^2, & m_{24} &= \sum_{s=1}^4 \omega_s x_s^2 y_s^4, & m_{42} &= \sum_{s=1}^4 \omega_s x_s^4 y_s^2. \end{aligned}$$

The formulas in (5.33) and (5.34) lead to

$$m_0 = \sum_{s=3}^4 \omega_s, \quad m_2 = \sum_{s=3}^4 \omega_s x_s^2, \quad m_4 = \sum_{s=3}^4 \omega_s x_s^4, \quad m_6 = \sum_{s=3}^4 \omega_s x_s^6,$$

implying that the following moment equations are true:

$$(B.2) \quad m_{00} = \sum_{s=1}^4 \omega_s, \quad m_{02} = \sum_{s=1}^4 \omega_s x_s^2, \quad m_{04} = \sum_{s=1}^4 \omega_s x_s^4, \quad m_{06} = \sum_{s=1}^4 \omega_s x_s^6.$$

The moment equations in (B.1) and (B.2) imply the CAD (5.28) satisfies the feasibility condition (i). The weights and coordinates are plotted in Figure 8, which demonstrates that  $x_s, y_s \in [0, 1]$  and  $\omega_s \geq 0$ . Thus, the feasibility condition (ii) and (iii) are satisfied and the CAD (5.28) is feasible.

Next, we will show that the boundary weight  $\bar{\omega}_*$  given in (5.29) is equal to  $\phi^*(\theta, (\mathbb{P}^3)^2)$ . According to Theorem 3.29,  $\phi^*(\theta, (\mathbb{P}^3)^2)$  is the smallest real root of polynomial  $\mathcal{F}_\theta(\phi)$  in the following form

$$\mathcal{F}_\theta(\phi) = \frac{3^{14} 5^8 7^2}{4096} \mathcal{F}_\theta^{(1)}(\phi) \mathcal{F}_\theta^{(2)}(\phi) \mathcal{F}_\theta^{(3)}(\phi) \mathcal{F}_\theta^{(4)}(\phi)$$

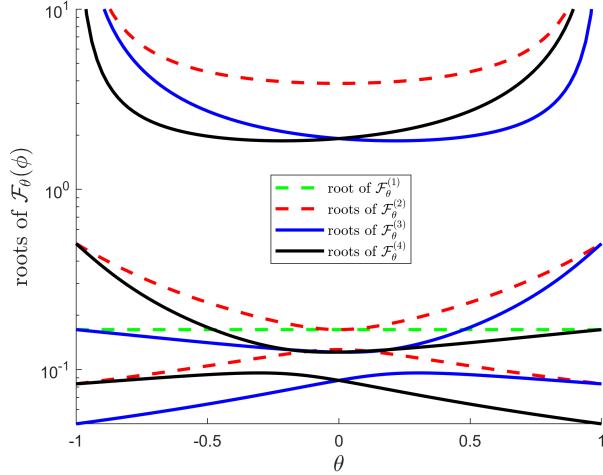


FIGURE 18. Roots of  $\mathcal{F}_\theta^{(1)}(\phi)$ ,  $\mathcal{F}_\theta^{(2)}(\phi)$ ,  $\mathcal{F}_\theta^{(3)}(\phi)$  and  $\mathcal{F}_\theta^{(4)}(\phi)$  in (B.3) as functions of  $\theta$ .

with

$$\begin{aligned}
 \mathcal{F}_\theta^{(1)}(\phi) &= 6\phi - 1, \\
 \mathcal{F}_\theta^{(2)}(\phi) &= (12\theta^2 - 12)\phi^3 + (50 - 26\theta^2)\phi^2 - 14\phi + 1 \\
 \mathcal{F}_\theta^{(3)}(\phi) &= (12\theta^3 - 48\theta^2 - 12\theta + 48)\phi^3 + (48\theta + 30\theta^2 - 102)\phi^2 + (-6\theta + 20)\phi - 1, \\
 \mathcal{F}_\theta^{(4)}(\phi) &= (12\theta^3 + 48\theta^2 - 12\theta - 48)\phi^3 + (48\theta - 30\theta^2 + 102)\phi^2 + (-6\theta - 20)\phi + 1.
 \end{aligned}
 \tag{B.3}$$

The real roots of  $\mathcal{F}_\theta^{(1)}(\phi)$ ,  $\mathcal{F}_\theta^{(2)}(\phi)$ ,  $\mathcal{F}_\theta^{(3)}(\phi)$  and  $\mathcal{F}_\theta^{(4)}(\phi)$  are plotted in Figure 18. It is clear that the smallest root of  $\mathcal{F}_\theta(\phi)$  is the root of either  $\mathcal{F}_\theta^{(3)}(\phi)$  (for  $\theta \in [-1, 0]$ ) or  $\mathcal{F}_\theta^{(4)}(\phi)$  (for  $\theta \in [0, 1]$ ). With the help of the cubic formula from [21], the smallest real root of  $\mathcal{F}_\theta^{(3)}(\phi)$  has the following explicit formula

$$\phi_1^{(3)}(\theta) = \left[ -2\theta + \frac{20}{3} + \frac{2}{3} \sqrt{126\theta^2 - 96\theta + 94} \cos \left( \frac{1}{3} \arccos \frac{-864\theta^3 + 2916\theta^2 - 288\theta - 532}{(126\theta^2 - 96\theta + 94)^{\frac{3}{2}}} \right) \right]^{-1},$$

and the smallest real root  $\mathcal{F}_\theta^{(4)}(\phi)$  has the following explicit formula

$$\phi_1^{(4)}(\theta) = \left[ 2\theta + \frac{20}{3} + \frac{2}{3} \sqrt{126\theta^2 + 96\theta + 94} \cos \left( \frac{1}{3} \arccos \frac{864\theta^3 + 2916\theta^2 + 288\theta - 532}{(126\theta^2 + 96\theta + 94)^{\frac{3}{2}}} \right) \right]^{-1}.$$

Thus,

$$\begin{aligned}
 \phi^*(\theta, (\mathbb{P}^3)^2) &= \begin{cases} \phi_1^{(3)}(\theta) & \text{if } \theta \in [-1, 0], \\ \phi_1^{(4)}(\theta) & \text{if } \theta \in [0, 1], \end{cases} \\
 &= \left[ 2|\theta| + \frac{20}{3} + \frac{2}{3} \sqrt{126\theta^2 + 96|\theta| + 94} \cos \left( \frac{1}{3} \arccos \frac{864|\theta|^3 + 2916\theta^2 + 288|\theta| - 532}{(126\theta^2 + 96|\theta| + 94)^{\frac{3}{2}}} \right) \right]^{-1}.
 \end{aligned}$$

So far, we have proved that (5.28) is a feasible CAD and  $\bar{\omega}_* = \phi^*(\theta, (\mathbb{P}^3)^2)$ . By Theorem 3.27, (5.28) is the symmetric OCAD for  $\mathbb{P}^6$  and  $\mathbb{P}^7$  spaces. The proof is completed.  $\square$

#### APPENDIX C. FULLY SYMMETRIC OCADS FOR $\theta = 0$ AND $\mathbb{P}^8$ TO $\mathbb{P}^{14}$ SPACES

This appendix gives the fully symmetric OCADs for  $\mathbb{P}^k$  spaces with  $8 \leq k \leq 15$  in the case of  $\theta = 0$ . See Figures 19 and 20.

## REFERENCES

1. Martin Campos-Pinto, Frédérique Charles, and Bruno Després, *Algorithms for positive polynomial approximation*, SIAM J. Numer. Anal. **57** (2019), no. 1, 148–172.
2. Constantin Carathéodory, *Über Den Variabilitätsbereich Der Fourier’Schen Konstanten Von Positiven Harmonischen Funktionen*, Rendiconti del Circolo Matematico di Palermo **32** (1911), no. 1, 193–217.
3. Bernardo Cockburn and Chi-Wang Shu, *Runge–Kutta discontinuous Galerkin methods for convection-dominated problems*, J. Sci. Comput. **16** (2001), no. 3, 173–261.
4. Shumo Cui, Shengrong Ding, and Kailiang Wu, *Is the classic convex decomposition optimal for bound-preserving schemes in multiple dimensions?*, arXiv:2207.08849 (2022).
5. Jie Du, Cheng Wang, Chengeng Qian, and Yang Yang, *High-order bound-preserving discontinuous Galerkin methods for stiff multispecies detonation*, SIAM J. Sci. Comput. **41** (2019), no. 2, B250–B273.
6. Jie Du and Yang Yang, *Third-order conservative sign-preserving and steady-state-preserving time integrations and applications in stiff multispecies and multireaction detonations*, J. Comput. Phys. **395** (2019), 489–510.
7. Qiang Du, Lili Ju, Xiao Li, and Zhonghua Qiao, *Maximum bound principles for a class of semilinear parabolic equations and exponential time-differencing schemes*, SIAM Review **63** (2021), no. 2, 317–359.
8. Leopold Flatto, *Basic sets of invariants for finite reflection groups*, Bull. Am. Math. Soc. **74** (1968), no. 4, 730–734.
9. Sigal Gottlieb, David I Ketcheson, and Chi-Wang Shu, *Strong stability preserving Runge-Kutta and multistep time discretizations*, World Scientific Publishing Co. Pte. Ltd., Hackensack, NJ, 2011.
10. Jean-Luc Guermond and Bojan Popov, *Invariant domains and second-order continuous finite element approximation for scalar conservation equations*, SIAM J. Numer. Anal. **55** (2017), no. 6, 3120–3146.
11. Guang-Shan Jiang and Chi-Wang Shu, *Efficient implementation of weighted eno schemes*, J. Comput. Phys. **126** (1996), no. 1, 202–228.
12. Yi Jiang and Hailiang Liu, *Invariant-region-preserving DG methods for multi-dimensional hyperbolic conservation law systems, with an application to compressible Euler equations*, J. Comput. Phys. **373** (2018), 385–409.
13. Jean B Lasserre, *A semidefinite programming approach to the generalized problem of moments*, Math. Program. **112** (2007), no. 1, 65–92.
14. Jean Bernard Lasserre, *Moments, positive polynomials and their applications*, Imperial College Press Optimization Series, vol. 1, Imperial College Press, London, 2010. MR 2589247
15. Jean-Bernard Lasserre, *An introduction to polynomial and semi-algebraic optimization*, Cambridge texts in applied mathematics, Cambridge University Press, Cambridge, 2015 (eng).
16. Tong Qin, Chi-Wang Shu, and Yang Yang, *Bound-preserving discontinuous Galerkin methods for relativistic hydrodynamics*, J. Comput. Phys. **315** (2016), 323–347.
17. Jianxian Qiu and Chi-Wang Shu, *Runge–Kutta discontinuous Galerkin method using WENO limiters*, SIAM J. Sci. Comput. **26** (2005), no. 3, 907–929.
18. Sergei L’vovich Sobolev, *The formulas of mechanical cubature on the surface of a sphere*, Sibirskii Matematicheskii Zhurnal **3** (1962), no. 5, 769–796.
19. Bernd Sturmfels, *Algorithms in invariant theory*, Springer Science & Business Media, 2008.
20. Cheng Wang, Xiangxiong Zhang, Chi-Wang Shu, and Jianguo Ning, *Robust high order discontinuous Galerkin schemes for two-dimensional gaseous detonations*, J. Comput. Phys. **231** (2012), no. 2, 653–665.
21. Eric W Weisstein, *Cubic formula*, <https://mathworld.wolfram.com/CubicFormula.html> (2002).
22. Kailiang Wu, *Design of provably physical-constraint-preserving methods for general relativistic hydrodynamics*, Phys. Rev. D **95** (2017), no. 10.
23. ———, *Positivity-preserving analysis of numerical schemes for ideal magnetohydrodynamics*, SIAM J. Numer. Anal. **56** (2018), no. 4, 2124–2147.
24. ———, *Minimum principle on specific entropy and high-order accurate invariant region preserving numerical methods for relativistic hydrodynamics*, SIAM J. Sci. Comput. **43** (2021), no. 6, B1164–B1197.
25. Kailiang Wu and Chi-Wang Shu, *A provably positive discontinuous Galerkin method for multidimensional ideal magnetohydrodynamics*, SIAM J. Sci. Comput. **40** (2018), no. 5, B1302–B1329.
26. ———, *Provably positive high-order schemes for ideal magnetohydrodynamics: analysis on general meshes*, Numer. Math. **142** (2019), no. 4, 995–1047.
27. ———, *Provably physical-constraint-preserving discontinuous Galerkin methods for multidimensional relativistic MHD equations*, Numer. Math. **148** (2021), 699–741.
28. Kailiang Wu and Chi-Wang Shu, *Geometric quasilinearization framework for analysis and design of bound-preserving schemes*, SIAM Review **in press** (2022).
29. Kailiang Wu and Huazhong Tang, *High-order accurate physical-constraints-preserving finite difference WENO schemes for special relativistic hydrodynamics*, J. Comput. Phys. **298** (2015), 539–564.
30. Yulong Xing, Xiangxiong Zhang, and Chi-Wang Shu, *Positivity-preserving high order well-balanced discontinuous Galerkin methods for the shallow water equations*, Adv. Water Resour. **33** (2010), no. 12, 1476–1493.
31. Tao Xiong, Jing-Mei Qiu, and Zhengfu Xu, *Parametrized positivity preserving flux limiters for the high order finite difference WENO scheme solving compressible Euler equations*, J. Sci. Comput. **67** (2016), no. 3, 1066–1088.
32. Zhengfu Xu, *Parametrized maximum principle preserving flux limiters for high order schemes solving hyperbolic conservation laws: one-dimensional scalar problem*, Math. Comp. **83** (2014), no. 289, 2213–2238.

33. Zhengfu Xu and Xiangxiong Zhang, *Bound-preserving high order schemes*, Handbook of Numerical Methods for Hyperbolic Problems: Applied and Modern Issues, edited by R. Abgrall and C.-W. Shu (North-Holland, Amsterdam), vol. 18, Elsevier, 2017.
34. Weiqun Zhang and Andrew I MacFadyen, *RAM: a relativistic adaptive mesh refinement hydrodynamics code*, Astrophys. J. Suppl. Ser. **164** (2006), no. 1, 255.
35. Xiangxiong Zhang, *On positivity-preserving high order discontinuous Galerkin schemes for compressible Navier-Stokes equations*, J. Comput. Phys. **328** (2017), 301–343.
36. Xiangxiong Zhang and Chi-Wang Shu, *On maximum-principle-satisfying high order schemes for scalar conservation laws*, J. Comput. Phys. **229** (2010), no. 9, 3091–3120.
37. ———, *On positivity-preserving high order discontinuous Galerkin schemes for compressible Euler equations on rectangular meshes*, J. Comput. Phys. **229** (2010), no. 23, 8918–8934.
38. ———, *Maximum-principle-satisfying and positivity-preserving high-order schemes for conservation laws: survey and new developments*, Proc. R. Soc. A **467** (2011), 2752–2776.
39. Xiangxiong Zhang, Yinhua Xia, and Chi-Wang Shu, *Maximum-principle-satisfying and positivity-preserving high order discontinuous Galerkin schemes for conservation laws on triangular meshes*, J. Sci. Comput. **50** (2012), no. 1, 29–62.
40. Yifan Zhang, Xiangxiong Zhang, and Chi-Wang Shu, *Maximum-principle-satisfying second order discontinuous Galerkin schemes for convection–diffusion equations on triangular meshes*, J. Comput. Phys. **234** (2013), 295–316.

DEPARTMENT OF MATHEMATICS, SOUTHERN UNIVERSITY OF SCIENCE AND TECHNOLOGY, SHENZHEN, GUANGDONG 518055, CHINA

*Email address:* `cuism@sustech.edu.cn`

DEPARTMENT OF MATHEMATICS, SOUTHERN UNIVERSITY OF SCIENCE AND TECHNOLOGY, SHENZHEN, GUANGDONG 518055, CHINA

*Email address:* `dingsr@sustech.edu.cn`

CORRESPONDING AUTHOR. DEPARTMENT OF MATHEMATICS & SUSTECH INTERNATIONAL CENTER FOR MATHEMATICS, SOUTHERN UNIVERSITY OF SCIENCE AND TECHNOLOGY, AND NATIONAL CENTER FOR APPLIED MATHEMATICS SHENZHEN (NCAMS), SHENZHEN, GUANGDONG 518055, CHINA

*Email address:* `wukl@sustech.edu.cn`

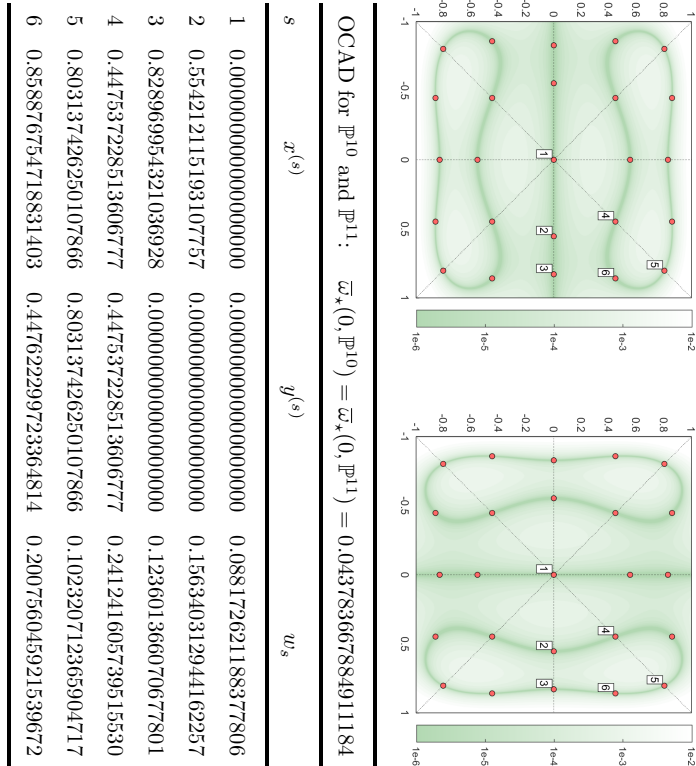
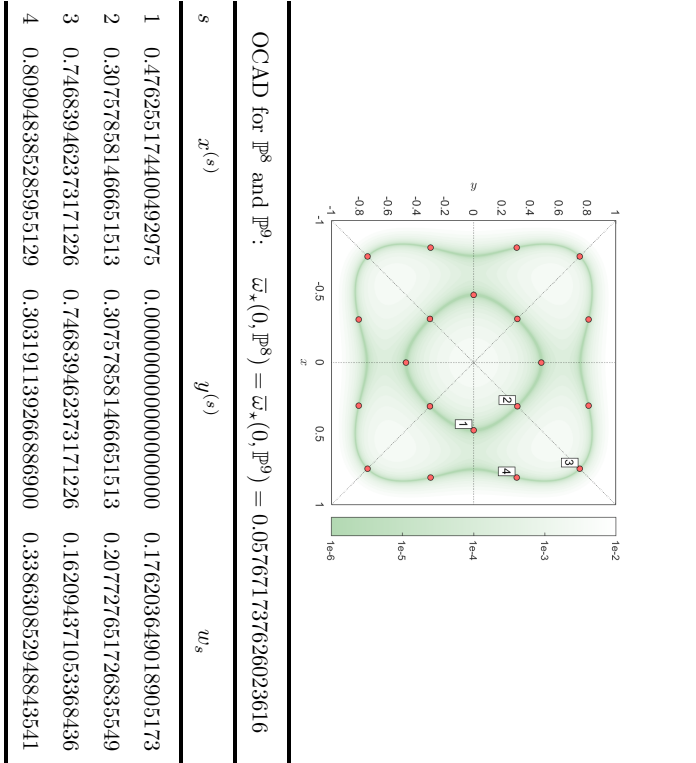
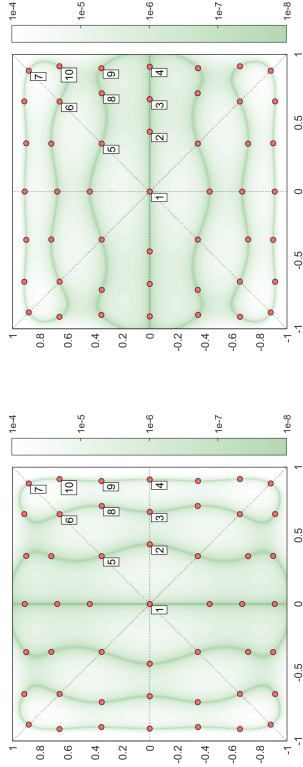
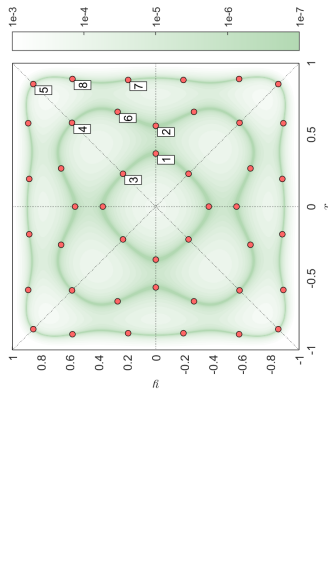


FIGURE 19. Fully symmetric OCADs in the case of  $\theta = 0$ . Left:  $\mathbb{P}^8$  and  $\mathbb{P}^9$ ; Right:  $\mathbb{P}^{10}$  and  $\mathbb{P}^{11}$ . The background shows the critical positive polynomials, which vanish at all the internal nodes. Note that there are two independent critical positive polynomials for both  $\mathbb{P}^{10}$  and  $\mathbb{P}^{11}$ .



OCAD for  $\mathbb{P}^{14}$  and  $\mathbb{P}^{15}$ :  $\bar{\omega}_*(0, \mathbb{P}^{14}) = \bar{\omega}_*(0, \mathbb{P}^{15}) = 0.026235904303028568$

$s$	$x^{(s)}$	$y^{(s)}$	$w_s$
1	0.0000000000000000	0.0000000000000000	0.053164403393148263
2	0.436392399477797233	0.0000000000000000	0.092145111611692213
3	0.67356529843208610	0.0000000000000000	0.101065021968679156
4	0.910301579799071447	0.0000000000000000	0.055756993653433708
5	0.350029230273781800	0.350029230273781800	0.161824595000403304
6	0.656381489508818472	0.656381489508818472	0.099307085270020912
7	0.881053772502435772	0.881053772502435772	0.038118523352566075
8	0.716669518597241706	0.349444864340185291	0.158536291138303115
9	0.899037349937064634	0.351871191587682486	0.106699680399639993
10	0.913328178951963054	0.657387736756496754	0.080910485606056695



OCAD for  $\mathbb{P}^{12}$  and  $\mathbb{P}^{13}$ :  $\bar{\omega}_*(0, \mathbb{P}^{12}) = \bar{\omega}_*(0, \mathbb{P}^{13}) = 0.032438153462135161$

$s$	$x^{(s)}$	$y^{(s)}$	$w_s$
1	0.369890118757416453	0.0000000000000000	0.091059404176295738
2	0.563514986781431304	0.0000000000000000	0.045533011352710533
3	0.228778715984597453	0.228778715984597453	0.128662871669451007
4	0.584426213735658284	0.584426213735658284	0.123039786326433503
5	0.854866852568051616	0.854866852568051616	0.055733425609174367
6	0.660749749320902580	0.266375841680371372	0.215949847642931181
7	0.883206839937117461	0.192848696503398337	0.148218518501914781
8	0.890316258798109716	0.581533330276227556	0.126926827796818464

FIGURE 20. Fully symmetric OCADs in the case of  $\theta = 0$ . Left:  $\mathbb{P}^{12}$  and  $\mathbb{P}^{13}$ ; Right:  $\mathbb{P}^{14}$  and  $\mathbb{P}^{15}$ . The background shows the critical positive polynomials, which vanish at all the internal nodes. Note that there are two independent critical positive polynomials for both  $\mathbb{P}^{14}$  and  $\mathbb{P}^{15}$ .